Simulation Model of Ray Patterning in Zebrafish Caudal Fins

By

Valerie Tweedle

Thesis submitted to the
Faculty of Graduate and Postdoctoral Studies
In partial fulfillment of the requirements
For the M.Sc. degree in Biology

Department of Biology
Faculty of Science
University of Ottawa

Abstract

The bony fin rays of the zebrafish caudal fin are a convenient model system for studying bone morphogenesis and patterning. Joints and bifurcations in fin rays follow predictable spatial patterns within and between rays as they develop. Despite a growing body of literature on the genetics of bone patterning and the development of the first model of ray growth, the mechanisms underlying observed joint and bifurcation patterns are not well understood. We developed simulation models to explore ray pattern formation mechanisms in growing fins. In all models, fin ray growth rates are based on quantitative experimental data. The different models simulate ray joint formation and ray bifurcation formation in growing rays using different hypothetical mechanisms. To select the most plausible model, we compared model outputs to qualitative experimental data on joint and bifurcation patterns. In the selected model, ray joint and bifurcation formation result from the accumulation of two substances, arbitrarily named $J_{r,t}$ and $B_{r,t}$, produced at the distal end of the fin. The rates of production of $J_{r,t}$ and $B_{r,t}$ follow a bimodal distribution across the medio-lateral axis of the fin, and decrease over time. Model parameters were optimized to find the best fit between model output and quantitative experimental data on ray joint and bifurcation patterns. The model will be tested further in the future by evaluating how well it can predict fin ray patterns of mutant zebrafish fins, as well as fin ray patterns of species with different fin shapes and sizes.

Acknowledgements

I would like to start by thanking my supervisor, Dr. Anne-Gaëlle Rolland-Lagan, for everything she has done for me during my undergraduate and graduate research projects. I would not have been able to complete them without her support, guidance, and encouragement.

Second, I would like to thank my committee members, Dr. Marie-Andrée Akimenko (Professor of Biology, University of Ottawa) and Dr. Tom Sherratt (Professor of Biology, Carleton University), for their comments and guidance throughout the course of my project and my external committee member Dr. John Lewis.

I would like to thank Vishal Saxena, Jing Zhang for their tutelage in experimental protocols and Dr. Marie-Andrée Akimenko for the use of her fish and equipment. I would also like to extend my gratitude to all the past and present members of the Rolland-Lagan laboratory. They provided me with helpful advice, camaraderie and made my time in the laboratory that much more enjoyable. I would also like to thank the members of the Ekker and Bonen laboratories for their encouragement.

Finally, I would like to thank my family, especially my parents, who have encouraged and supported me throughout my undergraduate and graduate degrees. I would also like to thank the University of Ottawa and the Ontario Graduate Scholarship Program for funding.

TABLE OF CONTENTS

List of Tables

List of Figures

List of Acronyms

Dpf – Days Post Fertilization

Dpa – Days Post Amputation

Shh – Sonic Hedgehog

sof – Short Fin Mutant

lof – Long Fin Mutant

alf – Another Long Fin Mutant

Fgf – Fibroblast Growth Factor

PSM – Pre-Somitic Mesoderm

Bmp – Bone Morphogenetic Proteins

Gdf5 – Growth Differentiation Factor 5

Vegf – Vascular Endothelial Growth Factors

Cx43 – Connexin 43

Ptc1 – Patched-1

RMSE – Root Mean Square Error

NRMSE – Normalized Root Mean Square Error

Chapter 1 - Introduction

1.1. The Study of Pattern Formation

Development of an organism from a single cell to its final form involves not only the creation of necessary tissue types, but also the proper spatial organization of these tissues within the organism as growth proceeds. Pattern formation is the study of the mechanisms responsible for the spatial organization of cell and tissue types (Wolpert 1969). Pattern formation mechanisms are typically responsible for the differentiation of cell types at given positions and/or the specification of growth at given positions in the organism. In particular, variations in growth between tissues can generate changes in the overall shape of the organism (reviewed in Wolpert 2002). The mechanisms behind pattern formation must be tightly regulated to ensure proper organization into functioning structures, in addition to working with growth to ensure proper final form. The processes of growth and pattern formation can occur in various ways, including sequentially, simultaneously, and/or in an interactive manner.

The sequential occurrence of patterning and growth often involves first the formation of a pattern, followed by growth. This can be illustrated conceptually by imagining a deflated balloon with black stripes drawn on it. As the balloon is inflated, representing growth, the stripe pattern is simply deformed by growth as it enlarges in proportion to the balloon (Figure 1.1A). An example of this sequential patterning and growth in nature is the patterning of a zebra's stripes. Zebra stripe patterns are established during embryogenesis, and simply enlarge after birth - no new stripes are added (Bard 1977).

Conversely, patterning and growth can occur simultaneously. In the balloon example, this is equivalent to painting new stripes on the balloon as it grows: the stripes originally drawn on the balloon begin to grow and move further apart with growth of the balloon, spreading out the pattern. Once the distance between stripes reaches a threshold, new stripes are painted in between the original stripes, so that the distance between the stripes is the same as it was before the balloon was inflated. Therefore, the size of the

balloon and the patterning of the stripes are changing simultaneously, so that the number of stripes increases but the spacing between stripes is maintained (Figure 1.1B). An example of this is the striped pattern of the angelfish. This number of stripes on the fish increases as the fish grows, to maintain relatively constant distance between stripes (Kondo and Asai, 1995).

Finally, the two processes can interact with one another in various ways. One possibility is that the pattern itself can affect growth. In the balloon example, this would happen if the striped pattern affected growth in those regions of the balloon. For instance, wherever stripes occur growth could be restricted, resulting in a ribbed balloon (Figure 1.1C). Another possibility is that the interaction between growth and patterning can cause alterations to the mechanisms of each. This commonly occurs during development as patterns of gene expression may affect growth, and growth in turn may affect patterning processes. This feedback between growth and patterning can be illustrated through the concept of morphogen gradients. Morphogens are substances involved in pattern formation. Their concentrations can vary over space and elicit differential gene expression (Ashe and Briscoe 2006, Rolland-Lagan *et al.*, 2012). We can use the French Flag model of pattern development to further explain this concept. In this model, each cell can differentiate to become blue, white, or red depending on their location (Wolpert 1969) as encoded by a morphogen gradient. The patterning mechanism is set-up such that a third of the cells will differentiate into one of the three colours, in likeness to the French Flag. We could imagine that the morphogen in this gradient is responsible for growth such that the area that differentiates to red has the highest growth. Therefore, the third of the flag that is red will be growing at a much more rapid pace. However, the patterning mechanism will re-specify the red portion of the flag such that it only takes up a third of the flag.

Differential gene activity due to morphogen concentrations plays an important role in the regulation of growth and patterning of an organism. The genes expressed during growth and patterning vary depending on the organism, location within the organism growing and/or being patterned, and the moment in time during development (reviewed in Wolpert 2002). In the following, we provide examples of genes involved in growth and patterning in vertebrates to illustrate the variety of genes involved and the roles they play.

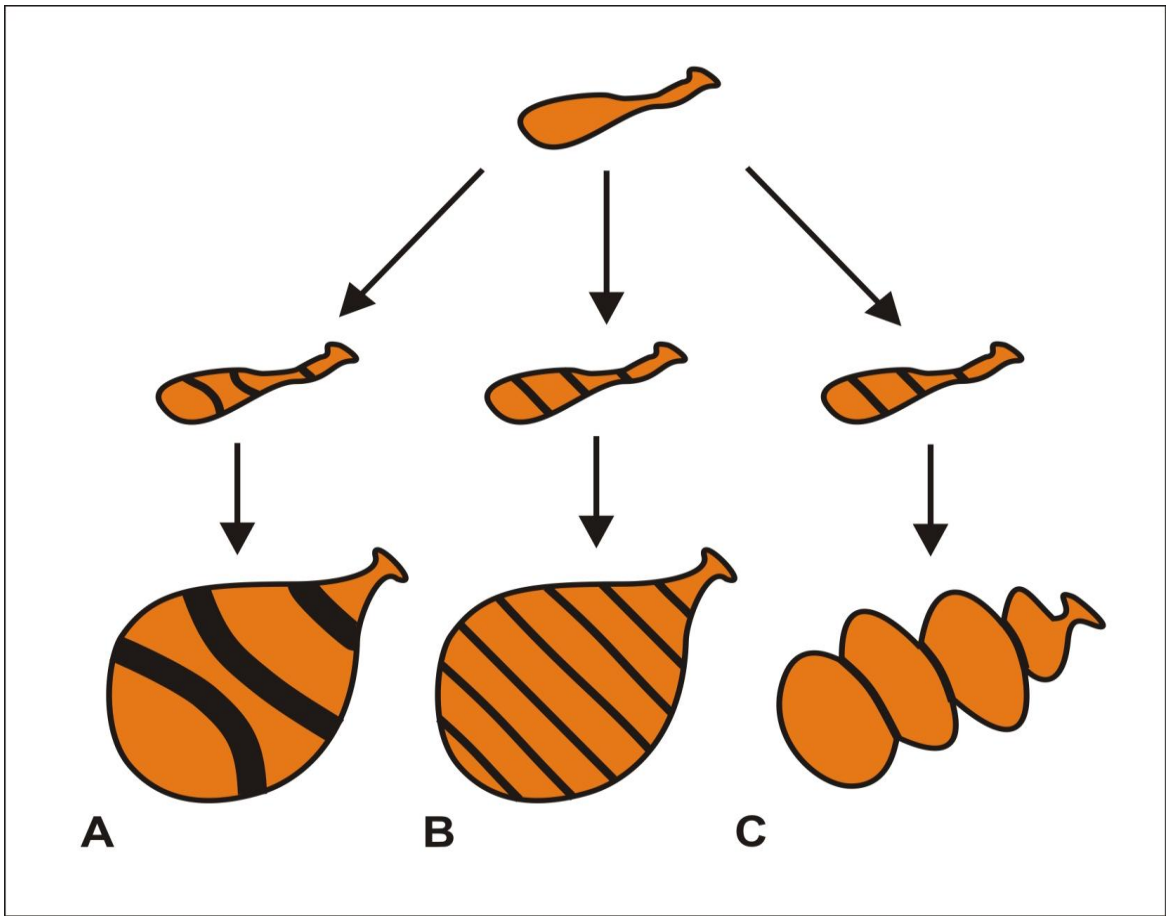

Figure 1.1 Schematic showing the interaction of patterning and growth processes using a balloon. **A:** patterning (stripes) occurring prior to growth. **B:** patterning of stripes occurring simultaneously with growth. The alteration of the pattern maintains stripe width during growth. **C:** effect of patterning on growth. Growth is restricted in striped areas.

1.2. Molecular Regulators of Growth

Some of the main regulators of growth are the members of the fibroblast growth factor (*Fgf*) gene family. FGF proteins have been shown to induce DNA synthesis and affect cell survival in many cell types. In addition, they are involved in gastrulation, angiogenesis, and tumour formation, to name a few (reviewed in Szebenyi and Fallon 1999, Branney *et al.*, 2009, Korc and Friesel 2009). A specific example of FGF requirement in growth is in the formation of the limbs. FGFs are required for the initiation of the fore- and hind-limb bud development in vertebrates, and ectopic expression of *Fgfs* induce the formation of extra limbs (Szebenyi and Fallon 1999, reviewed in Wolpert 2002). As the limb continues to develop, various FGFs continue to play roles in the growth of the limb tissues (Szebenyi and Fallon 1999).

1.3. Molecular Regulators of Vertebrate Patterning

Tissues and organs need to be patterned in an organism in order for it to attain its final form. Similar patterns can occur in many organs, even though the genes expressed in each may vary. For example, segmentation occurs not only in the vertebrate somites, but also in the patterning of limb bones. Similarly, bifurcation, or branching, occurs in blood vessels as well as in the respiratory tract.

1.3.1. Segmentation

The anterior-posterior patterning of vertebrates arises from the patterning of the somites during embryogenesis. Somites are segmented blocks of tissue formed sequentially from the pre-somitic mesoderm (PSM), and they are responsible for the formation of muscles, vertebrae, and dermis of the organism (Pourquié 2003, reviewed in Roellig *et al.*, 2011). It is postulated that the segmentation of the somites arises from a "Clock and Wavefront" model of condensation. This model implies a wavefront, or border, where the PSM differentiates and somite condensation occurs, working in conjunction with an oscillating molecular clock, which alternates between allowing this differentiation of somites or inhibiting it. Each oscillation of this clock thus is responsible for the formation

of a single pair of somites (Pourquié 2003, reviewed in Roellig *et al*., 2011). This oscillating molecular clock has been proposed to be a gene, *c-hairy1,* which has periodic expression in the PSM. This periodic *c-hairy1* expression is then transformed into a spatial pattern and a somite border through Notch signalling (Dale and Pourquié 2000), resulting in segmentation of the somites. Once the somites have condensed, various genes, such as the *hox* genes, play a role in the differentiation of the somites into their various structures, such as the vertebrae.

Segmentation occurs in other bony structures in the vertebrates, including bony appendages (i.e. positions of the joints cause the bony elements of the limbs to be segmented). The formation of vertebrate limbs involves the condensation of chondritic cells, branching, and segmentation (Baur *et al.,* 2000). Bone morphogenetic proteins (BMPs) are growth factors that play an important role in inducing the formation of cartilage and bone (Xiao *et al.,* 2007). growth differentiation factor 5 (*Gdf5*), a member of the BMP family, was shown to be expressed in mouse limbs in a series of stripes that corresponded to the position of the joints in the limb. In addition, mutant mice with null mutations in the *Gdf5* gene showed disruption in the formation of joints in all limbs and the fusion of bones (Storm and Kingsley 1996), implicating GDF5 in segmentation of the limb.

1.3.2. Bifurcation

The bifurcation, or branching, of structures is essential in vertebrates for providing adequate oxygen and nutrient supplies to the entire organism, in addition to removing waste, and/or providing structural support. Excellent examples of branching are found in the circulatory and the respiratory systems. The function of genes in bifurcation can vary, including functioning as chemoattractants to direct the movement of a branch, or through suppressing growth factors centrally to create a gap and form two branches.

The bifurcation of arteries and veins is pivotal in providing adequate nutrient and oxygen supplies to tissues in organisms with closed circulatory systems. Angiogenesis is the formation of blood vessels, and sprouting is a type of angiogenesis that involves the bifurcation of a blood vessel in two. This type of angiogenesis is commonly seen in the

vertebrate brain. One class of factors thought to direct new sprouts is the family of vascular endothelial growth factors (VEGFs) since they are chemotactic factors (reviewed in Risau 1997).

Another example of bifurcations is the branching of the trachea in the respiratory system into smaller tracheoles within the mammalian lungs. In the branching of a tracheole, SHH acts as a negative feedback signal to turn off *Fgf-10* expression in a central region of the trachea mesenchyme. This forms a gap in the center of the mesenchyme and results in two new branches arising from the single trachea (Pepicelli *et al.,* 1998).

The regulators of branching in these two systems vary and the bifurcations arise through different mechanism; however, they both result in a branched structure. This is an excellent example of the diversity of molecular regulators and their varied roles in patterning.

The study of segmentation and bifurcation patterning processes have been described in a variety organs and species independently, as illustrated by the examples above, mostly independently of growth processes. However, segmentation and bifurcation processes occur concurrently to growth. The caudal fin bony skeleton of the zebrafish not only grows indeterminately, but also forms segments and bifurcations continuously. The zebrafish caudal fin therefore provides a convenient system to study the processes of both segmentation and bifurcation patterning in the context of a growing tissue.

1.4. Zebrafish as a Model Organism

The caudal fin of the zebrafish (*Danio rerio*) has recently emerged as a model system to study bone patterning and appendage growth (Akimenko *et al.,* 2003, Iovine 2007). The zebrafish has the ability to regenerate its fins, which provides many opportunities to study the process of bone growth and patterning at a more rapid pace, since it is proposed that regeneration recapitulates ontogeny (Nabrit 1929, Poss *et al.,* 2003, Schebesta *et al.,* 2006, Iovine 2007). In addition, the zebrafish is amenable to genetic studies and large genetic screens, which can identify mutations in fin and bone

development (Haffter *et al.*, 1996, van Eeden *et al.*, 1996). The zebrafish is inexpensive to rear in large quantities, therefore making it an attractive system to study.

Candidate genes involved in dermal bone morphogenesis in fish fins (Akimenko and Ekker 1995, Borday *et al.*, 2001, Quint *et al.*, 2002, Iovine *et al.*, 2005, Sims *et al.*, 2009, Schulte *et al.*, 2011) have been shown to play roles in bone development in other species (Laforest *et al.*, 1998, Ingham and McMahon 2001, Iovine 2007). In addition, many of the genes involved in ontogenetic development in the caudal fin are also involved in regeneration (Laforest *et al.*, 1998, Iovine 2007). This is important in support of the statement that regeneration recapitulates ontogeny and in validating the use of regenerative studies for studying ontogenetic growth. However, unlike original development, gene expression levels in regeneration are usually higher, which could correlate with the more rapid pace of regeneration (Iovine 2007).

1.5. General Caudal Fin Structure and Terminology

Zebrafish possess paired pectoral and pelvic fins, and unpaired dorsal, caudal, and anal fins. Similar to other teleost fish, the fins are made up of a visible exoskeleton of dermal origin that is attached to an internal endoskeleton (Akimenko *et al.*, 2003). The zebrafish caudal fin is composed of approximately 16 - 18 bony rays (lepoditrichia), connected to one another by interray tissue (Figure 1.2B). At the distal tip of each ray are rod-like fibres, called actinotrichia. Each ray is composed of two concave structures called hemisegments (Figure 1.2C insert), which are connected to one another along the length of the ray by joints. Towards the distal end of all rays except the outer most dorsal and ventral rays, one or more bifurcations can occur (Figure 1.2C) (Haas 1962, Becerra *et al.*, 1983).

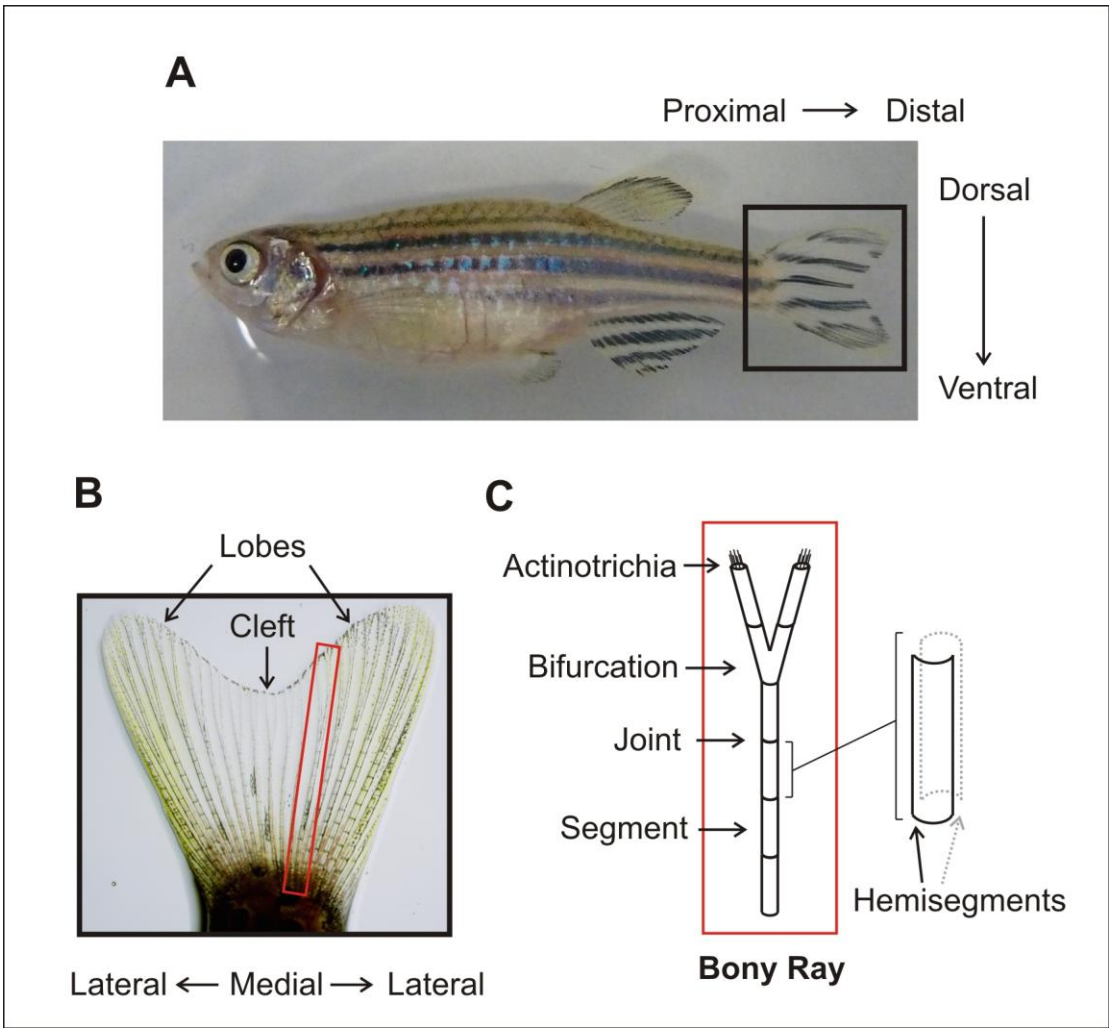

Figure 1.2 Zebrafish caudal fin structure and terminology **A:** Image of a zebrafish, and some axial terminology (surrounding image) for the caudal fin (black box). **B:** Larger image of a zebrafish caudal fin, highlighting various regions of the fin, a bony ray (red box), as well as other axis terminology. **C:** Schematic of a caudal fin bony ray, illustrating the segments, joints, bifurcations, and actinotrichia, including a finer view of the structure of a segment, including the two concave hemisegments (inset).

1.6. Growth in the Fin

1.6.1. Fin Development

Growth of the bony rays occurs in the distal margin of the fin (Haas H.J 1962, Iovine and Johnson 2000). Similar to other teleosts, the zebrafish displays indeterminate growth that slows with age (Iovine and Johnson 2000). During the juvenile stages of development, growth of the fin is allometric, or not in proportion, to body growth (Goldsmith *et al.,* 2006), but as the fish matures, this growth changes to be isometric, or in proportion, to body growth (Goldsmith *et al.,* 2003). The bi-lobed shape of the caudal fin can be attributed to variations in the growth rates between rays (Goldsmith *et al.,* 2003; Goldsmith *et al.,* 2006; Rolland-Lagan *et al.,* 2012). Studies have shown growth occurs by multiple bursts of cell proliferation (Goldsmith *et al.,* 2006), where the number of bursts of cell proliferation (Jain *et al.,* 2007) and the number of cells proliferating are higher in the lobe rays than the cleft rays (Goldsmith *et al.,* 2003). This difference in proliferation can be the cause of the differences seen in growth rates between lobe and cleft rays.

A recent paper published by Rolland-Lagan *et al.* (2012) presented the first model of fin ray growth control. The model hypothesizes the interaction of two morphogens, *G* and *X*, between compartments (representing cells or groups of cells) to control ray growth. The model proposes that *G* is involved in ray growth and is produced in a distal compartment in a growing ray. The level of *G* in the distal compartment determines the ray's growth rate. It has been shown that growth in the zebrafish fish slows with age (Iovine and Johnson 2000); therefore, to recreate this in the model, the production of *G* decreases over time. In addition, since growth only occurs in the distal part of the fin (Haas 1962), the diffusion constant of *G* is low, to restrict its presence to the distal region. The second morphogen, *X*, is proposed to be produced at the base of the ray, and it activates *G* production. *X* production increases with time, and it has a high diffusion constant to ensure it reaches the distal compartment of the ray to promote *G* production (Rolland-Lagan *et al.,* 2012). An example of the levels of the morphogens *G* and *X* at multiple time points in the model are shown in Figure 1.3, and below each graph a visualization of the ray is provided.

An early stage of development is shown in Figure 1.3A. The level of X in the distal compartment is high since the compartment is close to the base of the ray. This higher level of *X* promotes a greater level of *G* in the distal compartment, resulting in the rapid rate of juvenile ray growth. An adult fin is represented in Figure 1.3B, where the level of *X* is higher at the base of the fin than development, but because of the greater distance between the base of the fin and the distal compartment, the level of *X* in the distal compartment is low. This promotes a lower level of *G* and slower growth. The final panel, Figure 1.3C, shows the amputation of the fin ray, which will be discussed in a later section.

Rolland-Lagan *et al.* (2012) proposed possible candidates for the morphogens they presented in the model. This may provide key insight into the molecular regulators of growth.

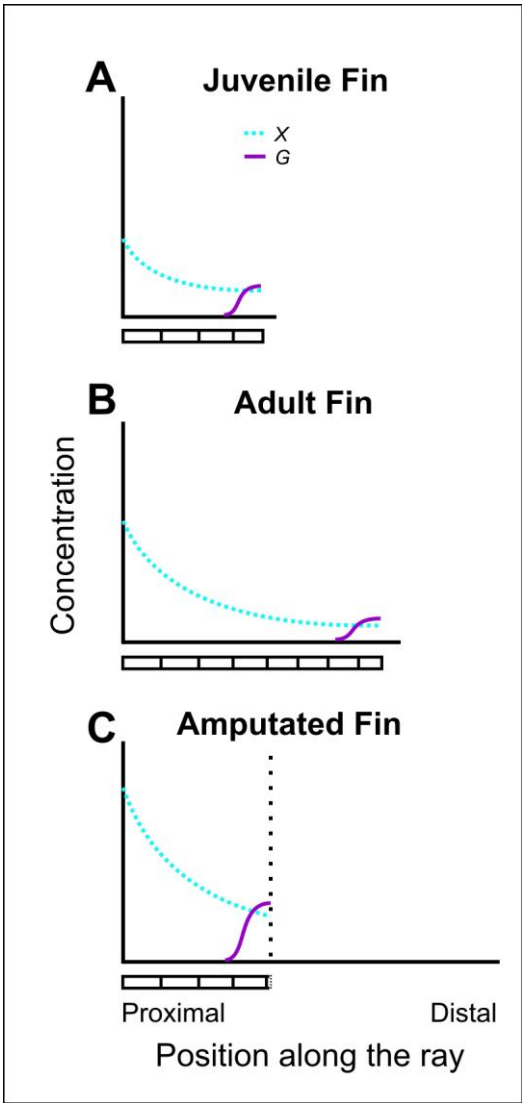

Figure 1.3. Schematics of the cellular model created by Rolland-Lagan *et al.* (2012). **A:** a juvenile fin showing the concentrations of X in cyan and G in purple. **B:** an adult fin, with corresponding levels of X and G. **C:** the adult fin at a later stage, after an amputation has been performed (amputation plane shown by the dotted line). Below each panel is a representation of the ray at each time point in the model.

1.6.2. Molecular Regulator of Growth

In the simulation model of ray growth presented by Rolland-Lagan *et al.* (2012), the morphogen *G* is postulated to represent a *fibroblast growth factor*. Fgfs have been shown to be involved in both patterning and growth (Schwank and Basler, 2010), including the initial formation of the limb bud in the chick embryo (reviewed in Wolpert 2002). In zebrafish, this family of factors has been shown to be involved in fin bud outgrowth, supporting its postulated inclusion in the model. A zebrafish mutant that does not develop pectoral fin buds completely lacks *fgf10* expression in early development. *fgf16,* which is induced by Fgf10, is involved in mediating the interactions of the apical ectodermal ridge and zone of polarizing activity in the developing pectoral fin bud, which is important in fin bud outgrowth (Nomura *et al.,* 2006). These studies highlight the importance of Fgfs in the initiation and development of the fin, supporting their role as regulators of growth.

Past initial fin development, Fgfs also play a role in homeostatic fin regeneration. Homeostatic regeneration is the day-to-day repair and maintenance of the fin tissue due to damage from regular use. Zebrafish fins showed distal fin loss in the absence of Fgf receptors, which would cause an inhibition of Fgf signalling, (Wills *et al.,* 2008). This provided evidence of the role of Fgfs in growth beyond initial fin bud development and growth; however, it is still unclear what role Fgfs play during juvenile development.

The majority of research conducted into the role of Fgfs during ontogenetic fin growth has been conducted in regenerating fins. This is due to the ease with which developmental processes can be studied during regeneration. We will discuss the role of this molecular regulator during regeneration in more detail in section 1.6.4 – Molecular Regulator of Regeneration.

1.6.3. Fin Regeneration

Zebrafish possess the ability to regenerate all of their fins, and regeneration has been proposed to follow a similar process to ontogenetic growth (Iovine 2007). Regeneration of the caudal fin after amputation occurs in three stages: wound healing, blastema formation and regenerative outgrowth. Wound healing involves the covering of

the wound by a thin layer of epithelial cells, called the wound epidermis, within 12 hours of amputation. Subsequently, mesenchymal cells of the connective tissue proximal to the amputation plane disorganize, dedifferentiate, and migrate up under the wound epidermis to form the blastema. Regenerative outgrowth occurs at around 4 days post amputation (dpa), and involves the differentiation of the blastema cells into the different tissues (Gross and Stagg 1959, Santamaria and Becerra 1991, Johnson and Weston 1995, Becerra *et al.*, 1996, Poss *et al.*, 2000, reviewed in Tal *et al.*, 2010). Gene expression patterns during ontogenetic and regenerative growth are often similar – although regenerative expression levels are higher (Iovine M.K. 2007). This could be important in the more rapid pace of regeneration compared to ontogeny.

The length of time for complete regeneration in teleosts is uncertain and varies by fish and fish species. Some studies state that in as few as 1 – 3 weeks, considerable to complete fin regeneration in teleosts can occur (Goss and Stagg 1957, Becerra *et al.*, 1996, Poss *et al.*, 2000). Conversely, other studies state that complete regeneration can take anywhere from 25 – 73 days (Tassava and Goss 1966, Géraudie *et al.*, 1995, Johnson and Weston 1995). Within the laboratory, experiments show that, depending on the level of amputation, average regenerate lengths attain pre-amputation length in 28 or 38 dpa for zebrafish (distal amputation versus proximal amputation, respectively) (n = 17, water temperature = 28.5ºC). However, it should be noted that those are averaged regenerate lengths, and the amount of time for all fins to attain pre-amputation length was greater than the 28 and 38 dpa, respectively (Rolland-Lagan *et al.*, 2012).

The rate of regeneration is highly variable and depends on the experimental conditions. This makes it difficult to determine exact timing for complete fin regeneration. Some factors that affect the rate of regeneration are the age of the fish (Broussonet 1786, Scott 1907), ambient water temperature (Johnson and Weston 1995), and the level of amputation (Morgan T.H. 1902, Tassava and Goss 1966, Lee *et al.*, 2005).

The impact of age on the rate of regeneration has not been well documented in recent years; however, early experiments in teleost fin regeneration state a more rapid rate of regeneration in juvenile fish (Broussonet 1786, Scott 1907). This could be because non-

amputated fin growth slows with age (Scott 1907, Iovine and Johnson 2000); therefore, an older fish grows slower and thus regenerates slower as well. Another cause of variability in regeneration is the effect of water temperature. A study showed that at a water temperature of 25 ºC, it takes approximately 12 days for a fin to reach 50% regeneration. However, if the temperature is increased to 33 ºC, the rate of regeneration doubles, such that 50% of regeneration occurs in 6 days (Johnson and Weston 1995). Therefore, the length of regeneration depends on the water temperature. The level of the amputation along the length of the fin also plays a key role in determining the rate of regeneration. It was noted in the killifish (*Fundulus*) that when the tail is cut obliquely, the more proximal region of the fin regenerates faster. This was thought to be because more tissue needs to be replaced in the proximal region of the fin versus the distal region (Morgan T.H. 1902). A more recent study showed that when a single fin is amputated at two different planes (in a stepwise manner), the regenerative growth rate is greater in the part of the fin that was cut more proximally (Akimenko et al. 1995, Lee *et al.,* 2005). Interestingly, in a similar regeneration study in *Trichogaster sp*. pelvic fins, proximal regenerates took longer to attain pre-amputation length than distal regenerates, although they had faster regeneration rates (Tassava and Goss 1966). This was also seen in the model presented by Rolland-Lagan *et al.* (2012). This indicates there is no set time in which regeneration occurs.

1.6.4. Molecular Regulator of Regeneration

This difference in regeneration rates between proximal and distal amputations can be attributed to the amount of fibroblast growth factor signalling in the caudal fin (Lee *et al.,* 2005). Initially, Fgfs were shown to be required for regeneration, specifically in blastema formation and maintenance, as well as regenerate outgrowth (Poss *et al.,* 2000), but their role was further elucidated by Lee *et al.* (2005). Fgfs were identified as part of the mechanism for assigning position-dependent properties of the blastema during regeneration. Both the level and the size of Fgf transcriptional target domains of expression (which can be used as a measure of Fgf signalling) were greater in amputations that were more proximal, indicating faster regeneration occurs with greater Fgf signalling. Further, a transgenic zebrafish line, which possesses heat-inducible Fgf inhibition, was used to test the effect of graded Fgf-signalling, mimicking the signalling of different levels of

amputation, on regeneration. The same results were achieved; the lowest levels of Fgf inhibition (representing high levels of Fgf signalling or a proximal amputation) showed the highest rates of regeneration. This suggests a molecular mechanism for the variation in regenerative rates between proximal and distal amputations (Lee *et al.*, 2005).

The simulation model of ray growth created by Rolland-Lagan *et al.* (2012) can also accurately model fin regeneration. It recreates the appropriate variation in regeneration rates described in the literature, including the more rapid rate than ontogeny and the variation in regeneration rate depending on amputation level. The model is set up such that when the fin is amputated, the new distal-most compartment located at the amputation plane has the ability to produce *G* in response to *X* (this mimics the formation of the blastema). The key component of the model that allows the appropriate regeneration of the fin is the increase in *X* production over time. At the level of the amputation plane, the concentration of *X* is greater than it would be at that level during ontogenetic growth (Figure 1.3C). This higher level of *X* promotes greater production of *G* in the amputation compartment and results in more rapid regeneration. Similarly, depending on the position of the amputation plane, the concentration of *X* varies depending on the distance from the base of the ray, therefore accounting for the variation in regeneration rates at different amputation planes.

The final morphology of the zebrafish caudal fin is in part due to this molecular regulator of growth, Fgf, but also is in part due to the patterning of the bony rays. Bony ray patterning is also controlled by a variety of genes; however, the mechanisms of their action are less understood.

1.7. Bone Patterning in the Fin

Visible patterns in the caudal fin can be broken down into the patterning of the joints and the patterning of the bifurcations within the bony rays. The patterning of these two features follows predictable spatial patterns within and between rays.

1.7.1. Patterning of Joints

Segments are the result of joints forming in the distal bone during bone morphogenesis (Haas 1962), and their length is determined by the amount of bone deposited in the interval between successive joint formation events. Segments located in the proximal region of a ray are longer than segments located in the distal part. Similarly, segments located in the lobe rays are longer than segments located in the cleft rays (Haas 1962; Iovine and Johnson 2000, Rolland-Lagan *et al.*, 2012). Finally, lobe rays are comprised of a higher number of segments than the cleft rays (Goldsmith *et al.*, 2006).

1.7.2. Molecular Regulators of Joint Patterning

Since a ray's length is dependent on the length and number of segments within it, researchers began studying zebrafish mutants with altered fin lengths to elucidate the mechanisms behind growth control in the fin (Iovine and Johnson 2000). In the processes, they identified various candidate genes involved in the regulation of joint formation and patterning. Some of the most well known ray length mutants include the *short fin* mutant (*sof*) (Johnson and Bennett, 1999, Iovine and Johnson 2000), the *long fin* mutant (*lof*) (Johnson and Weston 1995, van Eeden *et al.*, 1996, Iovine and Johnson 2000) and the *another long fin* mutant (*alf*) (van Eeden, *et al.*, 1996). The *sof* mutant possesses fins that are approximately half the size of wild type fins (Johnson and Bennett 1999), and contain fewer, shorter segments, which could be a result of their slower growth rate (Iovine and Johnson 2000). Conversely, the *lof* mutant displays longer fins than wild type, which could result from their fins continuing to grow at the rapid rate associated with juvenile development (Johnson and Weston 1995). In addition to this more rapid rate of growth, the *lof* rays also contain more segments than wild type; however, *lof* segments are

approximately the same length as wild type (Iovine and Johnson 2000). Finally, the heterozygous *alf* mutant phenotype is similar to the *lof* mutant, in that it possesses longer fins than wild type (Sims *et al.,* 2009), indicating faster growth rates; however, the rays contain segments of varied lengths, which are longer than the wild type (van Eeden *et al.,* 1996). Through molecular research into these fin length mutants, a few of the genes implicated in joint patterning have been identified.

Genetic analyses point to the protein connexin43 (Cx43) as playing a role in bone morphology. The protein was discovered by studying the *sof* mutant, whose phenotype is a result of a mutation in the *connexin* gene (Iovine *et al.,* 2005). Connexins are the subunits of gap junctions, which are responsible for communication between adjacent cells. What links this gene to the mutant phenotype is a reduced, although not absent, expression of *cx43*. In addition, during ontogenetic growth in wild type fins, *cx43* is expressed in three areas: a crescent-shaped domain at the distal end of each ray, proximal regions flanking the bone segments, and finally surrounding the newest joints. The authors concluded that *cx43* could act as a mechanism of measuring segment length, to determine segment size, and thus the placement of joints.

Further support for the role of *cx43* in regulating segment length came from an analysis of the *alf* mutant. Converse to the *sof* mutant, *alf* exhibits increased *cx43* expression. *cx43* gene knockdowns in *alf* show regular joint spacing, as opposed to their previously greater spacing, further suggesting an association between *cx43* and joint location in determining segment length (Sims *et al.*, 2009). From these mutants (*sof* and *alf*) we can assume the processes of joint formation and growth can be linked (Rolland-Lagan *et al.,* 2012), since their segment length is proportionate to the decrease or increase in fin length (*sof* and *alf*, respectively).

Although genetic analyses have not yet been performed to determine the cause of the *lof* phenotype, it possesses a morphology that sets it apart from the *sof* and *alf* mutants. Specifically, since the phenotype includes longer than wild type fins due to allometric growth, given what is known about the other two mutants, it could be assumed that the phenotype would include increased segment numbers and increased segment lengths. While

the mutant fin rays do contain more segments than wild type, the bony rays segments are of a similar size to wild type (Iovine and Johnson 2000). Since the segments are of a similar size to wild type with the increased growth rate, this implies that the mutant could be forming joints more rapidly, in addition to having an altered growth rate (Iovine and Johnson 2000).

Rolland-Lagan *et al*. (2012) built on their model of ray growth control by incorporating a mechanism of joint formation. They propose a third morphogen called *S,* in addition to *G* and *X,* which inhibits joint formation. When the levels of *S* and *G* fall below a threshold, joint formation is no longer inhibited and a joint forms. This creates a new source of *S* at the joint, ensuring other joints cannot be formed in the immediate vicinity. *S* is produced in response to *X*; therefore, the higher the level of *X*, the greater *S* production, and the further apart joints are formed. At the base of the fin, where *X* is produced, the concentration of *S* is high. The model does propose a mechanism by which the *lof* phenotype can arise. By increasing the transport rate of *X*, which influences the amount of *G* production (and thus the rate of growth), the mutant model rays grow longer than the wild type models rays, but show normal segment lengths typical of the *lof* mutant. Similarly, the model was also able to account for the *sof* phenotype of shorter fin length and segments, by decreasing the rate of *X* production. Therefore, because of *X*'s involvement in both growth and joint patterning in the model, they propose that this supports the coupling of the processes of growth and joint patterning. However, the phenotype can also be a result of an uncoupling of growth and segmentation, since fin length and segment length are not in proportion (Rolland-Lagan *et al.,* 2012). Genetic research into the mutant is needed to determine the genes and mechanism involved in this mutation.

Another gene implicated in joint formation is *evx1*. *evx1* belongs to the *even-skipped*-related gene family, which is a group of homeobox genes that play a role in segmentation by identifying segment borders (Macdonald *et al.,* 1986, reviewed in Wolpert 2002). The link between *evx1* and joint formation was discovered by Borday *et al.* (2001). They showed that *evx1* is expressed distal to each growing ray, where there is a crescent-shaped domain of expression, which varies in the level of expression preceding joint formation. More importantly, it is also expressed in a ladder-like fashion along the bony

rays, with each rung corresponding to the location of a joint. Further evidence for the role of *evx1* in joint formation comes from *evx1* homozygous mutants, which lack evx1 function. The mutants exhibit normal caudal fin length, implying *evx1* is not involved in ray growth; however, their fin rays completely lack joints (Schulte *et al.*, 2011), providing support for the role of *evx1* in identification of segment boundaries. However, because the fin lengths in these mutants are similar to wild type, this implies that segment formation does not affect growth.

Converse to the *sof* and *alf* mutants, and to some extent the *lof* mutant, which imply that the mechanism responsible for ray growth can affect joint patterning (Rolland-Lagan *et al.*, 2012), the *evx1* mutant indicates an uncoupling of these processes. Therefore, it is likely the mechanism responsible for joint patterning is a combination of many pathways, some of which are linked to growth and others that are not.

1.7.3. Patterning of Bifurcations

Rays bifurcate dichotomously as they grow. Bifurcations can occur multiple times within a single ray, except in the most dorsal and ventral rays which never bifurcate (Figure 1.4A) (Haas 1962, Becerra *et al.*, 1983). The spatial and temporal sequence of bifurcation events in the fin has recently been described (Rolland-Lagan *et al.*, in prep). In particular, bifurcations first appear in the lateral-most bifurcating rays and then proceed towards the medial rays. In addition, the positions of the bifurcation points follow a bi-lobed curve (Figure 1.4A). Rolland-Lagan *et al.* (in prep.) propose a nomenclature to label different sections of the fin rays, depending on their position relative to ray bifurcations, and we use this terminology in this thesis. The ray sections prior to the first bifurcation are identified as S1 ray sections; the sections between the first and second bifurcations are called S2 ray sections; the sections between the second and third bifurcations are called S3 ray sections, and so on. This is illustrated in Figure 1.4B

It is believed that the presence of interray tissue on either side of a ray influences bifurcation, because in the absence of interray tissue on both sides a ray does not bifurcate (Mari-Beffa *et al.*, 1996, Murciano *et al.*, 2002). This explains why the outermost rays in

the caudal fin, which only have interray tissue on one side, do not bifurcate. Conversely, on occasion, these normally non-bifurcating rays can be induced to form bifurcations if they are grafted into an inner ray's position (Murciano *et al.,* 2002). This supports the conclusion that interray tissue induces bifurcation, but it also implies that each ray has the potential to bifurcate if conditions are suitable.

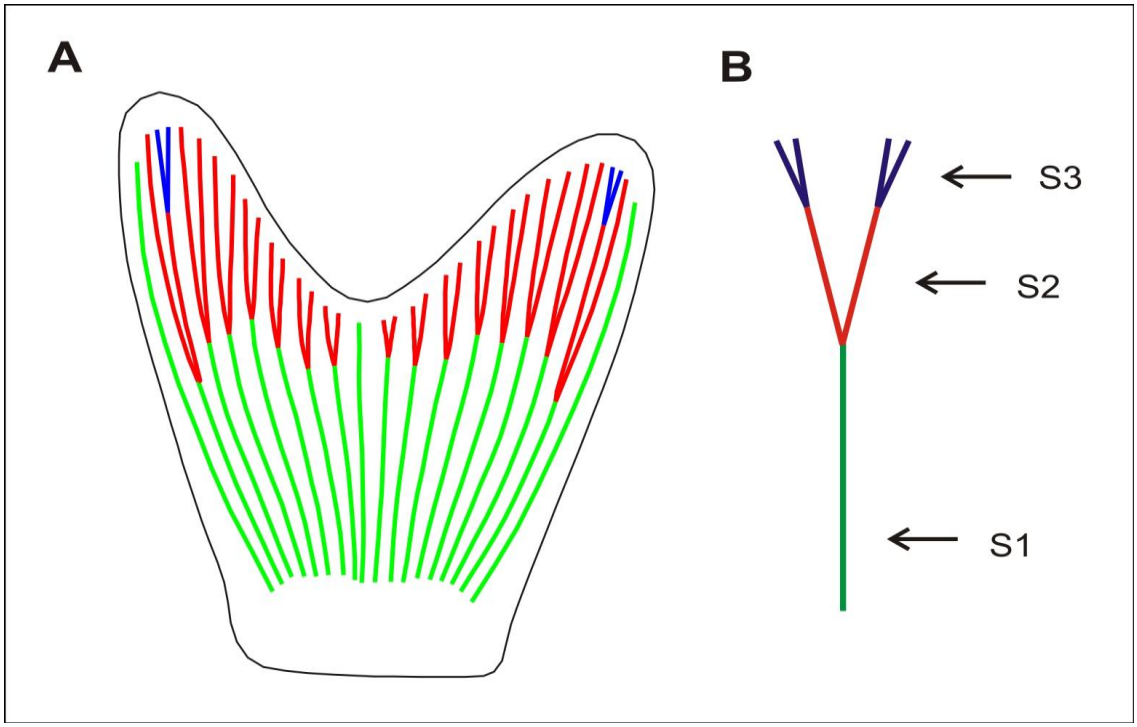

Figure 1.4. Schematic of zebrafish caudal fin ray bifurcations and ray section terminology. **A:** Schematic of a zebrafish caudal fin, showing 18 bony rays and the spatial distribution of bifurcations. **B:** individual bony ray, highlighting the terminology of each ray section. Ray sections are coloured such that S1 is green, S2 is red, and S3 is blue. Image courtesy of Rolland-Lagan *et al.* (in prep).

1.7.4. Molecular Regulators of Bifurcation

Although the presence of interray tissue in inducing bifurcations has been proposed, the molecular pathways responsible for the formation of bifurcations are not well characterized. A few genes have been identified that could be involved, and they are involved in the Sonic hedgehog (Shh) signalling pathway, including *shh*, its receptor *patched-1* (*ptc1*) and a downstream target of Shh, *bone morphogenetic protein 2b* (*bmp2b*).

Shh is a signalling molecule involved in the patterning and development of many different tissues and structures in a wide range of species. Some of these include regulating the ventral polarity of the neural tube in the frog, branching of the lungs in the mouse and limb patterning in the chick (reviewed in Ingham and McMahon 2001). Most of the work on Shh in zebrafish bone patterning has been through regeneration studies; however, s*hh* is also expressed during the ontogenetic growth of the paired fin rays (Akimenko and Ekker 1995, Laforest *et al.*, 1998).

Studies have shown that during the regeneration of the caudal fin a domain of *shh* expression exists distal to each of the regenerating rays that normally bifurcate. Preceding bifurcation of the ray itself, each domain splits in two, implicating *shh* in bone patterning (Laforest *et al.,* 1998, Akimenko *et al.*, 2003). The lateral most rays, which normally do not bifurcate, only display one *shh* domain of expression throughout regeneration. Ectopic expression of *shh* in the gap between branches of regenerating bifurcations can cause the fusion of the two branches, further supported the link between *shh* and bone morphogenesis and patterning (Laforest *et al.,* 1998, Quint *et al.,* 2002).

To examine if other members of the *shh* signalling pathway are involved in bone formation or patterning, expression of *ptc1* and *bmp* were observed during regeneration. Both of these genes are re-induced in the regenerating fin in a coordinated fashion with *shh* (Laforest *et al.,* 1998). In addition, ectopic expression of *bmp2b* alone has the ability to fuse rays (Quint *et al.,* 2002). Therefore, it could simply be the downstream target of shh which affect bone morphogenesis.

The presence of interray tissue around a ray, in addition to the presence of *shh* and other members of its signalling pathway, appear to be required for bifurcation. It is interesting that before any signs of bifurcation, all rays possess one domain of *shh* expression. Yet, prior to ray bifurcation, all the inner rays develop a second *shh* expression domain. Perhaps the interray tissue facilitates the transport of a molecule between rays, inducing the *shh* domain to split. Since the lateral most rays only have one neighbour, their domains are never signalled to split. However, what would trigger the *shh* domains to split is unknown.

Chapter 2 – Proposed Research

2.1 Systems Biology Approach

The quantity and quality of molecular information on fin development, regeneration, and patterning at the molecular level are increasing rapidly. However, this molecular information on its own does not provide sufficient insight into the mechanisms responsible for the formation of patterns within the fin. Theoretical models are useful in hypothesizing developmental mechanisms, based on the experimental data collected (Kholodenko *et al.*, 2005).

Systems biology utilizes literature and experimental data to theorize a model of the system of interest. Then, through comparison of the model to experimental data, the model can either be falsified or validated. This is an iterative process, which involves adjusting the theoretical model based on new experimental data collected. The drawback to using this approach is that the model will only be as good as the experimental data and the current literature available on the subject (Kholodenko *et al.*, 2005). However, a model that closely recreates the trends in the literature and experimental data can be further tested by altering model parameters and predicting the outcome of future experiments. Therefore, the power of a model lies in its predictive ability (Kholodenko *et al.*, 2005).

2.2 Objectives

We propose to study the mechanisms of joint and bifurcation pattern formation in zebrafish caudal fins using a systems biology approach. Rolland-Lagan *et al.* (2012) have already proposed a model of ray growth and regeneration; therefore, we do not focus on the control of ray growth in the model. In addition, a mechanism of joint formation has been proposed; however, none has been proposed for bifurcation.

With the emergence of quantitative data on fin patterning collected by Rolland-Lagan *et al.*, (*in prep*), in addition to the existing literature on the molecular aspects of fin patterning, we can study bony ray segmentation and bifurcation patterning using a systems biology approach. The objective of this thesis is to create a basic model with a set of rules

for how joints and bifurcation occur in one fin type in one species of fish, and from this we can attempt to predict the patterning of joint and bifurcations in different fin types and in different fish species.

Chapter 3 – Methods

3.1 Modelling Ray Growth

The purpose of the simulation model is to generate patterns of joint and bifurcation formation based on a set of developmental rules corresponding to postulated developmental mechanisms. Resulting simulated ray joint and bifurcation patterns can then be compared to experimental data. Fin rays grow at the same time as joints and bifurcations are formed; therefore, the model has to incorporate growth. However, the purpose of the model is not to uncover the developmental mechanisms underlying growth. Rather, it aims to identify developmental mechanisms for joint and bifurcation formation in growing fins. Therefore, we first create a model of ray growth such that rays grow at a rate that matches experimental data. With this ray growth model, we then incorporate postulated mechanisms to simulate joint and bifurcation formation.

The ray growth model is set up to recreate a caudal fish fin containing 18 bony rays. The model fin is oriented such that the proximal region of the fin is at the bottom of the figure output, the distal region is at the top, and on the left and right sides are the dorsal and ventral regions, respectively. We number the rays starting at -9 for the dorsal-most ray and proceeding to 9 for the ventral-most ray, skipping 0 in the center (Figure 3.1A). As segments form within the model, we assign each a unique segment number for the purposes of identification. The first segments in all rays appear simultaneously; therefore, the segment in the leftmost ray is numbered 1 and the segments in the remaining rays are numbered sequentially to the right. We continue to assign the following segment numbers to segments in order of appearance, regardless of their position in the fin.

The model of ray growth is set up as a particle model based on *shh* expression, due to its close association with bone patterning and morphogenesis (Laforest *et al.,* 1998, Akimenko and Ekker 1995, Quint *et al.,* 2002, Akimenko *et al.,* 2003). Particle models are well suited for describing patterning processes and have been previously used to describe venation patterns in leaves and angiogenesis in tumour progression (Runions *et al.,* 2005, Rafal and Witold 2008). In the model there are two sets of points, “source points” and

"bone points." The source points represent *shh* expression domains, localized at the distal tip of the fin rays, and are where growth occurs. The bone points represent newly differentiated osteoblasts which will form the rays. These bone points are localized proximal to each source point. This particle arrangement is shown in Figure 3.1B. As source points move distally, representing fin outgrowth, the bone points match the movement, representing differentiation of the bony cells, which causes bone formation. Each source point-bone point pair is responsible for the formation of an individual ray.

The time at which ray bone differentiation begins and when the first segments appear is not well documented; however, one study indicates the ray structures only begin forming approximately 4 weeks after fertilization (Laforest *et al.*, 1998). Within the model, we are modelling ray development; therefore, the model must represent a fin older than 0 dpf (days post fertilization). To determine what day the beginning of the model should represent we use unpublished ray 7 length data on fish aged 28 to 170 dpf (n = 18) which was collected outside of my Master's. We fit an inverse function (of the form $y = a + \frac{b}{x}$) to the plotted ray lengths over time and extrapolate backwards to determine where the function crosses the *x*-axis, which corresponds to 26.12 dpf (for more information, see Appendix 8.2 – Determining Growth and Regeneration). From this extrapolation, we assume the average bony rays first appear at 26.12 dpf. Images of fins taken between 22 and 28 dpf previously collected support this 26.12 dpf starting day, since some fins show visible bony rays and segments, and some do not (unpublished results). Therefore, the start of the model represents a fish fin at 26.12 dpf.

For more detailed information on the model, see Appendix 8.4 – Model.

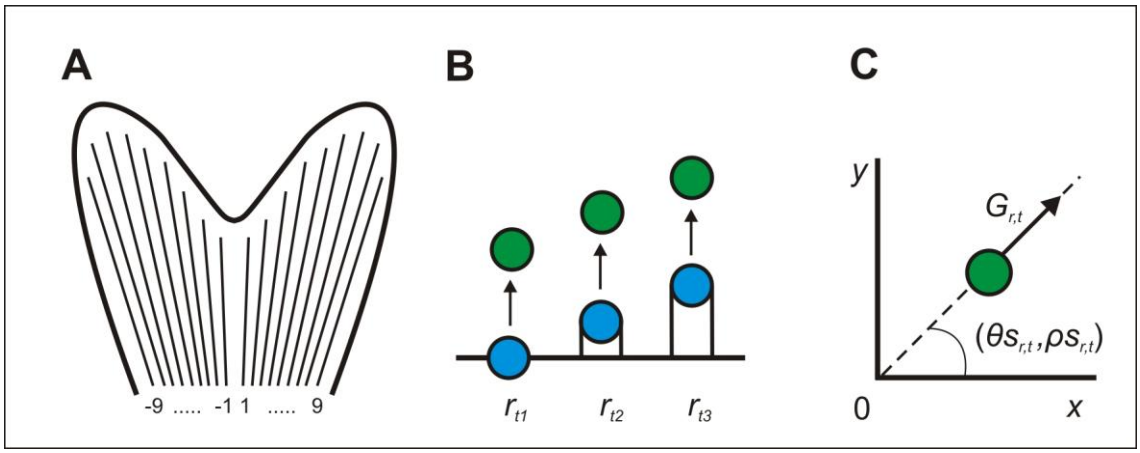

Figure 3.1. Ray numbering, set up and growth in the ray growth model. **A:** schematic of ray number assignment; ray numbers are assigned depending on the ray's position along the medio-lateral axis. **B:** the association between source (green) and bone (blue) points and the formation of a bony ray (vertical black lines) at three time intervals (t1, t2, t3). Arrows represent bone point movement to match source point growth. **C:** the position ($\theta s_{r,0}$ and $\rho s_{r,0}$) and movement of source points ($G_{r,t}$) in the polar coordinates system.

The shape of the caudal fin can be approximated to that of a triangle, with the vertex located proximally and the base distally. The zebrafish caudal fin is relatively flat and therefore can be visualized in a two dimensional plane. Because of this, we believe there is an underlying coordinate system upon which we can explain fin growth. We consider two coordinate systems to model ray growth, the polar and Cartesian coordinate systems.

In the polar coordinates system, every point in the system is defined as a function of the origin. Specifically, every point is described as being at an angle θ to the origin and a certain distance ρ away from it. Modelling ray growth in this system is achieved by changing the value of ρ over time; and the angle θ of growth will spread the rays, creating the triangular fin shape.

In the Cartesian coordinate system, to create this triangular shape, growth needs to occur along both the *x*- and *y*- axes. This complicates the model since growth rates need to be assigned to both axes. The quantitative experimental data we possess on ray growth is on the change in ray length over time, and does not contain any coordinate information. Therefore, it would be difficult to calculate the movement along *x* and *y* axes from this data for use in the Cartesian coordinate system. For this reasons, we choose to model ray growth in the polar coordinate system.

The point of origin is (0, 0) and the source and bone points are assigned starting angles and positions at an appropriate distance from the origin. The starting positions ($\rho s_{r,0}$ and $\rho b_{r,0}$, for the source and bone point respectively) and angles ($\theta s_{r,0}$ and $\theta b_{r,0}$ for the source and bone point respectively) are based loosely on experimental data on fin shape (for more information see Appendix 8.1 - Starting Angles and Positions).

We assign different growth rates to each source point to reflect the differences in growth between rays in the literature (Goldsmith *et al.*, 2003; Goldsmith *et al.*, 2006; Jain *et al.*, 2007, Rolland-Lagan *et al.*, 2012). The growth rates are calculated from experimental data collected on fish fin development from a juvenile stage (28 dpf) to adulthood (170 dpf) (n = 18, for more information see Appendix 8.2 - Determining Growth and Regeneration). We calculate a fin growth rate equation based on experimental data. The fin growth rate equation is the following:

$$G_{f,t} = \frac{209.4793690722447}{t^2} \qquad (1)$$

Where $G_{f,t}$ represents the fin growth rate (i.e. derivative of the equation of fin length as a function of time, see Appendix 8.2.1) and t represents the time in days. We then use a constant (which varies for each ray) to scale this fin growth rate (equation 1) to the 18 individual rays, representing individual ray growth ($G_{r,t}$). For more detail on the determination of individual ray growth rates, see Appendix 8.2.1 – Development Data Set. Growth, or the movement of the source and bone points, for each ray in the model is summarized by equation (2).

$$\frac{d\rho s_{r,t}}{dt} = \frac{d\rho b_{r,t}}{dt} = G_{r,t} \qquad (2)$$

Where $\rho s_{r,t}$ represents the source point position for ray r at time t, $\rho b_{r,t}$ the bone point position for ray r at time t, and $G_{r,t}$ the growth rate for ray r at time t. The change in a source point and bone point's position, for a single ray, is equal due to their close association. The movement of a source point is illustrated in Figure 3.1C.

Since we are interested in the patterning of joints and bifurcations, we focus on growth along the proximo-distal axis only. However, growth occurs along the medio-lateral axis as well. Therefore, we incorporate this growth only into the plotting portion of the model, once the simulation has finished. We do this by shifting each point in the fin rays

outward along the *x*-axis by a given distance to recreate a visually similar fin output. This shift in bone point position is shown by the following equation:

$$\rho b_{r,t} = X_r \rho b_{r,t} \qquad (3)$$

Where $\rho b_{r,t}$ the bone point position along the *x*-axis for ray r at time t, and X_r represents the amount of change in point position for ray r. This allows the model to reproduce a fin of similar size and shape to a real fin.

To determine the amount of movement along the medio-lateral axis, we use previously collected unpublished data on ray base positions from fish tracked from a juvenile stage to adulthood (Rolland-Lagan *et al., in prep*). We divide the *x* coordinate (in mm) of the leftmost ray in the adult fish by its initial position (in its juvenile stage) to determine the fold change in position (the change in position was 4-fold). Then we take the base position of the model rays and multiply their *x* coordinate by this fold change, which gives us the amount of growth in *x* for each ray (X_r in equation 3). We then shift all the remaining bone points out by this amount of growth in *x*, spreading the fin along the *x*-axis.

The next step is to incorporate the postulated mechanisms for joint formation and bifurcation formation within growing fins into the model.

3.2 Patterning Mechanism Selection

To select the best mechanisms for joint and bifurcation formation we create multiple versions of the ray growth model, each testing a different mechanism of joint and bifurcation formation. We tested models where joint and/or bifurcation formation occurred at regular time intervals, at set positions from the fin base, and where joint and/or bifurcation formation was controlled by patterning substances. We found the best results with the mechanisms based on the patterning substances; therefore, we present those mechanisms here. For more information on the other mechanisms tested, see Appendix 8.4.1 – Mechanisms Tested.

Initially, we model joint formation independent of bifurcation formation to simplify the model selection process. A set of eight models test possible methods of joint pattern formation (equations 4, 5 and 6) and another set of six models test possible methods of bifurcation formation (equations 9, 10 and 11). We compare each model's output to expected trends in joint and bifurcation patterns to determine which recreates the trends best. Once best models of joint formation and bifurcation formation have been identified, we combine them into one model.

The trends in joint patterning we want to recreate are that segment length decreases along the proximo-distal axis as well as along the medio-lateral axis (Haas 1962; Iovine and Johnson 2000, Rolland-Lagan *et al.*, 2012), and that there are a greater number of segments in the lateral than medial rays (Goldsmith *et al.*, 2006). The patterns we want to recreate in bifurcation patterning are that bifurcations occur first in the lateral bifurcating rays and then proceed inward, and that they have a bi-modal distribution of S1 ray section lengths (Rolland-Lagan *et al., in prep*).

3.2.1 Joint Formation

We postulate that joint formation is based on the production of a substance, which we call "joint forming substance" $J_{r,t}$, to a threshold T_J. When the concentration of $J_{r,t}$ reaches T_J, a joint forms. We hypothesize that $J_{r,t}$ is produced and accumulates in the bone points, since they are responsible for ray formation. This process is illustrated in Figure 3.2A.

The initial concentration of $J_{r,0}$ is zero and it is produced at a rate $A_{r,t}$, as described in equations (4a) and (4b).

$$\frac{dJ_{r,t}}{dt} = A_{r,t} - \delta * J_{r,t} \quad \text{if } J_{r,t} < T_J \qquad (4a)$$

$$J_{r,t} = 0 \quad \text{if } J_{r,t} \geq T_J \qquad (4b)$$

Where $J_{r,t}$ is the concentration of joint forming substance for ray r at time t, $A_{r,t}$ is the rate of $J_{r,t}$ production for ray r at time t. $A_{r,t}$ can either be constant or vary in space and/or time, as is outlined below. δ is the decay rate of the joint forming substance $J_{r,t}$, which is proportional to the concentration, and T_J is the threshold for joint formation. When the concentration of $J_{r,t}$ reaches T_J, a joint forms, the concentration of $J_{r,t}$ returns to zero (equation 3b) and $J_{r,t}$ production begins anew.

We can alter the rate of $J_{r,t}$ production, $A_{r,t}$, in both space and time to test hypothesized methods of $J_{r,t}$ production and accumulation. The variations in $A_{r,t}$ will result in different joint patterns within the fin, which we can then use to select the model that best recreates joint patterns. In space, the rate of $J_{r,t}$ production can be constant between rays; therefore, joints form at the same time in all rays. Otherwise, the rate of $J_{r,t}$ production can vary between rays, resulting in varied joint formation. The following equations outline these possibilities:

$$A_{r,t} = \alpha \qquad (5a)$$

$$\tilde{A}_{r,t} = \tilde{\alpha}_r \qquad (5b)$$

Where $A_{r,t}$ and $\tilde{A}_{r,t}$ are the rates of $J_{r,t}$ production for ray r at time t. Equation 5a represents the model where $A_{r,t}$ is constant over both space and time, and equation 5b represents the model where $A_{r,t}$ varies in space (and is therefore noted $\tilde{A}_{r,t}$) but is constant in time. α is the value assigned to the rate of $J_{r,t}$ production for all rays, and $\tilde{\alpha}_r$ is the value assigned to the rate of $J_{r,t}$ production for ray r.

To alter the rate of $J_{r,t}$ production in time, the values of $A_{r,t}$ and $\tilde{A}_{r,t}$ must change over time. To recreate the decrease in segment length along the proximo-distal axis, the

value of $A_{r,t}$ should decrease. We explore the following methods of altering $A_{r,t}$ in time only:

$$A_{r,t} = mG_{r,t} \qquad (6a)$$

$$A_{r,t} = \frac{h}{(t+t_0)^e} \qquad (6b)$$

$$\frac{dA_{r,t}}{dt} = -c_J A_{r,t} \qquad (6c)$$

Where $A_{r,t}$ is the rate of $J_{r,t}$ production for ray r at time t, m is a constant, $G_{r,t}$ is the growth rate of ray r at time t, h is a constant for all rays, e is a constant, t represents the time in days, t_0 represents the starting day of the model and c_J is a decay constant. The equations are similar to the models where $A_{r,t}$ varies in space as well as time:

$$\tilde{A}_{r,t} = \tilde{m}_r G_{r,t} \qquad (7a)$$

$$\tilde{A}_{r,t} = \frac{\tilde{h}_r}{(t+t_0)^e} \qquad (7b)$$

$$\frac{d\tilde{A}_{r,t}}{dt} = -c_J \tilde{A}_{r,t} \qquad (7c)$$

Where $\tilde{A}_{r,t}$ is the rate of $J_{r,t}$ production for ray r at time t, $\tilde{m}_r$ is the constant for ray r, $\tilde{h}_r$ is a the constant for ray r, e is a constant, t represents the time in days, t_0 represents the starting day of the model, and c_J is the decay constant. In equations 4, 5 and 6 the threshold for joint formation will vary.

The equations we test represent various ways the rate of $J_{r,t}$ production can decrease over time. Since the growth rate is already decreasing, we test the situation where

$\tilde{A}_{r,t}$ varies as a function of the growth rate (equations 6a and 7a). We test a model where the $\tilde{A}_{r,t}$ decreases with an equation (equations 6b and 7b) of the same form as the equation for growth (equation 1); however, the parameter values in the equation are different so that the curves do not overlap. The model proposed by Rolland-Lagan *et al.* (2012), suggests that the rate of growth is controlled by the interaction of two morphogens, and that joint formation is also controlled by the interaction of morphogens. Therefore, since these equations (6b and 7b) have the same form as the equation for growth, this suggests that joint formation could be the result of substance interaction as well. Finally, we test the situation where $\tilde{A}_{r,t}$ decreases proportionally to its level (equations 6c and 7c).

We run each simulation model testing these proposed methods of joint forming substance (equations 5, 6, and 7) and extract data on the number of segments within the ray and the length of the segments. We compare the data collected from each model qualitatively to the expected joint patterns to determine which method of joint forming substance production and accumulation recreates the trends the best.

Table 3.1 Summary of the methods of joint and bifurcation substance accumulation being tested.

Equation	Description
$A_{r,t} = \alpha$ (5a)	Method where the rate of $J_{r,t}$ production ($A_{r,t}$) is constant between rays, and is constant in time.
$\tilde{A}_{r,t} = \tilde{\alpha}_r$ (5b)	Method where the rate of $J_{r,t}$ production ($\tilde{A}_{r,t}$) varies between rays, but is constant in time.
$A_{r,t} = mG_{r,t}$ (6a)	Method where the rate of $J_{r,t}$ production ($A_{r,t}$) varies in time depending on each ray's the growth rate, but is constant between rays.
$\tilde{A}_{r,t} = \tilde{m}_r G_{r,t}$ (7a)	Method where the rate of $J_{r,t}$ production ($\tilde{A}_{r,t}$) varies in time depending on each ray's the growth rate, and varies between rays.
$A_{r,t} = \frac{h}{(t+t_0)^e}$ (6b)	Method where the rate of $J_{r,t}$ production ($A_{r,t}$) varies in time depending on an equation for growth of the form $y = a + \frac{b}{x}$, but is constant between rays.
$\tilde{A}_{r,t} = \frac{\tilde{h}_r}{(t+t_0)^e}$ (7b)	Method where the rate of $J_{r,t}$ production ($\tilde{A}_{r,t}$) varies in time depending on an equation for growth of the form $y = a + \frac{b}{x}$, and varies between rays.
$\frac{dA_{r,t}}{dt} = -c_J A_{r,t}$ (6c)	Method where the rate of $J_{r,t}$ production ($A_{r,t}$) varies in time proportionally to its level, but is constant between rays.
$\frac{d\tilde{A}_{r,t}}{dt} = -c_J \tilde{A}_{r,t}$ (7c)	Method where the rate of $J_{r,t}$ production ($\tilde{A}_{r,t}$) varies in time proportionally to its level, and varies between rays.
$Q_{r,t} = \beta$ (9a)	Method where the rate of $B_{r,t}$ production ($Q_{r,t}$) is constant between rays, and is constant in time.
$\tilde{Q}_{r,t} = \tilde{\beta}_r$ (9b)	Method where the rate of $B_{r,t}$ production ($\tilde{Q}_{r,t}$) varies between rays, but is constant in time.
$Q_{r,t} = pG_{r,t}$ (10a)	Method where the rate of $B_{r,t}$ production ($Q_{r,t}$) varies in time depending on each ray's the growth rate, but is constant between rays.
$\tilde{Q}_{r,t} = \tilde{p}_r G_{r,t}$ (11a)	Method where the rate of $B_{r,t}$ production ($\tilde{Q}_{r,t}$) varies in time depending on each ray's the growth rate, and varies between rays.
$\frac{dQ_{r,t}}{dt} = -c_B Q_{r,t}$ (10b)	Method where the rate of $B_{r,t}$ production ($Q_{r,t}$) varies in time proportionally to its level, but is constant between rays.
$\frac{d\tilde{Q}_{r,t}}{dt} = -c_B \tilde{Q}_{r,t}$ (11b)	Method where the rate of $B_{r,t}$ production ($\tilde{Q}_{r,t}$) varies in time proportionally to its level, and varies between rays.

Where $A_{r,t}$ and $\tilde{A}_{r,t}$ are the rates of $J_{r,t}$ production for all rays, or ray r, respectively, at time t; α and $\tilde{\alpha}_r$ are the values assigned to the rate of $J_{r,t}$ production for all rays, or ray r; m and $\tilde{m}_r$ are the constants for all rays, or ray r; $G_{r,t}$ is the growth rate of ray r at time t; h and $\tilde{h}_r$ are the constants for all rays, or ray r; e is a constant; t represents the time in days; t_0 represents the starting day of the model; and c_J is the decay constant. $Q_{r,t}$ and $\tilde{Q}_{r,t}$ are the rates of $B_{r,t}$ production for all rays, or ray r at time t; β and $\tilde{\beta}_r$ are the values assigned to the rate of $B_{r,t}$ production value for all rays, or ray r; p and $\tilde{p}_r$ are constants for all rays, or ray r; and c_B is a decay constant.

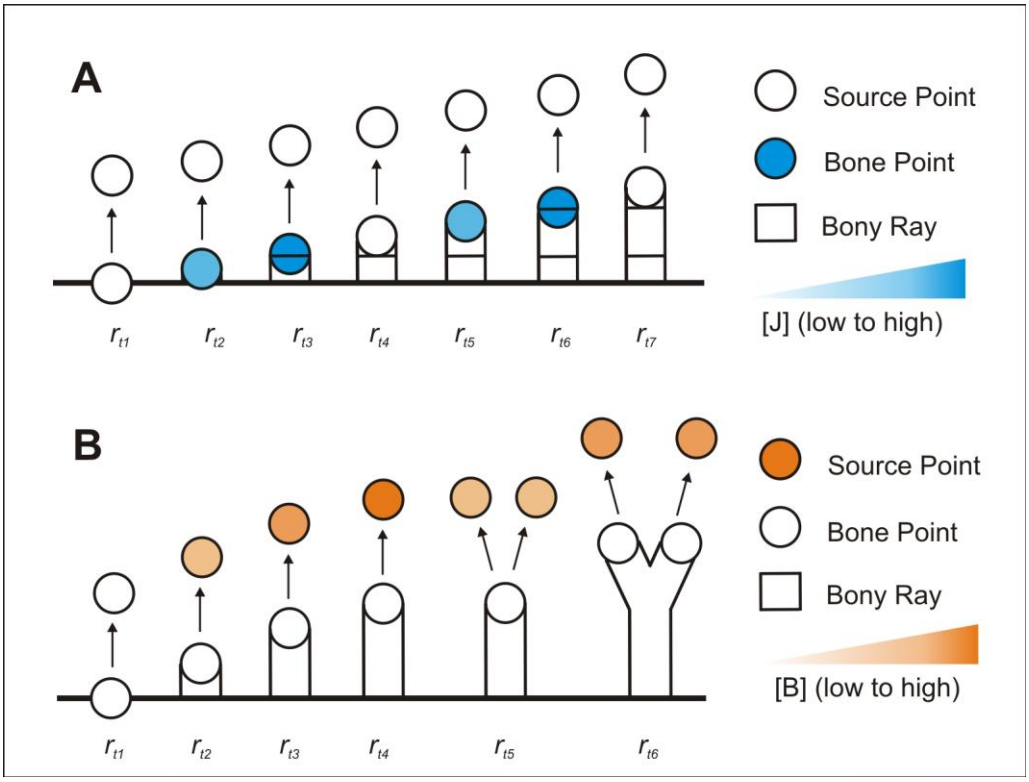

Figure 3.2. Schematic of bifurcation and joint formation in the ray growth model. **A:** joint formation over seven time points (t_1, t_2, t_3, etc.) for one ray (r), showing the production of the joint forming substance (J) in the bone point to threshold (cyan) and the formation of a joint. **B:** bifurcation formation over six time points (t_1, t_2, t_3, etc.) for one ray (r), showing the production of the bifurcation forming substance (B) in the source point to threshold (orange) and the splitting of the source and bone points.

3.2.2 Bifurcation Formation

We are also testing bifurcation formation based on the production of a substance, which we call "bifurcation forming substance" $B_{r,t}$, to a threshold T_B. When the concentration of $B_{r,t}$ reaches T_B, a bifurcation forms. We hypothesize the substance is produced and accumulates in the source points, since they represent *shh* which has been linked to bone deposition and patterning in zebrafish fins (Laforest *et al.*, 1998, Akimenko and Ekker 1995, Quint *et al.*, 2002, Akimenko *et al.*, 2003).

Once a source point splits, the bone point associated with it detects two source points in close proximity to one another and this cues the bone point to split as well, creating two bony branches. Each of these new source-bone point pairs continues to grow forming the two branches of the bifurcation. This process is illustrated in Figure 3.2B.

The production of $B_{r,t}$ is based on the rate $Q_{r,t}$, as described in equations (8a) and (8b).

$$\frac{dB_{r,t}}{dt} = Q_{r,t} - \delta * B_{r,t} \quad \text{if } B_{r,t} < T_B \qquad (8a)$$

$$B_{r,t} = 0 \quad \text{if } B_{r,t} \geq T_B \qquad (8b)$$

Where $B_{r,t}$ is the concentration of bifurcation substance for ray *r* at time *t,* $Q_{r,t}$ is the rate of $B_{r,t}$ production for ray r at time t. $Q_{r,t}$ can either be constant or vary in space and/or time, as is outlined below. δ is the decay rate of the bifurcation forming substance, which is proportional to its concentration, and T_B is the threshold for bifurcation formation.

Once a ray reaches T_B and the source point divides, there are two possibilities to what happens to the concentration of bifurcation forming substance. The first possibility is that the concentration of $B_{r,t}$ returns to zero in the two source points that arose from the bifurcation (equation 8b), and production begins anew. The alternative possibility is to

reduce the concentration of $B_{r,t}$ to half in each of the source points (equation 8c). The reasoning behind splitting the concentration of $B_{r,t}$ is that it appears that when the *shh* expression domain splits prior to bifurcation, the two new domains are smaller than the original (Akimenko *et al.,* 2003). However, the sizes of the *shh* expression domains have not been quantified. We posit that if there is a reduction in domain size, perhaps the concentration of shh is also reduced, which can influence when the next bifurcation occurs. Therefore, we model this by assigning half the concentration of $B_{r,t}$ into the two source points, as explained by the following equation:

$$B_{r,t} = \frac{1}{2} B_{r,t} \qquad \text{if } B_{r,t} \geq T_B \qquad (8c)$$

Where $B_{r,t}$ is the concentration of bifurcation substance for ray *r* at time *t*, and T_B is the threshold for bifurcation formation. Since the outermost rays of the fin (i.e. the most ventral and most dorsal rays) do not bifurcate, these two rays in the model are excluded from bifurcation, even if their concentration of $B_{r,t}$ reaches threshold.

Similar to joint formation, to test methods of bifurcation substance production for bifurcation formation, we can alter the value of $Q_{r,t}$ in both space and time, which alters the bifurcation patterns within the fin. In space, the rate of $B_{r,t}$ production can be constant between rays, resulting in all rays bifurcating at once. Otherwise, we can vary the rate of production between rays, resulting in rays bifurcating at different times. The following equations outline these possibilities:

$$Q_{r,t} = \beta \qquad (9a)$$

$$\tilde{Q}_{r,t} = \tilde{\beta}_r \qquad (9b)$$

Where $Q_{r,t}$ and $\tilde{Q}_{r,t}$ are the rates of $B_{r,t}$ production for ray r at time t, β is the value assigned to the rate of $B_{r,t}$ production value for all rays, and $\tilde{\beta}_r$ is the value assigned

to the rate of $\tilde{B}_{r,t}$ production for ray r. Equation 9a represents the model where the rate of $B_{r,t}$ production is constant over both space and time. Equation 9b represents the model where the rate of $B_{r,t}$ production varies over space, but is constant in time.

To alter the rate of $B_{r,t}$ production in time, we must alter the values of $Q_{r,t}$ and $\tilde{Q}_{r,t}$ over time. We explore the following methods of altering $Q_{r,t}$ in time only:

$$Q_{r,t} = pG_{r,t} \qquad (10a)$$

$$\frac{dQ_{r,t}}{dt} = -c_B Q_{r,t} \qquad (10b)$$

Where $Q_{r,t}$ is the rate of $B_{r,t}$ production for ray r at time t, p is a constant, $G_{r,t}$ is the growth rate of ray r at time t, and c_B is a decay constant. The equations are similar in the model where $\tilde{Q}_{r,t}$ varies over space and time:

$$\tilde{Q}_{r,t} = \tilde{p}_r G_{r,t} \qquad (11a)$$

$$\frac{d\tilde{Q}_{r,t}}{dt} = -c_B \tilde{Q}_{r,t} \qquad (11b)$$

Where $\tilde{Q}_{r,t}$ is the rate of $B_{r,t}$ production for ray r at time t, $\tilde{p}_r$ is the constant for ray r, $G_{r,t}$ is the growth rate of ray r at time t, and c_B is a decay constant. In equations 9, 10 and 11 the threshold for bifurcation formation will vary.

The equations we test represent various ways the rate of $B_{r,t}$ production can decrease over time. Since the growth rate is already decreasing, we test the situation where $\tilde{Q}_{r,t}$ varies as a function of the growth rate (equations 10a and 11a). Finally, we test the situation where $\tilde{Q}_{r,t}$ decreases proportionally to its level (equations 10b and 11b).

We run each simulation model testing these proposed methods of bifurcation forming substance (equations 9, 10, and 11) and extract data on the occurrence of first bifurcations and the S1 ray section lengths. We compare the data collected from each model qualitatively to the expected bifurcation patterns to determine which method of bifurcation forming substance production and accumulation recreates the trends the best.

3.3 Modelling of Regeneration

For regeneration to occur in the model, the user is asked whether an amputation should be made. Upon selection of amputation, the model performs a cut along the fin at a designated fin length (amputation plane). The sections of the fin ray that are distal to the amputation plane are removed and regenerative growth occurs from the ray stumps.

Model regeneration is similar to ontogenetic growth. From the literature, we know that regeneration occurs more rapidly (Iovine 2007). We assign varying regenerative growth rates to each ray, to maintain the bi-lobed shape of the fin, that are higher than the ontogenetic growth rates. The regenerative growth rates are calculated from experimental data collected on adult fin development similar to what was done to calculate ontogenetic growth rates (for more information see Appendix 8.2 - Determining Growth and Regeneration). We calculate a fin regeneration rate equation based on experimental data. The fin regeneration rate equation is the following:

$$R_{f,t} = \frac{11.24537040987619}{t^2} \qquad (12)$$

Where $R_{f,t}$ represents the fin regeneration rate and t represents the time in days. We then scale this fin growth rate to represent individual ray regeneration ($R_{r,t}$). Regenerative growth in the model is summarized by equation (13).

$$\frac{d\rho s_{r,t}}{dt} = \frac{d\rho b_{r,t}}{dt} = R_{r,t} \qquad (13)$$

Where $\rho s_{r,t}$ represents the source point position for ray r at time t, $\rho b_{r,t}$ the bone point position for ray r at time t, and $R_{r,t}$ the growth rate for ray r at time t. Similar to ontogenetic growth, the change in a source point and bone point's positions, for a single ray, is equal due to their close association.

We keep the mechanism for joint formation the same as in ontogenetic development. Since production of the joint forming substance occurs in the distal bone point, upon amputation this source of joint forming substance is removed. Therefore, we assume a new source of joint forming substance is formed at the amputation plane, with the concentration set to zero ($J_{r,t} = 0$).

Similarly, the mechanism for bifurcation formation in regenerating fins is kept the same as the mechanism for bifurcation during ontogeny. The concentration of bifurcation forming substance is also reset to zero ($B_{r,t} = 0$) in each ray upon amputation. The bifurcation forming substance is produced in the distal source point and upon amputation this source is lost; therefore, a new source is created at the amputation plane.

3.4 Model Optimization

Once we determine the best method of joint and bifurcation substance production and accumulation from the selection process above, we need to optimize the model parameters to determine if we can quantitatively recreate the experimental trends in joint and bifurcation patterning.

3.4.1 Length of Simulation

Before we begin the optimization of the parameters of joint and bifurcation formation mechanisms, we need to optimize the length of the simulation. This ensures the model fin is a similar size to the experimental fins to which we will compare it for joint and bifurcation optimization.

There is little precedence in developmental biology of model and experimental data comparisons; therefore, we looked to these comparisons in other fields of study. We selected to use the Root Mean Square Error (RMSE) analysis (and the normalized Root Mean Square Error (NRMSE)) for our comparisons since it is widely used, particularly in (although not limited to) climatology studies (Willmott and Matsuura 2005). RMSE analysis is used for comparing model values to true values to determine the amount of error between them. The NRMSE is the normalization of the RMSE. To optimize the length of the model simulation we run the model for a range of times (in days) and calculate the length of ray 7 at each time. We use these two analyses to compare the length of ray 7 between model and experimental data. The model with the smallest amount of error between model and experimental data (lowest RMSE) is selected as the length of the simulation (i.e. the model that matches experimental data the best).

3.4.2 Joint Formation Mechanisms

Since the growth rate we use in the model is based on experimental data on fin length for the third ray from the right (ray 7), we focus on optimizing the match between model and experimental data for that ray.

We adjust the parameters in the equations for joint forming substance production as explained by equation 7b to increase the fit between the model and experimental data.

$$\tilde{A}_{r,t} = \frac{\tilde{h}_r}{(t + t_0)^e} \qquad (7b)$$

Where $\tilde{A}_{r,t}$ is the rate of $J_{r,t}$ production for ray r at time t, $\tilde{h}_r$ is the constant for ray r, e is a constant, t represents the time in days and t_0 represents the starting day of the model. We optimize the values for the threshold for joint formation T_J, the exponent in the rate of $J_{r,t}$ production equation e, and the constant in the equation $\tilde{h}_r$. To optimize the parameters, we test a range of parameter values and compare quantitative data on the

number of segments in the ray, as well as average segment lengths between the model and experimental data.

To narrow down the number of parameter combinations that we analyze with RMSE and NRMSE, we begin with an elimination of parameter combinations based on segment number. From experimental data collected in the laboratory, we know that the rays in a fin contain approximately 13 – 22 segments, with the longer rays containing segment numbers at the higher end of that range (Rolland-Lagan *et al., in prep*). We are optimizing the longest ray; therefore, we eliminate any parameter set with fewer than 18 or greater than 22 segments. When counting segments within a ray, we only count the segments that are flanked on the proximal and distal ends by joints, i.e. complete segments. We then perform RMSE and NRMSE on the average segment length in this smaller set of models.

3.4.3 Bifurcation Formation Mechanism

We adjust the parameters in the equations for bifurcation forming substance production as explained by equation 11a to increase the fit between the model and experimental data.

$$\tilde{Q}_{r,t} = \tilde{p}_r G_{r,t} \qquad (11a)$$

Where $\tilde{Q}_{r,t}$ is the rate of $B_{r,t}$ production for ray r at time t, $\tilde{p}_r$ is the constant for ray r, and $G_{r,t}$ is the growth rate of ray r at time t. We optimize the threshold for bifurcation formation T_B, and the coefficient from the equation for the rate of production $\tilde{p}_r$. Within this method of substance production, the value of $\tilde{p}_r$ varies between rays. Therefore, to optimize this parameter, the value needs to be changed for each ray individually, increasing the computation time. Therefore, to simplify this process, we input a second constant into the equation, v, which will alter each value of $\tilde{p}_r$. The new equation for substance production operates in the same manner as equation 11a. When $v = 1$, the value of $\tilde{p}_r$ is unchanged; and when $v \neq 1$ the value of $\tilde{p}_r$ is altered. The new equation is as follows:

$$\tilde{Q}_{r,t} = (v\tilde{p}_r) * G_{r,t} \qquad (11a - 2)$$

Where $\tilde{Q}_{r,t}$ is the rate of $B_{r,t}$ production for ray r at time t, $\tilde{p}_r$ is the constant for ray r, $G_{r,t}$ is the growth rate of ray r at time t, and v is a constant.

To optimize the parameters in the mechanism for bifurcation pattern formation, we run the model for a range of parameter values and compare quantitative data on the length of S1 and S2 ray sections using RMSE and NRMSE analyses.

Chapter 4 – Results

4.1 Modelling Ray Growth

The parameter values in the model for the growth rates, starting positions, and starting angles for each ray and the amount of shifting along the *x*-axis are provided in Table 4.1. The model represents 44 days of fin development, starting at 26.12 dpf. We use this length of time because it recreates a fin length similar to that of adult fish *in vivo* (for more information see section 4.4.1 – Length of Simulation). The growth rates are determined from unpublished data on fin development collected outside my Master's (n=18, for more information see Appendix 8.2 – Determining Growth and Regeneration). From this experimental data we calculate an equation for fin growth, which we scale to determine individual ray growth rates and we input those into the model.

To confirm that our growth model calculations based on experimental data are correct we compare the model fin length, the ray length experimental data, and the inverse line of best fit through the experimental data points. This is shown in Figure 4.1A, where the points represent individual ray length data points, the gray solid line is the inverse line of best fit, and the dashed black line is the model fin length. We can see that the two lines overlap, which indicates the model is an accurate replication of fin growth.

Now that the model fin is growing correctly, we need to check if individual model ray length matches experimental ray lengths. The individual ray growth rates are determined by scaling the fin growth rate to each ray. A comparison of the model ray lengths to the experimental fin ray lengths between 18 rays is shown in figure 4.1B. In this figure, overall model ray lengths are similar to experimental fin lengths, with most model data falling within the error bars of the experimental data (16/18); indicating the model is an accurate model of individual ray growth.

Table 4.1. Parameter values assigned for model set up and individual ray growth.

	Value Assigned																	
	Ray Number																	
Parameter*	**-9**	**-8**	**-7**	**-6**	**-5**	**-4**	**-3**	**-2**	**-1**	**1**	**2**	**3**	**4**	**5**	**6**	**7**	**8**	**9**
$\rho s_{r,0}$	0.450	0.449	0.446	0.440	0.432	0.425	0.419	0.416	0.414	0.414	0.416	0.419	0.425	0.432	0.440	0.446	0.449	0.450
$\theta s_{r,0}$	2.174	2.094	2.020	1.951	1.883	1.813	1.742	1.681	1.608	1.534	1.460	1.400	1.328	1.259	1.191	1.121	1.048	0.968
$\rho b_{r,0}$	0.445	0.445	0.442	0.435	0.428	0.421	0.415	0.412	0.410	0.410	0.412	0.415	0.421	0.428	0.435	0.442	0.445	0.445
$\theta b_{r,0}$	2.174	2.094	2.020	1.951	1.883	1.813	1.742	1.681	1.608	1.534	1.460	1.400	1.328	1.259	1.191	1.121	1.048	0.968
$G_{r,0}$	0.287	0.292	0.282	0.260	0.233	0.207	0.183	0.160	0.151	0.157	0.176	0.202	0.223	0.244	0.260	0.271	0.275	0.283
X_r	-0.758	-0.667	-0.576	-0.485	-0.394	-0.303	-0.212	-0.136	-0.455	0.455	0.136	0.212	0.303	0.394	0.485	0.576	0.667	0.758

* Where $\rho s_{r,0}$ and $\rho b_{r,0}$ represents the source point and bone point positions for ray r at time $t = 0$ respectively, $\theta s_{r,0}$ and $\theta b_{r,0}$ are the starting angles of the source and bone points for ray r at time $t = 0$ respectively, $G_{r,0}$ is the growth rate for ray r at time $t = 0$, and X_r represents the amount of change in bone point position for ray r.

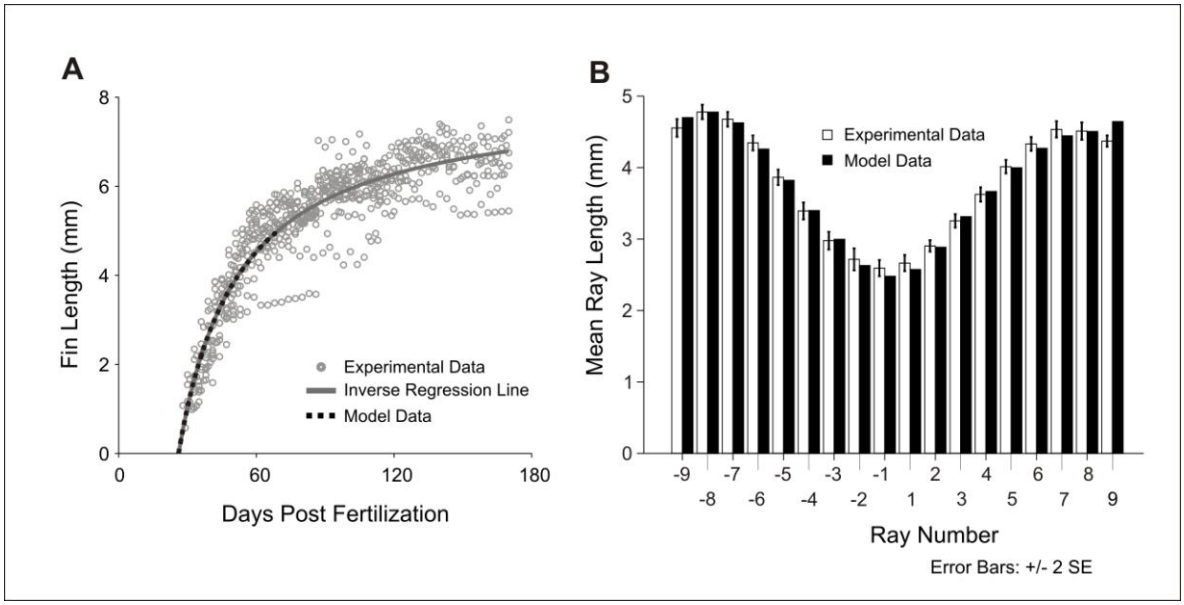

Figure 4.1. Comparison of model and experimental fin and ray length data. **A:** Comparison of the model fin length (black dashed line) to experimental fin lengths (grey circles) and the inverse line of best fit (grey solid line, $R^2 = 0.864$). See Appendix 8.2.1 and Table 8.1 for further details on the curve fitting and the results of the statistical analysis. **B:** Model ray lengths (black bars) compared to experimental ray lengths (white bars). The model was grown using an equation of growth determined from experimental data.

4.2 Patterning Mechanism Selection

4.2.1 Joint Pattern Formation

We test eight joint substance production models (equations 5, 6 and 7). The parameter values for each model of joint patterning substance production are listed in Table 4.2.

For each tested model, we extract quantitative data on the number of segments and the segment lengths in each ray. We then qualitatively compare these values to the expected trends in joint patterning, which are based on experimental data. The expected trends are illustrated in Figure 4.2, and they include fewer segments in the medial rays, compared to the lateral rays (Figure 4.2A), a decrease in segment length along the proximo-distal axis (Figure 4.2B), as well as a decrease in segment length between lateral and medial rays (Figure 4.2B).

Within each individual ray, we assign the segments segment ID numbers, which can be used to identify the segment's position in the ray. The most proximal segment is numbered 1, the second is numbered 2, and so on. This segment ID number represents the position of a segment along the proximo-distal axis of a ray, where the smaller the segment ID number, the more proximal the segment.

The quantitative data we extract from the models is provided in Figure 4.3, showing the number of segments (A-H), the segment lengths (I-P) and the visualization of each fin (Q-X). The eight methods of joint patterning substance production we test include where the rate of $J_{r,t}$ production remains constant over time and space (equation 5a), and where the rate of $J_{r,t}$ production remains constant over time and varies in space (equation 5b). The remaining six methods involve the rate of $J_{r,t}$ production varying over time in three ways and either remaining constant in space, or varying (respectively). The methods of varying the rate of production over time are decreasing as a function of the growth rate (equations 6a and 7a, respectively), decreasing with an equation of the same form as the

growth equation (or equation 6b and 7b), or decreasing proportionally to its level (or equation 6c and 7c).

Within the figure, panels A, I, Q correspond to equation 5a and panels B, J, R, correspond to equation 5b. For the methods in which production varies in time but remains constant in space, panels C, K, S correspond to equation 6a; panels E, M, U correspond to equation 6b**;** panels G, O, W correspond to equation 6c. For the methods in which production varies in time and in space, panels D, L, T correspond to equation 7a; panels F, N, V correspond to equation 7b**;** panels H, P, X correspond to equation 7c. In panels I-P the black lines represents a lateral ray (ray 7) and the lighter line represents a medial ray (ray 1). Visualizations of the fins for each model are provided in Figure 4.3Q-X. All fins are plotted based on segment length. Segments are color-coded by length and black points represent joints within the rays.

To determine which model and associated method of joint forming substance production recreates the expected trends, we can compare Figure 4.2 to Figure 4.3. For the number of segments in the rays (Figure 4.2A and Figures 4.3A-H) we can see that four models (Figures 4.3B, C, F, and H) generate the appropriate decrease in segment numbers between the lateral and medial rays. These panels correspond to the mechanism of joint pattern formation described by equations 5b, 6a, 7b, and 7c, respectively. For segment length (Figure 4.2B and Figures 4.3I-P), only two models (Figures 4.3M and N) give rise to the appropriate decrease in segment length along the proximo-distal axis, and between lateral and medial rays. Panels M and N correspond to the joint formation mechanism described by equations 6b and 7b, respectively.

From these two comparisons, only one model correctly generates the trends in the number of segments between rays and in segment lengths. That is the model described by equation 7b, when the rate of accumulation varies between rays and decreases over time as a function of an equation of the same form as the growth equation ($y = a + \frac{b}{x}$). Therefore, we select this model of joint forming substance production as representing a likely joint formation mechanism.

Table 4.2. Parameter values assigned for testing models where joints form as a result of substance accumulation.

		Value Assigned																	
		Ray Number																	
Equation	Parameter	**-9**	**-8**	**-7**	**-6**	**-5**	**-4**	**-3**	**-2**	**-1**	**1**	**2**	**3**	**4**	**5**	**6**	**7**	**8**	**9**
4a	δ	0.001																	
5a	α	1.000																	
5b	$\tilde{\alpha}_r$	1.000	1.000	1.000	0.930	0.850	0.840	0.800	0.730	0.680	0.680	0.730	0.800	0.840	0.850	0.930	1.000	1.000	1.000
5a & 5b	T_J	0.900																	
6a	m	0.029																	
7a	$\tilde{m}_r$	0.029	0.029	0.029	0.030	0.032	0.037	0.040	0.042	0.043	0.043	0.042	0.040	0.037	0.032	0.030	0.029	0.029	0.029
6a & 7a	T_J	0.008																	
6b	h	6.000																	
7b	$\tilde{h}_r$	6.000	6.000	6.000	5.580	5.100	5.040	4.800	4.380	4.080	4.080	4.380	4.800	5.040	5.100	5.580	6.000	6.000	6.000
6b & 7b	t_0	26.120																	
6b & 7b	e	1.900																	
6b & 7b	T_J	0.011																	
6c	$A_{r,t}$	α (equation 4a)																	
7c	$\tilde{A}_{r.t}$	$\tilde{\alpha}_r$ (equation 4b)																	
6c & 7c	c_J	0.003																	
6c & 7c	T_J	0.900																	

* δ is the decay constant for joint forming substance decay, α is the value assigned to the rate of accumulation for all rays, and $\tilde{\alpha}_r$ is the value assigned to the rate of accumulation for ray r, m and h are constants which are equal among all rays, $\tilde{m}_r$ and $\tilde{h}_r$ are constants for ray r, T_J is the threshold for joint formation, e is a constant, t_0 represents the initial day of the model, c_J is the rate of accumulation decay for all rays, $A_{r,t}$ and $\tilde{A}_{r,t}$ are the rates of production for ray r at time $t = 0$.

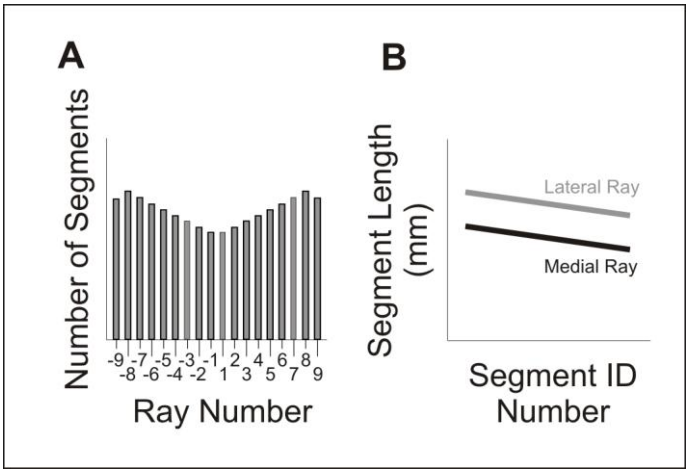

Figure 4.2. Expected trends in joint patterning. **A:** the trends in number of segments per ray. **B:** the trends in segment lengths along the proximo-distal axis and between rays.

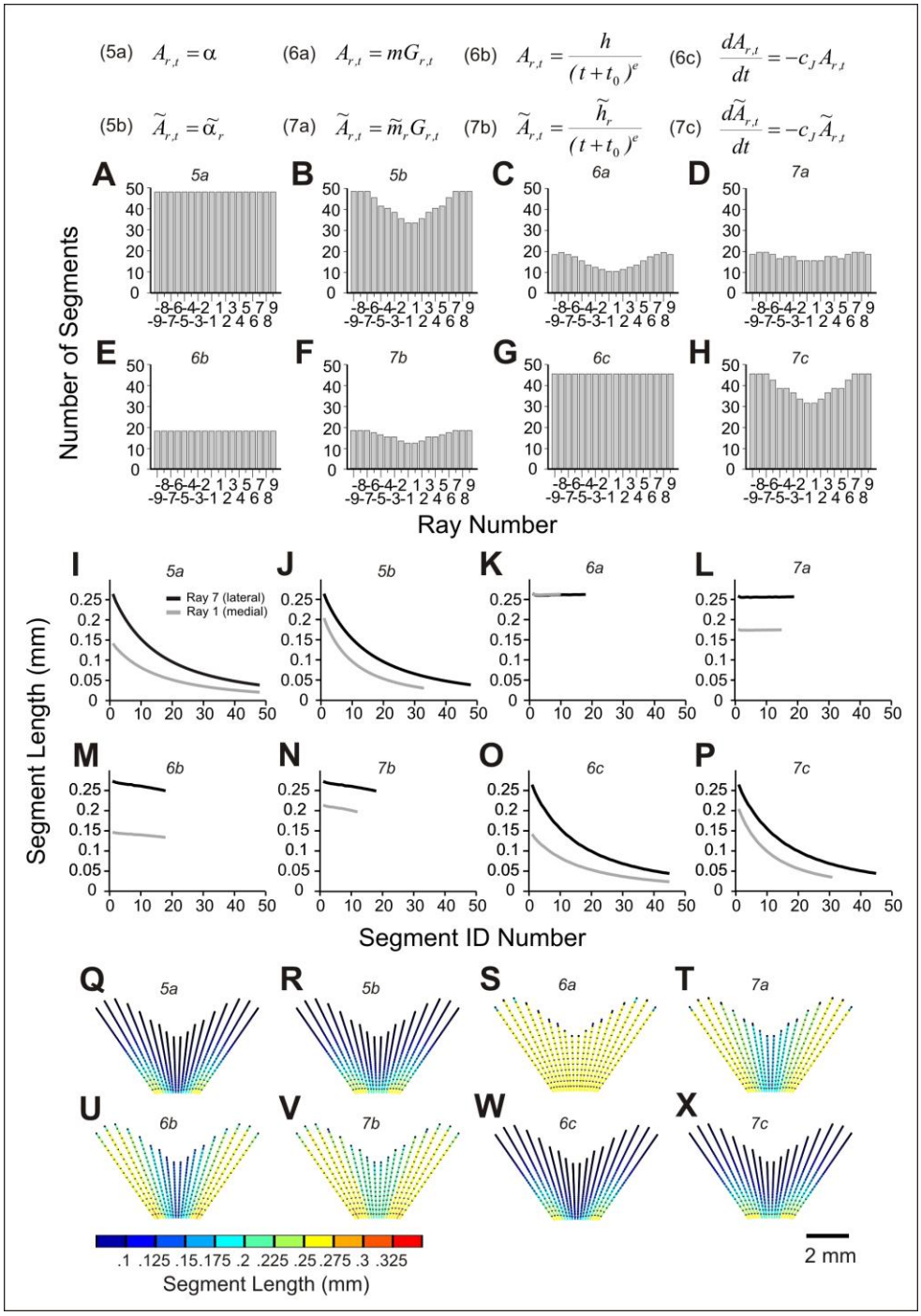

Figure 4.3. Quantitative data extracted from the joint forming substance accumulation models. Number of segments (**A-H**), segment lengths (**I-P**) and model output (**Q-X**) as shown for the eight hypothesized mechanisms of joint forming substance accumulation (equations 5, 6 and 7). At the top of each panel, the method acronym is provided. The model was run for 44 days on 18 rays. The parameters used in each model are outlined in Table 4.2. In panels I-P the black lines represents a lateral ray (ray 7) and the light grey lines represent a medial ray (ray 1).

4.2.2 Bifurcation Pattern Formation

We postulate two concentrations of bifurcation forming substance after bifurcation, either the concentration is divided in half, or the concentration is reset to zero. The first case results in second bifurcations occurring too much too soon after the first bifurcations no matter which equation parameters were used. Therefore, we set the concentration of bifurcation forming substance to zero after bifurcation. The parameter values we use to test the methods of bifurcation substance production in the mechanism for bifurcation formation are listed in Table 4.3.

We test six bifurcation substance accumulation models. From each model of bifurcation formation, we extract data on the occurrence of bifurcations (in time) and S1 ray section lengths for qualitative comparison to the expected trends in bifurcation patterning. The trends we want to recreate are illustrated in Figure 4.4. These trends include bifurcations occurring first in the outermost bifurcating rays, and proceeding inward (Figure 4.4A), and a bi-lobed distribution of S1 ray section lengths in bifurcating rays across the medio-lateral axis of the fin (Figure 4.4B).

The quantitative data extracted from the tested models is presented in Figure 4.5, showing the time of first bifurcations (A-F), S1 ray section lengths (G-L) and the visualization of each model (M-R). The six methods of bifurcation patterning substance production we test include the model where the rate of $B_{r,t}$ production remains constant over time and space (equation 9a) and where the rate of $B_{r,t}$ production remains constant over time and varies in space (equation 9b). The other four methods involve the rate of production varying over time in multiple ways; in two of these cases, the rate of $B_{r,t}$ production is constant in space, and in the other two it varies in space. The rate of production can decrease either as a function of the growth rate (equations 10a and 11a, where the rate is constant over space or varies, respectively), or proportionally to its level(equations 10b and 11b).

Within Figure 4.5, panels A, G, M correspond to equation 9a; and panels B, H, N correspond to equation 9b. For the methods in which production varies in time, but remains

constant in space, panels C, I, O correspond to equation 10a; and panels E, K, Q correspond to equation 10b. For the methods in which production varies in both space and time, panels D, J, P correspond to equation 11a; and panels F, L, R correspond to equation 11b. For each fin visualization (M-R) the S1 ray sections are coloured green, S2 sections are red, and S3 sections are blue.

We can compare Figure 4.4 to Figure 4.5 to determine which method of bifurcation substance production recreates the expected trends in bifurcation patterning. For the time of first bifurcation occurrence (Figure 4.4A and Figure 4.5A-F), four models recreate the appropriate trend (Figures 4.5B, C, D and F). These panels correspond to the method of bifurcation substance production described by equations 9b, 10a, 11a, and 11b, respectively. Similarly, for S1 ray section lengths (Figure 4.4B and Figure4.5 G-L), three methods show a bi-lobed distribution of ray section lengths (H, J, and L). These panels correspond to the bifurcation substance production methods described by equations 9b, 11a, and 11b, respectively.

Therefore, three models of bifurcation substance accumulation generate the expected trend in bifurcation patterning. To narrow down which of these models provides the best match to the expected trends we look at the length of S2 ray sections. We know from unpublished data previously collected in the laboratory, that S2 ray section in the lateral-most bifurcating rays are relatively similar in length to the S1 section, and that the length of inner S2 ray sections are shorter than the prior S1 section (Rolland-Lagan *et al., in prep*). If we compare panels N, P and R from Figure 4.5 we can see the S2 ray sections (shown in red) in the lateral-most rays in panels N and R are smaller than the prior S1 ray sections (shown in green). Whereas, panel P does not have second bifurcations and thus the S2 ray sections are long. Therefore, we can conclude that the model of bifurcation substance accumulation described by equation 11a, where the rate of accumulation decreases over space and time as a function of the growth rate, best recreates the expected trends in bifurcation patterning. Therefore, we select this method of bifurcation substance production for the mechanism of bifurcation formation in the final model of bony ray patterning.

Table 4.3. Parameter values assigned for testing the models where bifurcations form as a result of substance accumulation.

		Value Assigned																	
		Ray Number																	
Equation	Parameter	**-9**	**-8**	**-7**	**-6**	**-5**	**-4**	**-3**	**-2**	**-1**	**1**	**2**	**3**	**4**	**5**	**6**	**7**	**8**	**9**
8a	δ	0.001																	
9a	β	0.500																	
9b	$\tilde{\beta}_r$	0.530	0.500	0.440	0.420	0.430	0.460	0.480	0.500	0.510	0.510	0.500	0.480	0.460	0.430	0.420	0.440	0.500	0.530
9a & 9b	T_B	0.170																	
10a	p	0.500																	
11a	$\tilde{p}_r$	0.530	0.500	0.440	0.420	0.430	0.460	0.480	0.500	0.510	0.510	0.500	0.480	0.460	0.430	0.420	0.440	0.500	0.530
10a & 11a	T_B	0.013																	
10b	Q_t	1.000																	
11b	$\tilde{Q}_{r.t}$	0.530	0.500	0.440	0.420	0.430	0.460	0.480	0.500	0.510	0.510	0.500	0.480	0.460	0.430	0.420	0.440	0.500	0.530
10b & 11b	c_B	0.030																	
10b & 11b	T_B	9.000																	

* δ is the decay rate of the bifurcation forming substance, which is proportional its the concentration, β is the value assigned to the rate of accumulation value for all rays, and $\tilde{\beta}_r$ is the value assigned to the rate of accumulation for ray r, p is a constant assigned to all rays, $\tilde{p}_r$ is a constant assigned to ray r, c_B is a decay constant assigned to all rays, Q_t and $\tilde{Q}_{r,t}$ are the rates of production for ray r at time $t = 0$ and T_B is the threshold for bifurcation.

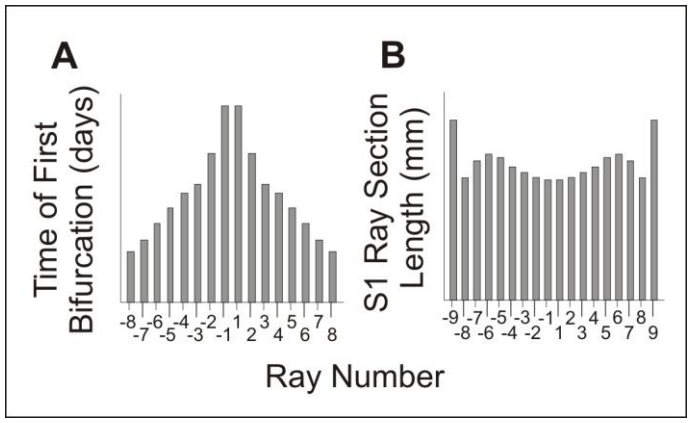

Figure 4.4. Expected trends in bifurcation patterning. **A:** the trend in first bifurcation occurrence between rays. **B:** the bi-lobed distribution of S1 ray section lengths in the branching rays. It should be noted that the lateral-most rays (rays -9 and 9) do not bifurcate.

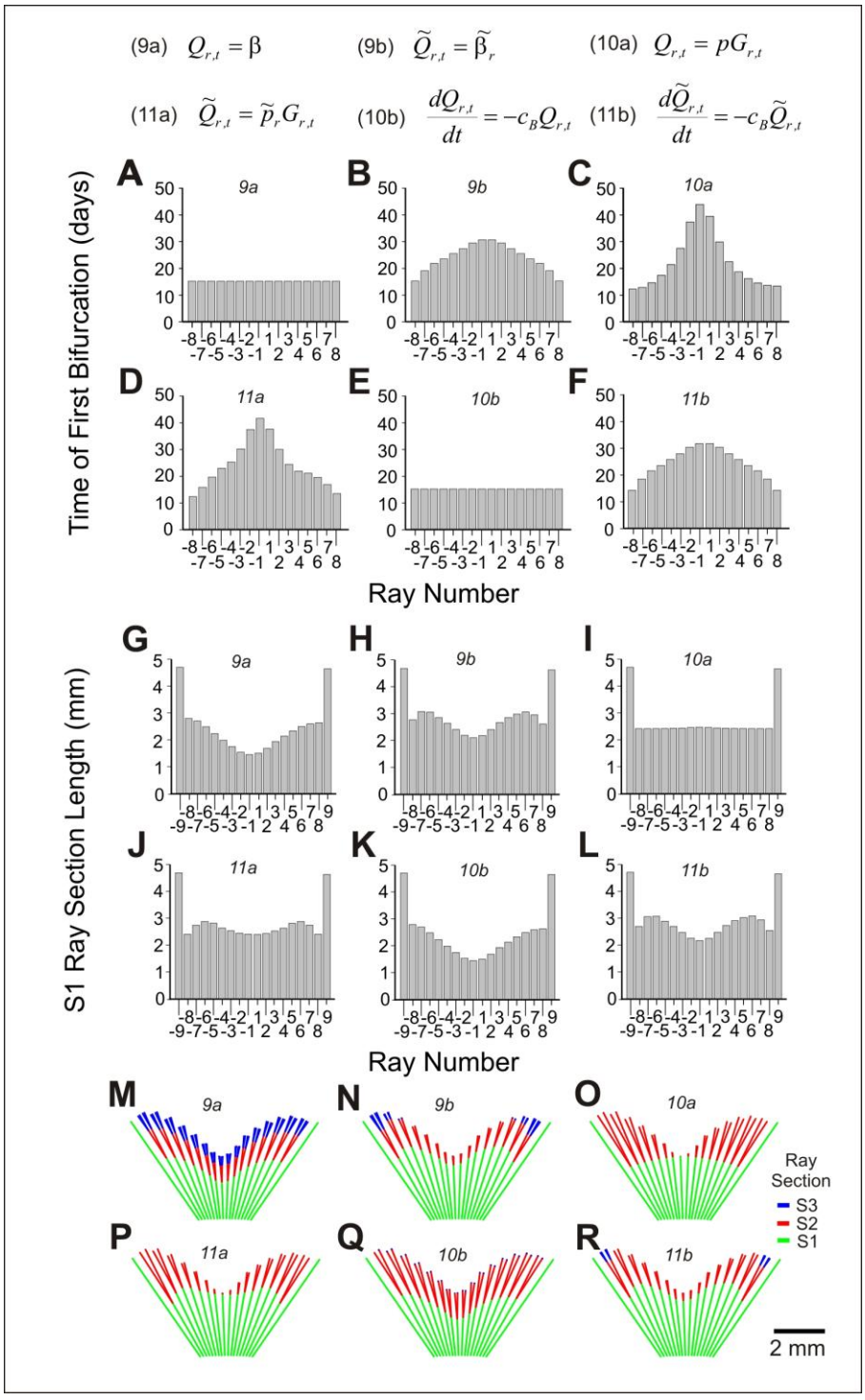

Figure 4.5. Quantitative data from the bifurcation forming substance accumulation models. First bifurcation occurrence (A-F), S1 ray section lengths (G-L) and visual model output (M-R) for the six hypothesized methods of bifurcation forming substance accumulation (equations 9, 10 and 11). At the top of each panel, the method acronym is provided. The model was run for 44 days and 18 rays. Parameters used in the models are outlined in Table 4.3. S1 ray sections are shown in green, S2 ray sections in red, and S3 sections in blue.

4.3 Modelling of Regeneration

The starting positions and angles of the regenerating rays are listed in Table 4.4, as well as the regeneration growth rates and the height along the *y*-axis where the fin was amputated. Once again, to recreate a visually similar fin, scaling along the medio-lateral axis is done at the very end of the simulation, after regeneration has occurred.

The process of regeneration can be highly variable. In goldfish, it has been reported that the older the fish, the slower regeneration occurs (Broussonet 1786, Scott 1907), although the rate is more rapid than ontogenetic development. Regeneration is dependent on the ambient water temperature (Johnson and Weston 1995), and although regeneration recapitulates ontogenetic growth, regeneration occurs more rapidly if the amputation is performed proximally versus distally (Tassava and Goss 1966, Poss *et al.,* 2000, Lee *et al.,* 2005). Therefore, to incorporate complete regeneration into the model, a tremendous amount of quantitative data is required to calibrate these variations in regenerative growth.

We do not possess data on each of these variations in regeneration; however, we do possess one set of unpublished regeneration data collected before my Master's program. This regeneration data set is on a small number of fish (n=12), older than 100 dpf, which were amputated proximally and allowed to regenerate at 28.5°C. From this data set, we calculate individual ray regeneration rates and input them into the model in an identical manner as the ontogenetic growth rates. For more information on this regeneration data set, see Appendix 8.2 – Determining Growth and Regeneration.

We run the ontogenetic ray development model for 100 days to match the age of the fish from the data set, to recreate a realistic model fin. Since the model begins at day 26.12, the total age of the model fins at amputation are 126.12 dpf. In the experimental data set, the fins were amputated 2-3 segments below the lowest bifurcation. Therefore, we amputate the fin at 2 mm on the *y*-axis since it falls below the lowest bifurcation, and the ray sections distal to the amputation plane are removed. The amputated ray stumps act as the starting positions for the individual ray regenerates.

The model fin then regenerates for 40 days, since it has been documented that regeneration can take anywhere from 1 week to 73 days in *Trichogaster sp.*, *Fundulus heteroclitus* and zebrafish(Goss and Stagg 1957, Tassava and Goss 1966, Géraudie *et al.*, 1995, Johnson and Weston 1995, Becerra *et al.*, 1996, Poss *et al.*, 2000). A similar length of time (28-38 days) was documented in the laboratory as being the time required for the average length of amputated fins to attain pre-amputation length (Rolland-Lagan *et al.*, 2012). The visualization of the fin from ontogenetic growth (A), after amputation (B) and after regeneration (C) are illustrated in Figure 4.6.

The mechanisms of joint and bifurcation formation are identical to those from ontogenetic development. Therefore, the parameter values for the mechanisms are the same (Table 4.2 – parameters for equation 6b). However, when the values are kept the same, we see in the regenerated fin (Figure 4.6C) the segments distal to the amputation are much larger than we would expect in a real regenerate. Therefore, we alter the parameter values in the equation for joint formation to recreate a more realistic segmentation pattern. These new parameters are listed in Table 4.4 and the visualizations of the fin prior to amputation (D), after amputation (E), and after regeneration (F) with the new parameters are provided in Figure 4.6.

We extract quantitative data on fin pattern parameters between the ontogenetic fin and the regenerated fin (Figure 4.7) to make comparisons between the original fin and the regenerate. The fin pattern parameters we extract are S1 ray section lengths (A), number of segments per ray (B), and segment lengths (C for a medial ray, and D for a lateral ray). We can see from the longer S1 ray section lengths in the regenerated ray, bifurcation in the regenerate is delayed (Figure 4.7A). This delay has also been documented in the literature (Géraudie *et al.*, 1994).

The comparison between the number of segments in ontogenetic and regenerated fin rays has not been documented in the literature. Therefore, it is difficult to determine whether the regenerated model fin rays recreate the expected pattern in that respect. However, we can see that in the model, the regenerated fin rays contain the same number, if not more segments than the ontogenetic fin rays (Figure 4.7B).

In the mechanism for joint formation, we reset the concentration of joint forming substance to zero upon amputation. This results in regenerated segments at the amputation plane that are longer than segments located in the same position in non-regenerated fins. This is consistent with a recently published paper on zebrafish (Rolland-Lagan *et al.,* 2012), and another study on goldfish (Mari-Beffa *et al.,* 1999), which showed that the first regenerated segments are longer than segments found in that position in a non-regenerated ray. This increase in segment length is seen in both medial (Figure 4.7C) and lateral (Figure 4.7D) rays, which is also supported by previous research. The first regenerated segment is longer than the non-regenerated segment in the same position (Rolland-Lagan *et al.,* 2012). However, regenerate segment length decreases along the proximo-distal axis such that the difference between average segment lengths of fins before amputation and after regeneration are not statistically different (Becerra *et al.,* 1999, Rolland-Lagan *et al.,* 2012).

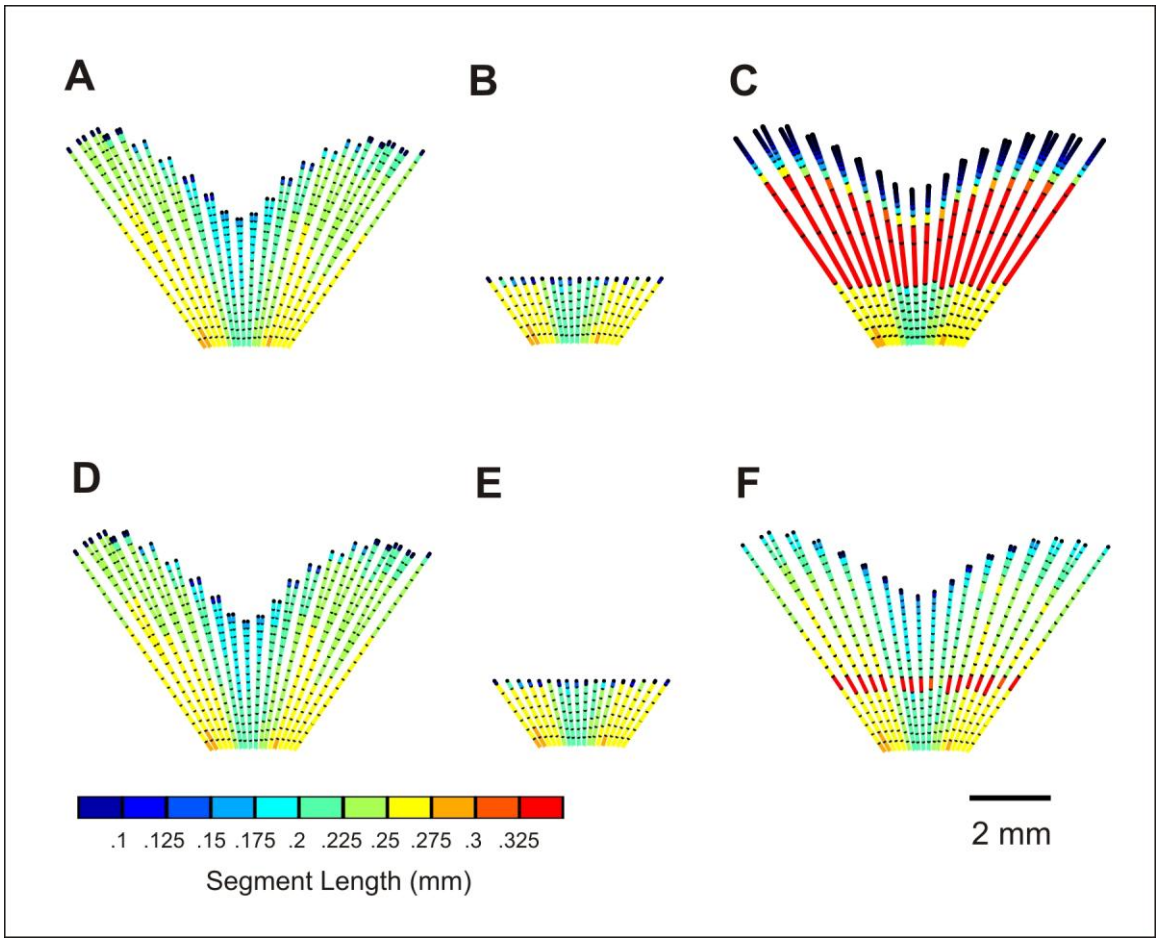

Figure 4.6. Visualizations of the model fin after ontogenetic development, amputation, and regeneration. **A-C:** no changes were made to the parameters in the mechanism of joint formation. **D-F:** alterations were made to the parameters in mechanism of joint formation. **A and D**: the model fin after 100 days of growth. **B and E**: the fin amputated at 2 mm. **C and F**: the fin regenerated after 40 days. Mechanisms of joint and bifurcation formation are the best models from the selection process. The parameters used in ontogenetic growth are those outlined by the best models in Tables 4.1, 4.2 and 4.3 (**A and D**). The parameters used in regenerative growth in **C** are outlined in Table 4.2 for equation 6b, and the parameters used in regenerative growth in **F** are outlined in Table 4.4.

Table 4.4. Parameter values assigned for fin regeneration.

	Value Assigned																	
	Ray Number																	
Parameter*	**-9**	**-8**	**-7**	**-6**	**-5**	**-4**	**-3**	**-2**	**-1**	**1**	**2**	**3**	**4**	**5**	**6**	**7**	**8**	**9**
$\rho s_{r,0}$	2.453	2.332	2.243	2.175	2.122	2.081	2.050	2.032	2.021	2.021	2.032	2.050	2.081	2.122	2.175	2.243	2.332	2.453
$\theta s_{r,0}$	2.174	2.094	2.020	1.951	1.883	1.813	1.742	1.681	1.608	1.534	1.460	1.400	1.328	1.259	1.191	1.121	1.048	0.968
$\rho b_{r,0}$	2.429	2.308	2.221	2.154	2.101	2.060	2.030	2.012	2.001	2.001	2.012	2.030	2.060	2.101	2.154	2.221	2.308	2.429
$\theta b_{r,0}$	2.174	2.094	2.020	1.951	1.883	1.813	1.742	1.681	1.608	1.534	1.460	1.400	1.328	1.259	1.191	1.121	1.048	0.968
$R_{r,0}$	1.870	1.902	1.840	1.694	1.520	1.351	1.191	1.045	0.985	1.023	1.147	1.317	1.458	1.590	1.698	1.768	1.794	1.878
Y	2.000																	
δ	0.001																	
$\tilde{h}_r$	0.400	0.400	0.400	0.372	0.340	0.336	0.320	0.292	0.272	0.272	0.292	0.320	0.336	0.340	0.372	0.400	0.400	0.400
t_0	2.360																	
e	1.850																	
T_J	0.012																	
$\tilde{p}_r$	0.531	0.475	0.418	0.399	0.409	0.437	0.456	0.475	0.485	0.485	0.475	0.456	0.437	0.409	0.399	0.418	0.475	0.531
T_B	1.050																	

* Where $\rho s_{r,0}$ and $\rho b_{r,0}$ represents the source point and bone point positions for ray r at time $t = 0$ during regeneration, respectively; $\theta s_{r,0}$ and $\theta b_{r,0}$ are the starting angles of the source and bone points for ray r at time $t = 0$ during regeneration, respectively; and $R_{r,t}$ is the growth rate for ray r at time $t = 0$ during regeneration. Y represents the level of amputation along the *y*-axis and δ represents the decay constant for the rate of accumulation for both the joint and bifurcation forming substances. $\tilde{h}_r$ is a constant for ray r; e is a constant; t_0 represents the initial day of the regenerating model; and T_J is the threshold for joint formation. $\tilde{p}_r$ is a constant assigned to ray r; and T_B is the threshold for bifurcation.

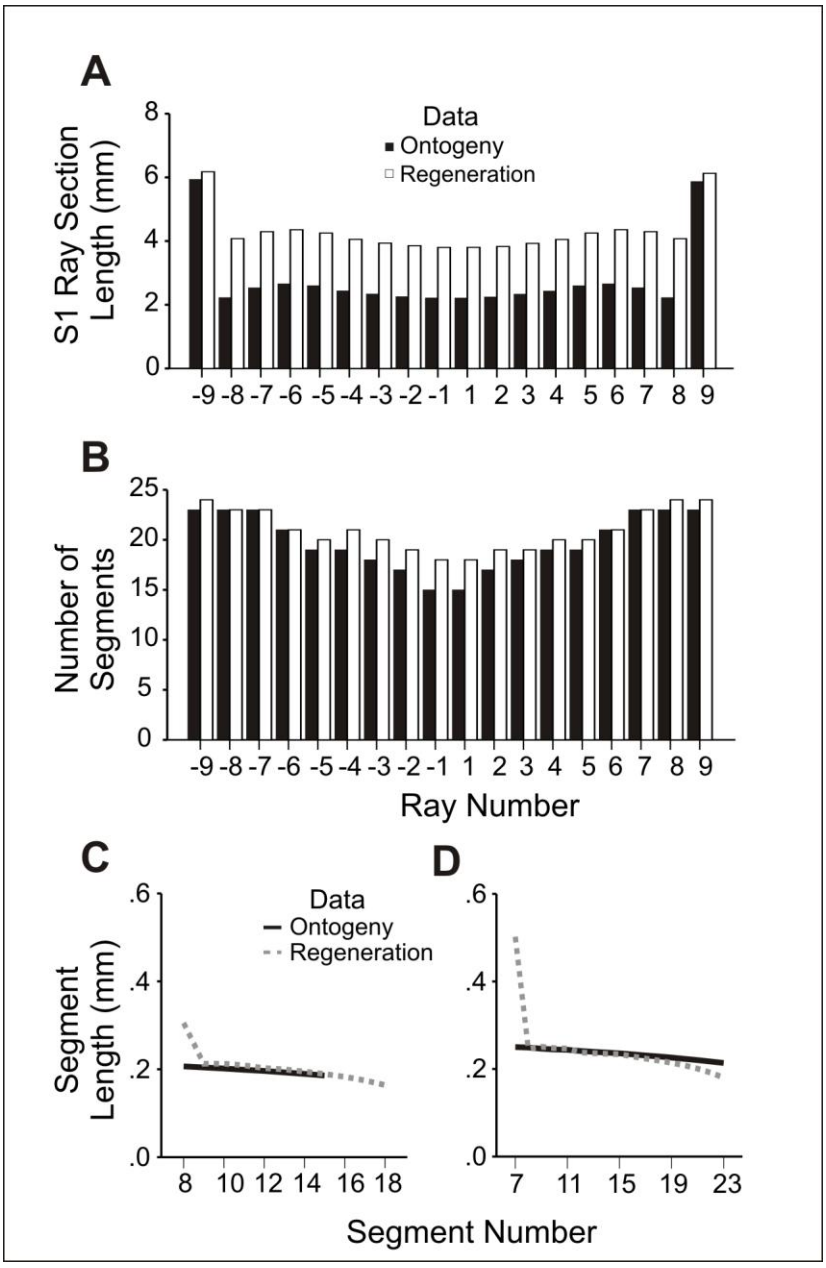

Figure 4.7. Quantitative data extracted on fin pattern parameters for the ontogenetic and regenerated fish fins. The fin pattern parameters extracted include **A:** S1 ray section lengths, **B:** number of segments, **C:** segment lengths in a medial ray (Ray 1) and **D:** segment lengths in a lateral ray. (Ray 7)

4.4 Model Ray Development Optimization

The parameter values in the models outlined above were arbitrarily chosen so the patterning of the joint and bifurcations was visually similar to experimental data. However, it is unclear if the arbitrary parameter values assigned provide the best fit to the experimental data. Therefore, we run each model for a range of parameter values to determine the amount of error between model and experimental data. The parameter combination that results in the lowest amount of error between model and experimental data is then selected as the optimized parameter values and are used in the final version of the model. We optimize the parameters in three areas of the model: the length of the simulation, the mechanism for joint formation, and the mechanism for bifurcation formation. Here we will discuss the results of the optimizations.

To perform all three optimizations, we first test a range of parameter values at large intervals. This identifies a smaller range of parameter values that give the best RMSE results. We then run the optimization again, using the smaller range of values identified above, with a smaller interval between the values. From this finer optimization we can identify the value with the best RMSE.

We use the same experimental data set for the optimization of simulation length, the joint formation mechanism and the bifurcation formation mechanism. It was collected previously within the laboratory and we only use the data representing adult wild type zebrafish (n=12). For more information, see Appendix 8.2.3 – Optimization Data Set.

4.4.1 Length of Simulation

The range of days tested for length of simulation optimization is listed in Table 4.5. We optimize the length of the simulation to ensure the size of the model fin is similar to the size of the experimental fins that we will use in the optimization of the patterning mechanisms.

To optimize the length of the simulation we compared average experimental ray lengths to the model ray lengths. The average experimental ray lengths were used for 18 rays, from all 12 fish from the experimental data et. In the model, we measure ray length from the base of each fin to the most distal point on the ray. We then use the ray length of all 18 rays for both the model and experimental data and performed a RMSE analysis and NRMSE analysis to determine the amount of error between model and experimental data. The RMSE and NRMSE gave us similar results; therefore, we used the RMSE value for selection.

The number of days that results in the lowest RMSE value was chosen as the length of simulation. This number was 44 days (RMSE = 0.093, NRMSE = 0.041). Therefore, since the model starts at 26.12 dpf, if we run the simulation for 44 days, the total age of the modeled fin is 70.12 dpf.

Table 4.5. Range of parameter values for the optimization of the best model of ray growth and patterning.

Parameter*	Range of Values (increment)
t	4200 – 4800 (20)
T_J	0.006 – 0.014 (0.0005)
e	1.84 – 2.20 (0.02)
$\tilde{h}_r$	5 – 6 (0.2)
T_B	0.8 – 1.3 (0.05)
v	0.07 – 1.10 (0.05)

* t is the time (in days) that the simulation was run, T_J is the threshold for joint formation, e is the exponent in the rate of accumulation equation (7b), $\tilde{h}_r$ is the coefficient in the same equation (7b), T_B is the threshold for bifurcation formation, and v is the coefficient in the equation (11a – 2).

4.4.2 Joint Formation

For joint formation, the best mechanism was equation 7b, where the rate of accumulation varied in both space and time. The parameters to optimize are the threshold for joint formation T_J, the exponent in the rate of production equation e, and the constant in the same equation, $\tilde{h}_r$. The range of parameter values tested is outlined in Table 4.5.

Since the calibration of growth in the model is based on experimental growth data for the third ray from the right (ray 7), we focus on optimizing that ray only. However, we do compare the number of segment and lengths in all rays to ensure we can identify any rays that are noticeably different.

To narrow down the number of parameter combinations that we analyze with the RMSE and NRMSE analyses, we begin with an elimination of parameters sets based on segment number. From the experimental data previously collected in the laboratory on wild type zebrafish (n=12), we know that the fin rays contain approximately 13 – 22 segments, with the longer lobe rays containing segment numbers at the higher end of that range (Rolland-Lagan *et al., in prep*). Therefore, since we are optimizing the longest ray, we eliminate any parameter combination that produces a ray with fewer than 18 or greater than 22 segments. When counting segments in a ray, we only count the segments that are flanked on the proximal and distal ends by joints, i.e. complete segments.

With the remaining parameter combinations, we perform the RMSE and NRMSE analyses on average ray segment length between model and experimental data. For the analysis, each segment within the ray is assigned a segment ID number depending on its position along the proximo-distal axis. The most proximal segment is number 1, the second proximal segment is 2, and the more distal segments are numbered sequentially. To compare segment lengths, we only use segments with ID numbers present in both data sets. In other words, if there are 18 model segments and 22 experimental segments, we only use segments lengths for the first 18 segments in both data sets and compare those values using RMSE and NRMSE. The RMSE and NRMSE give us similar results; therefore, we use the RMSE value for parameter selection.

The five parameter combinations that result in the lowest RMSE values are provided in Table 4.6. Model segment lengths compared to the experimental segment lengths for the parameter value combination that resulted in the lowest RMSE value are shown in Figure 4.8A. In panel 4.8B, each point on the graph represents the RMSE analysis result of one of the parameter combinations. The corresponding threshold, exponent, and coefficient values that produced those RMSE values are shown on the *x*, *y*, and *z*-axes respectively and the coloration of the point represents the RMSE value. Dark blue represents low RMSE values, and red are high.

To further support the selected mechanism of joint formation, we investigate the match between experimental and model data further. Since we optimize based on the longest ray in the fin, we also check that the number of segments and the lengths of those segments line-up between the remaining rays in the fin in the model and experimental data.

The comparison of the number of segments between the experimental fin and the model fin are shown in Figure 4.9. We can see that there is variation in the number of segments between the dorsal and ventral sides of the fin in both data sets and that half of the model rays fall within the error bars of the experimental rays. Figure 4.10 shows the comparison between model and experimental segment lengths for rays 1 – 9 on the ventral side of the fin. Although there is more variation in experimental segment lengths, the model segment lengths fall close to the experimental data. In all 18 rays, for the segment ID numbers that appear in both data sets, 67% of the model segment lengths (180/268) fall within the error bars of the experimental data.

These results indicate a reasonably good fit between the model and experimental data for all fin rays; especially considering we only optimized the mechanism for joint formation on one ray. This implies that the developmental rules created by the mechanism of joint formation could be similar to what occurs *in vivo*.

Table 4.6 Results for the parameter optimization of the joint formation model. The five models presented provided the lowest Root Mean Square Error values based on the parameter ranges outlined in Table 4.5.

Parameter Values			Root Mean Square Error	Normalized Root Mean Square Error	Number of Segments
T_J	e	$\tilde{h}_r$			
0.0120	1.86	5.4	0.0268	0.1186	18
0.0115	1.90	6.0	0.0269	0.1189	18
0.0115	1.86	5.2	0.0269	0.1188	18
0.0115	1.88	5.6	0.0271	0.1199	18
0.0110	1.86	5.0	0.0275	0.1217	18

* T_F is the threshold for joint formation, e is the exponent in the rate of accumulation equation (6b) and $\tilde{h}_r$ is the coefficient in the same equation (6b).

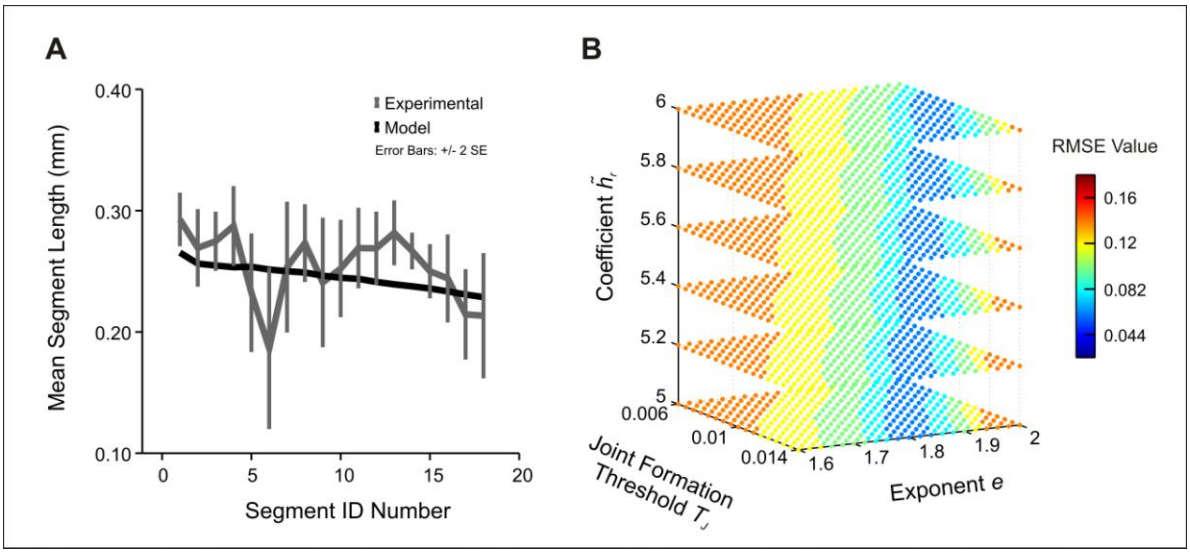

Figure 4.8. Results of the parameter optimization in the joint pattern formation mechanism. **A:** comparing segment length between model (black line) and experimental data (grey line) for ray 7. The parameter values used resulted in the lowest Root Mean Square Error (RMSE) value. **B:** the RMSE results for all parameter combinations used in the optimization. The range of parameters used in the optimization is listed in Table 4.5.

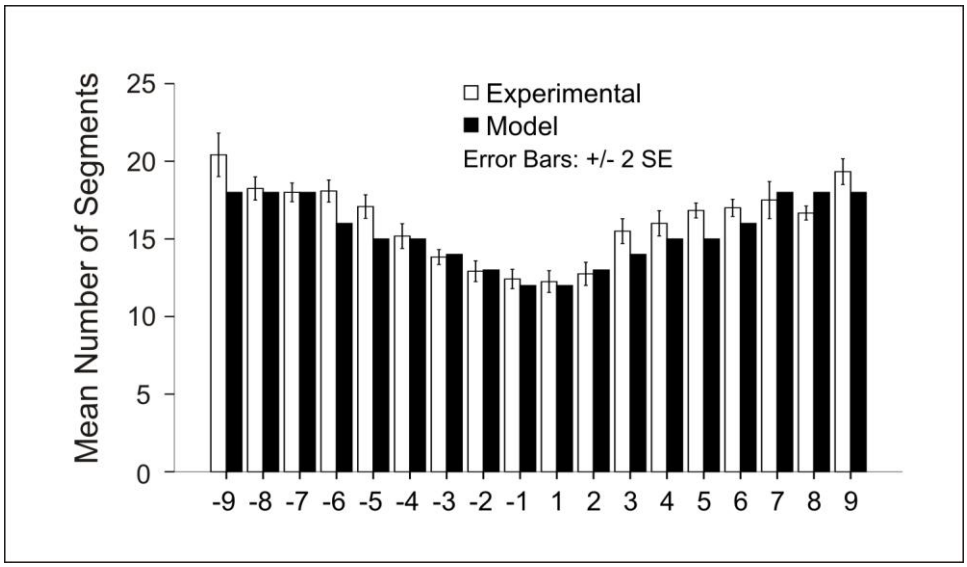

Figure 4.9. Comparison of segment numbers between the optimized parameters in the joint formation mechanism and experimental data for all rays within the fin. Model data is shown in black and experimental data is shown in white.

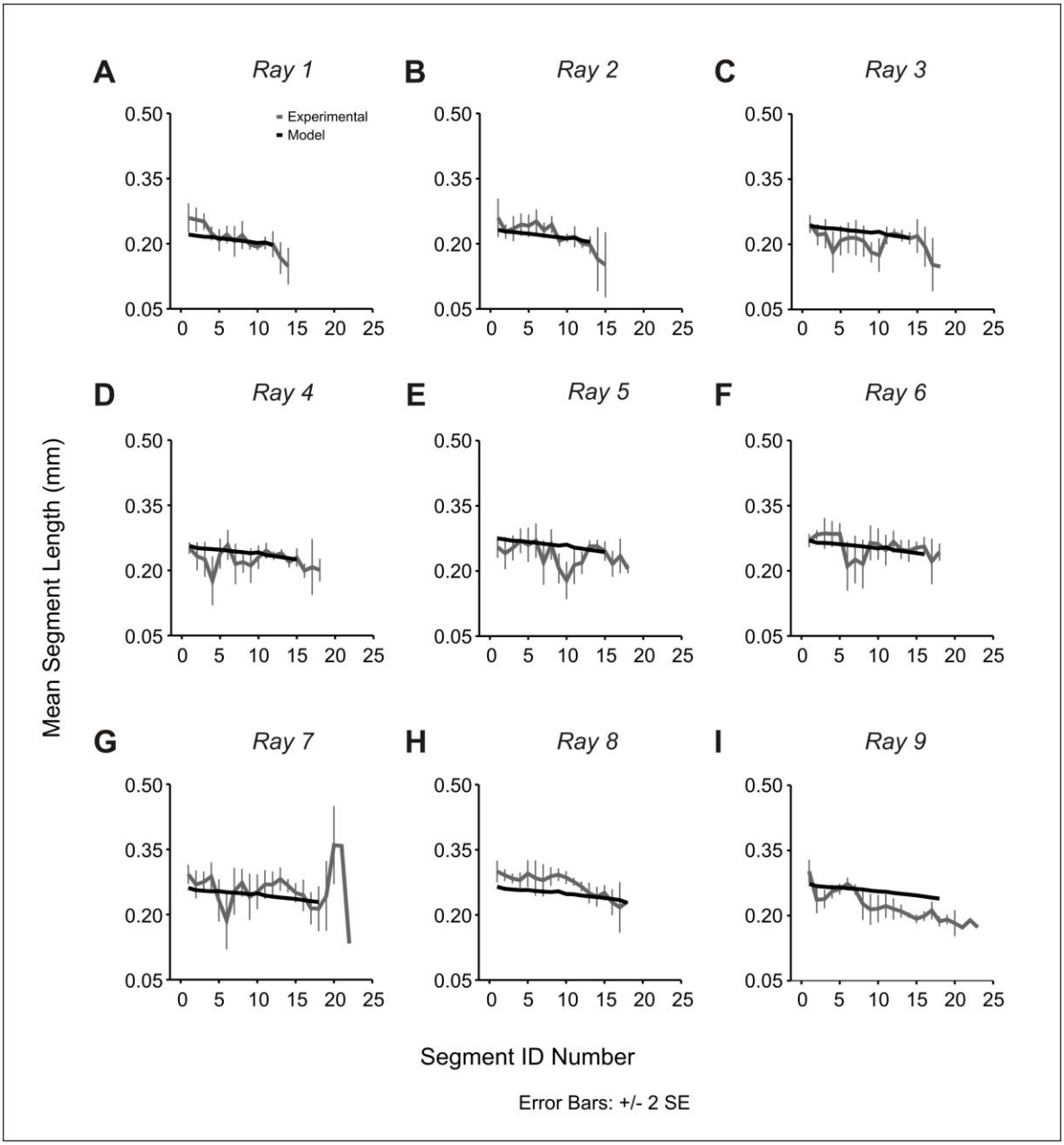

Figure 4.10. Comparing segment lengths between the model with optimized parameters in the joint formation mechanism and experimental data. Data is shown for the 9 rays on the ventral side of the fin. Experimental data is shown in grey, and model data is shown in black.

4.4.3 Bifurcation formation

For bifurcation formation, the best mechanism was equation 11a, which we modified to equation 11a – 2, where the rate of $B_{r,t}$ production varies in both space and time. Within this equation, we optimize the threshold for bifurcation formation T_B, and the new constant v in the equation (11a – 2). The range of parameter values we test are outlined in Table 4.5.

To perform the RMSE and NRMSE analysis, we compare model and experimental average S1 and S2 ray section lengths for all rays of the fin. Since the experimental data set contains little information on S3 ray sections, we exclude S3 data from the analysis. The RMSE and NRMSE give us similar results; therefore, we use the RMSE value for parameter selection.

We then compare the model S1 section lengths to the experimental S2 section lengths for all rays using RMSE analysis and NRMSE analysis. We average both S2 ray sections for each ray in the experimental and do the same for the model data. We then also perform RMSE and NRMSE analyses on the averaged S2 ray sections for all rays in the model and experimental data.

The parameter values for the five parameter combinations that resulted in the lowest RMSE values are provided in Table 4.7. The S1 and S2 ray section lengths for the parameter combination that resulted in the lowest RMSE value are shown in Figure 4.11A. The darker colors represent the model ray sections (S1 - black and S2 - green, respectively); and the lighter colors show the data for the experimental ray sections (S1 - white and S2 - light green, respectively). In panel 4.11B, the results of all the parameter combinations are illustrated as a surface. The threshold and constant values for each RMSE result are on the *x* and *y* axes, and the *z*-axis represents the RMSE values. The coloration of the surface simply allows better distinction between the different regions of the surface.

Table 4.7. Results for the parameter optimization of the bifurcation formation model. The five models presented provided the lowest Root Mean Square Error values based on the parameter ranges outlined in Table 4.5.

Parameter Values		**Root Mean Square Error for S1**	**Normalized Root Mean Square Error for S1**	**Root Mean Square Error for S2**	**Normalized Root Mean Square Error for S2**
T_B	v				
1.05	0.95	0.1412	0.0549	0.1709	0.0667
1.10	1.00	0.1415	0.0550	0.1718	0.0670
1.00	0.90	0.1418	0.0552	0.1709	0.0667
1.15	1.05	0.1427	0.0555	0.1731	0.0675
0.95	0.85	0.1438	0.0559	0.1697	0.0662

* T_B is the threshold for joint formation, and v is the new constant in the rate of accumulation equation (11a – 2).

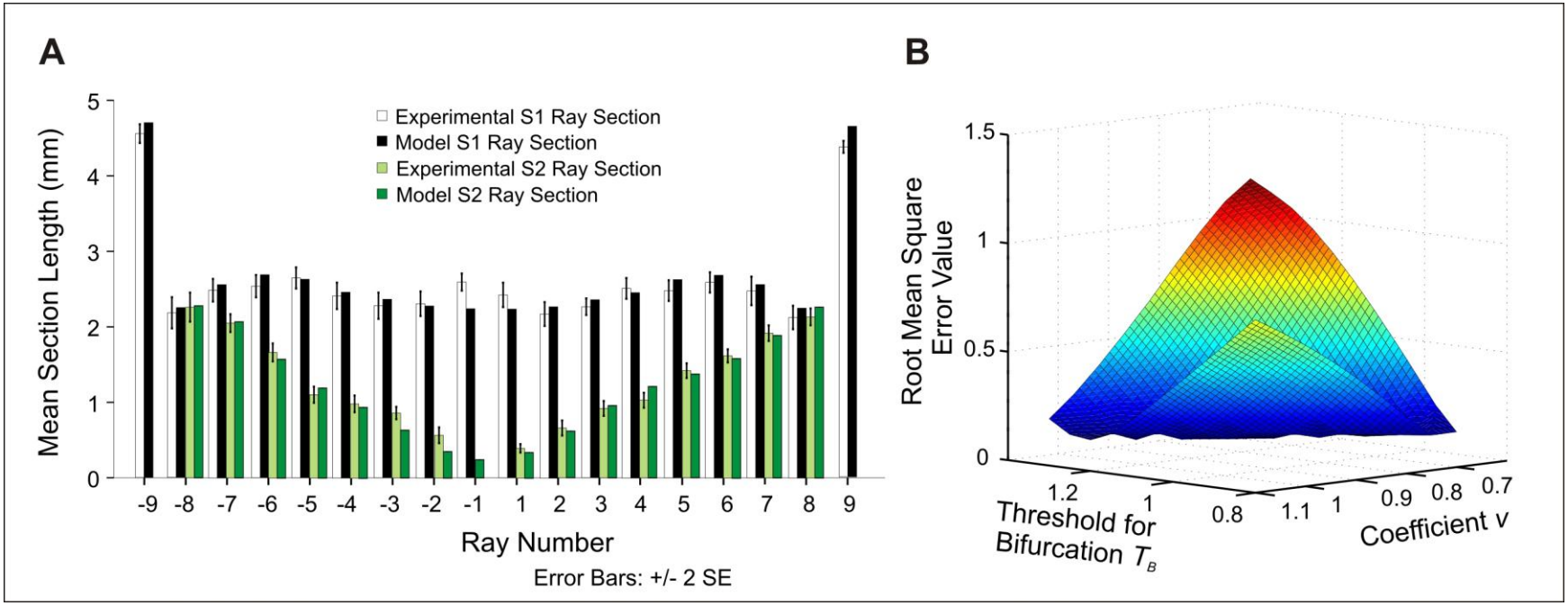

Figure 4.11. Results from the parameter optimization in the bifurcation patterning formation mechanism. **A:** shows ray section lengths for the S1 and S2 ray sections for the parameter values that resulted in the lowest RMSE values. **B:** shows the resulting RMSE values for each parameter combination; the coloration of the mesh allows distinction between the various regions. The parameter values are listed in Table 4.5.

4.5 Optimized Model

We created a model of fin ray growth for which we postulated mechanisms of joint and bifurcation formation. We then selected the appropriate joint and bifurcation mechanisms that recreated the correct trends in joint and bifurcation patterning. Both of the selected mechanisms for joint and bifurcation formation utilize the accumulation of patterning substances to a threshold to trigger joint or bifurcation formation. Parameter optimization improved the fit of the model ray patterning to the experimental ray patterning data, producing the final optimized model. The final model fin is visualized in Figure 4.12. This figure shows 18 bony rays, after 44 days of development (representing a fin aged 70.12 days). The mechanism for joint formation is based on the method of substance production described by equation 6b; where the rate of joint forming substance production $J_{r,t}$ decreases as a function of an equation with the same form as the equation for growth. Similarly, the mechanism for bifurcation formation is based on the method of substance production described by equation 11a; where the rate of bifurcation forming substance production decreases as a function of growth $B_{r,t}$. The parameter values assigned in the optimized version of the model are outlined in Table 4.8. A comparison of the growth rates, $J_{r,t}$ production rates, and $B_{r,t}$ production rates are shown in Figure 4.13. In Panel A we can see the values assigned at $t = 0$, and how they vary between rays in the fin. The change in the rates over time for one lateral ray (ray 7) is shown in Panel B.

Table 4.8. Parameter values assigned for the best model of ray growth. The best methods of joint and bifurcation pattern formation have had the parameters optimized and a visualization of the fin is shown in Figure 4.12.

	Value Assigned																	
	Ray Number																	
Parameter*	**-9**	**-8**	**-7**	**-6**	**-5**	**-4**	**-3**	**-2**	**-1**	**1**	**2**	**3**	**4**	**5**	**6**	**7**	**8**	**9**
$\rho s_{r,0}$	0.450	0.449	0.446	0.440	0.432	0.425	0.419	0.416	0.414	0.414	0.416	0.419	0.425	0.432	0.440	0.446	0.449	0.450
$\theta s_{r,0}$	2.174	2.094	2.020	1.951	1.883	1.813	1.742	1.681	1.608	1.534	1.460	1.400	1.328	1.259	1.191	1.121	1.048	0.968
$\rho b_{r,0}$	0.445	0.445	0.442	0.435	0.428	0.421	0.415	0.412	0.410	0.410	0.412	0.415	0.421	0.428	0.435	0.442	0.445	0.445
$\theta b_{r,0}$	2.174	2.094	2.020	1.951	1.883	1.813	1.742	1.681	1.608	1.534	1.460	1.400	1.328	1.259	1.191	1.121	1.048	0.968
$G_{r,0}$	0.287	0.292	0.282	0.260	0.233	0.207	0.183	0.160	0.151	0.157	0.176	0.202	0.223	0.244	0.260	0.271	0.275	0.283
X_r	-0.758	-0.667	-0.576	-0.485	-0.394	-0.303	-0.212	-0.136	-0.455	0.455	0.136	0.212	0.303	0.394	0.485	0.576	0.667	0.758
δ	0.001																	
$\tilde{h}_r$	5.400	5.400	5.400	5.022	4.590	4.536	4.320	3.942	3.672	3.672	3.942	4.320	4.536	4.590	5.022	5.400	5.400	5.400
t_0	26.120																	
e	1.860																	
T_J	0.012																	
$\tilde{p}_r$	0.531	0.475	0.418	0.399	0.409	0.437	0.456	0.475	0.485	0.485	0.475	0.456	0.437	0.409	0.399	0.418	0.475	0.531
T_B	1.050																	

* Where $\rho s_{r,0}$ and $\rho b_{r,0}$ represents the source point and bone point positions for ray r at time $t = 0$ respectively; $\theta s_{r,0}$ and $\theta b_{r,0}$ are the starting angles of the source and bone points for ray r at time $t = 0$ respectively; $G_{r,0}$ is the growth rate for ray r at time $t = 0$; X_r represents the amount of change in bone point position for ray r; δ is the decay constant for joint forming substance decay; $\tilde{h}_r$ is the decay constant for ray r in the equation for joint forming substance; T_J is the threshold for joint formation; e is the exponent in the equation for joint forming substance; t_0 represents the initial day of the model; $\tilde{p}_r$ is a constant assigned to ray r; and T_B is the threshold for bifurcation.

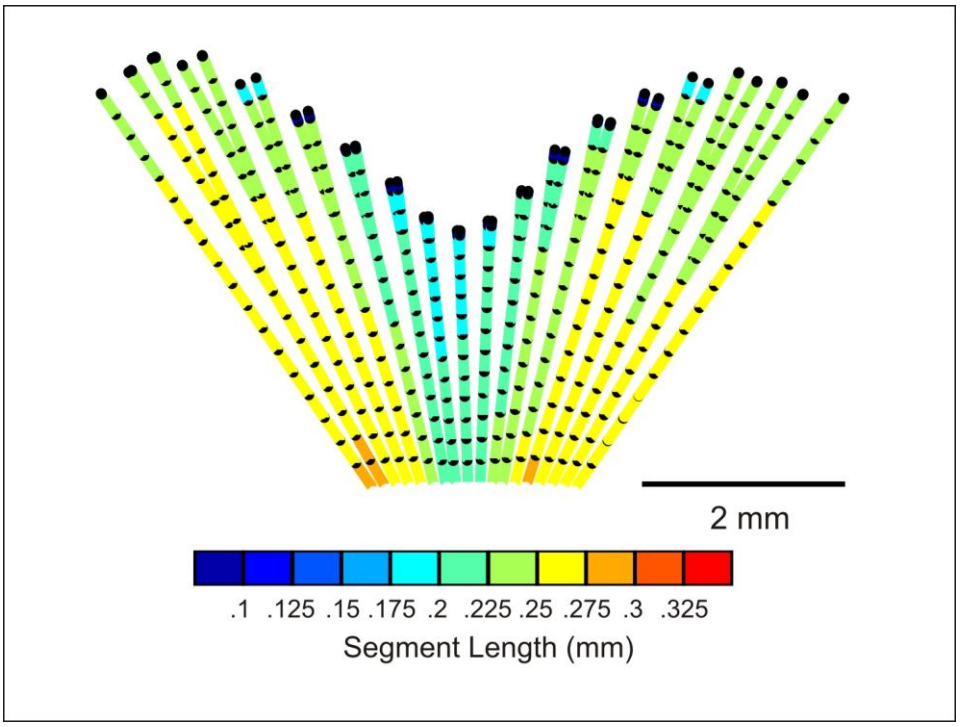

Figure 4.12. Fin visualization of the best model of ray growth and joint and bifurcation patterning. Segment colouration indicates segment length and black points represent joints or the distal tip of the ray. The mechanisms of joint and bifurcation formation are based on the accumulation of joint and bifurcation forming substances to a threshold; when the rates of accumulation vary in space and time. The mechanisms have been selected and parameters optimized to recreate experimental data as closely as possible. The model has been run for 18 rays and for 44 days.

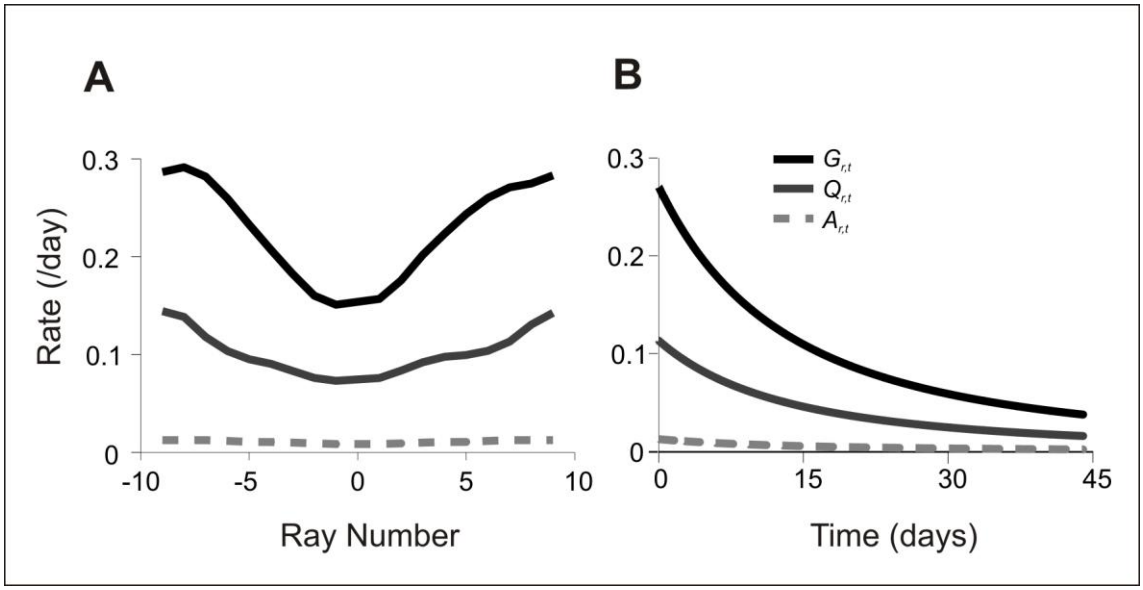

Figure 4.13. Graphical representation of growth, and production rates in the model. **A**: initial $G_{r,0}$ (growth), $A_{r,0}$ ($J_{r,t}$ production), and $Q_{r,0}$ ($B_{r,t}$ production) rates in the rays of the fin. **B**: $G_{r,t}$, $A_{r,t}$, and $Q_{r,t}$ rates over the length of the simulation for ray 7. Growth rates ($G_{r,t}$) are shown by black solid lines, $J_{r,t}$ production rates ($A_{r,t}$) are shown by dark grey solid lines, and $B_{r,t}$ production rates ($Q_{r,t}$) are shown by light grey dashed lines.

4.6 Parameter Variation

With this final model of joint and bifurcation patterning, we can now test the effect on fin shape and ray patterning when the parameters within the model are altered. Since there are numerous parameters that can be altered, we specifically look at altering the growth rates within the fin.

There is a variety of fin shapes and sizes found in nature. Not only between different species, but also within a single fish. If we compare the caudal fin of the killifish (*Fundulus heteroclitus*) to the zebrafish, we can see that the killifish has a mono-lobed fin, whereas the zebrafish has a bi-lobed fin (Nabrit 1929). In addition, from simple observation of the zebrafish itself, there are apparent differences in fin shapes between the paired pectoral and pelvic fins, as well as the anal, caudal and dorsal fins. The variation in fin shapes can be the result of differences in growth rates between rays in the fins (Goldsmith *et al.,* 2003, Goldsmith *et al.,* 2006, Rolland-Lagan *et al.*, 2012). Because joints and bifurcations are formed within growing fins, manipulating the model growth rates could drastically alter not only the fin shape and size, but also the patterning of the rays. In particular, segment length in the model relies heavily on the amount of bone development between joint formation events. Therefore, if we alter the rate of growth, joint patterns will no doubt be affected as a result.

However, the shape of the fin may not be solely due to the variation in growth between rays. The lepidotrichia of the fin are attached at their proximal end to the endoskeletal bones (Akimenko *et al.,* 2003); therefore, the position endoskeleton may influence fin shape. This concept is illustrated in Figure 4.14. Imagine a fin that has equal growth rates between rays. If the endoskeletal bones are positioned next to one another in a straight line, the fin would have a flattened shape (Fig. 4.14A). However, if we shift the positions of the endoskeletal bones, such that they slope upwards from left to right, the resulting fin shape would be sloped as well (Fig 4.14B). Therefore, it is possible that fin shape is also influenced by endoskeletal bone position. We can recreate this influence in the model by changing the base positions of the rays to reflect differences in endoskeletal bone

positions. However, further research is required to determine to what extent endoskeletal bone position has on fin shape.

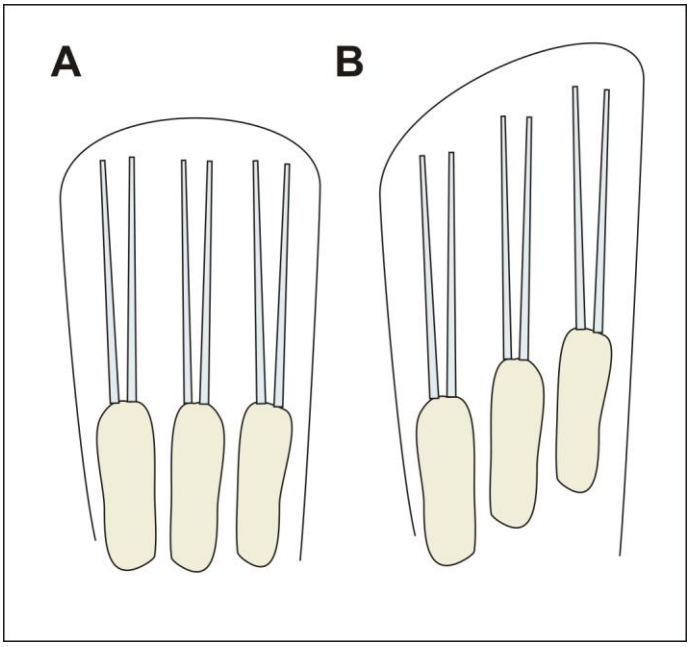

Figure 4.14 Schematic of the effect of endoskeletal bone position on fin shape. **A**: endoskeletal bones (light yellow) positioned in a straight line with lepidotrichia (light grey) attached, note that growth rates are equal among rays. **B**: endoskeletal bones positioned on an angle with lepidotrichia attached, note that growth rates are equal among rays.

Studies have shown that some fin length mutants, such as *alf* and *sof* (van Eeden *et al.,* 1996, Johnson and Bennet 1999, Iovine and Johnson 2000) have longer segments and rays or shorter segments and rays, respectively - linking joint formation and growth. This close link between growth and joint patterning has also been supported by the cellular model of ray growth and joint patterning presented by Rolland-Lagan *et al.* (2012). In particular, they propose that growth affects joint patterning, but joint patterning can be uncoupled from growth. The latter is supported by the *evx1* mutant, which lacks joints and has relatively normal ray lengths (Schulte *et al.,* 2011).

We test altering the growth rates between rays, as well as altering the growth rates globally (in all rays). The growth rates we assign to each variation are outlined in Table 4.9. The first three growth rates cause changes in fin shape by altering individual ray growth rates, and the last three growth rates cause changes in fin size by either globally increasing or decreasing the growth rates.

The results of the modeled fin when growth rates are altered are shown in Figure 4.15. Panels A-C show the effect on fin shape and joint and bifurcation patterning when the growth rate for each ray is varied independently. In A, we see the effect of equal growth rates among all rays. In B, the growth rates have been assigned such that the fastest growth rates are in the center of the fin, resulting in a mono-lobed fin. Finally, in C, we see the fin shape as described in the model, where the growth rates are fastest in the lobe rays, resulting in the typical bi-lobed caudal fin shape. Panels D-F illustrate the effect on fin size and joint and bifurcation patterning when the growth rates are altered equally in all rays. In D, we see the normal growth rates (as described above in this report), resulting in a wild-type fin. In E, the growth rates were reduced in all rays by 25%. Conversely, in F, we see the resulting ray and segment lengths in the fin when the growth rates are increased by 25% in all rays.

Through parameter variation we can attempt to predict joint and bifurcation patterns in various fish species, fin types and fish mutants. Although there is not a lot of quantitative data on the patterning of mutant zebrafish fins, we do know general trends in fin

morphology. For example, the *sof* mutant possesses shorter fin rays, as well as shorter segments than wild type, in addition to having fewer segments per ray (Johnson and Bennett, 1999, Iovine and Johnson 2000). If we examine Figure 4.15E, we can see that the model output exhibits these same properties in ray and segment length, as well as numbers of segments. Similarly, Figure 4.15F resembles the *alf* heterozygous fin mutant, which has longer than wild type rays and segments. However, no information is available on the number of segments within a ray in the *alf* heterozygote mutant; therefore, no qualitative comparisons can be made. Similarly, quantitative data on fin patterning in these mutants is not available; therefore, any comparison made is strictly qualitative.

Table 4.9. Growth rate used in the parameter variation tests. Fin visualizations can be found in Figure 4.15.

	$G_{r,0}$ **Values**																	
	Ray Number																	
Panel in Figure 4.X	**-9**	**-8**	**-7**	**-6**	**-5**	**-4**	**-3**	**-2**	**-1**	**1**	**2**	**3**	**4**	**5**	**6**	**7**	**8**	**9**
A	0.307	0.307	0.307	0.307	0.307	0.307	0.307	0.307	0.307	0.307	0.307	0.307	0.307	0.307	0.307	0.307	0.307	0.307
B	0.157	0.176	0.202	0.223	0.244	0.260	0.271	0.275	0.283	0.283	0.275	0.271	0.260	0.244	0.223	0.202	0.176	0.157
C	0.287	0.292	0.282	0.260	0.233	0.207	0.183	0.160	0.151	0.157	0.176	0.202	0.223	0.244	0.260	0.271	0.275	0.283
D	0.287	0.292	0.282	0.260	0.233	0.207	0.183	0.160	0.151	0.157	0.176	0.202	0.223	0.244	0.260	0.271	0.275	0.283
E	0.215	0.219	0.212	0.195	0.175	0.155	0.137	0.120	0.113	0.118	0.132	0.151	0.168	0.183	0.195	0.203	0.206	0.212
F	0.358	0.364	0.352	0.324	0.291	0.259	0.228	0.200	0.189	0.196	0.220	0.252	0.279	0.305	0.325	0.339	0.344	0.354

* Where $G_{r,0}$ is the growth rate for ray r at time $t = 0$.

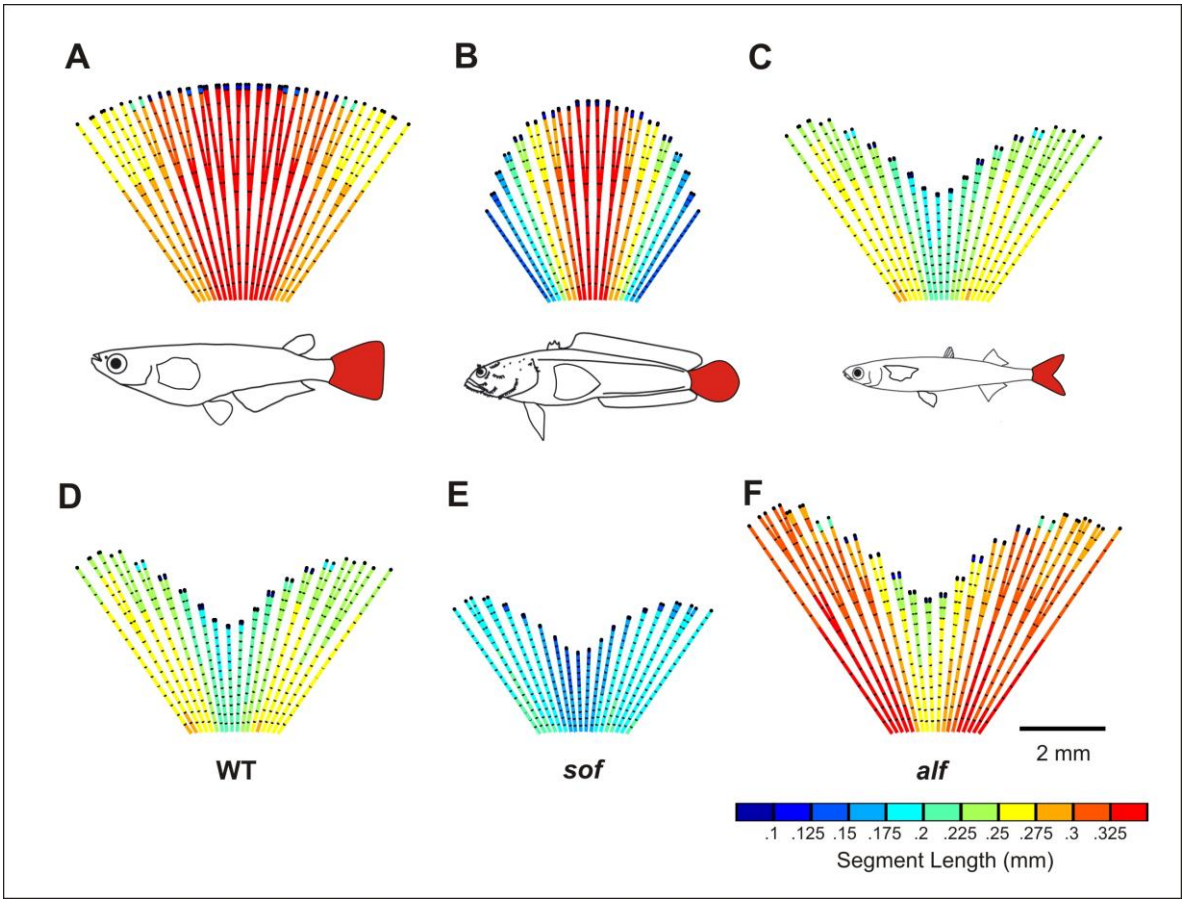

Figure 4.15. Fin visualizations for parameters variation tests. **A –C**: effect of changing the growth rate between rays on overall fin shape and joint and bifurcation patterning. Examples of teleostean orders with similar caudal fin shapes reproduced from Yamanoue *et al.* 2010 with permission from John Wiley and Sons (**A** – Beloniformes, **B** - Batrachoidiformes, **C** – Atheriniformes). **D-F:** effect on fin and segment length when the growth rates are maintained (**D**), when the rates are decreased by 25% in all rays (**E**) and when they are increased by 25% in all rays (**F**). Each model was run for 44 days on 18 rays. Parameter values are listed in Table 4.8.

Chapter 5 – Discussion

5.1 Model

5.1.1 Ray growth and Regeneration

Growth in the zebrafish fin is a highly dynamic process. Juvenile fin development begins continuous and allometric to body growth (Goldsmith *et al.*, 2006) and becomes saltatory and isometric to body growth with age (Goldsmith *et al.*, 2003). Multiple bursts of cell proliferation have been linked to the growth of the bony rays and variations in the frequency of proliferation bursts between rays underlie differences in length between rays (Jain *et al.*, 2007). A simulation model based on the transport of morphogens between compartments (representing cells or groups of cells) qualitatively accounts for observed growth patterns during fin ray development and regeneration (Rolland-Lagan *et al.*, 2012). However, output from this cellular model cannot be quantitatively compared to experimental data as the number of cells in real fin rays precludes modeling of whole fins at the cellular level. Here we decide to focus on a non-cellular, higher-level model that does not include cells but encompasses developmental rules and makes it possible to quantitatively compare model and experimental data.

Since a mechanism for the control of growth in the cellular model already exists, we focus on patterning of ray joints and bifurcations. Therefore, we incorporated growth rates from experimental data rather than model the mechanisms of growth. Similarly, we incorporate regenerative growth into the model using experimental regeneration rates. Although the amount of quantitative data on ray patterning during regeneration to which we can compare the model is lacking, this section of the model can be used to predict the patterning of joint and bifurcation in the regenerated ray.

This calibrated model of ray growth and regeneration provides a strong foundation upon which mechanisms of joint and bifurcation pattern formation can be tested, independent of the mechanism for growth.

5.1.2 Joint and Bifurcation Formation

Substance accumulation models for joint and bifurcation formation provide us with the easiest way to manipulate fin patterning. We can alter the rate of substance production in time and space, and thus we can test a variety mechanisms, such as a time-based mechanism (by keeping the rate of production constant over time). In addition, changing the rate of production over time can be modeled in any number of ways, i.e. linearly, exponentially, etc. This provides us with the opportunity to test multiple fin patterning models without drastically changing the core of the model.

Previous research showed that joint patterning and growth could be coupled (Sims *et al.*, 2009, Rolland-Lagan *et al.,* 2012). Moreover, simulation studies suggest that growth affects joint patterning, but joint patterning does not affect growth (Rolland-Lagan *et al.*, 2012). Therefore, we believe it is valid to investigate the mechanisms of joint pattern formation independently of the mechanisms of growth, but within the context of a growing fin.

Within the model, the lateral most rays do not bifurcate, as is the case experimentally. From studies done on ray-interray interactions, it was shown that the presence of interray tissue on either side of a ray is required for bifurcation (Murciano *et al.*, 2002). Since the rays in the leftmost and rightmost positions within the model are not surrounded by interray tissue, we simply exclude them from the bifurcation process. We believe this exclusion is valid, because we are not removing the capacity of the rays themselves to bifurcate, rather we are ensuring any ray in those positions will not. The rays in the outermost positions still produce and accumulate bifurcation forming substance ($B_{r,t}$); therefore, if these rays were to be grafted into positions with interray tissue on either side, they could form bifurcations. This matches the bifurcation potential of grafted rays seen in the study by Murciano *et al.* (2002).

Within the regenerative part of the model, the mechanism for joint and bifurcation patterning are the same as ontogenetic growth. However, the joint patterns that result from these mechanisms are not consistent with expected patterns. The regenerated segments distal to the amputation are considerably longer than those in the non-regenerated region of

the fin. In addition, the segments in the regenerate decrease in size much too quickly. Therefore, we increase the rate of $J_{r,t}$ production in the mechanism of joint formation to create an appropriate joint pattern in the regenerate. This implies that within the model presented here, growth affects segmentation. This is consistent with the model Rolland-Lagan *et al.* (2012) presented, where the mechanism for joint formation was partially dependent on the two morphogens that control ray growth.

Bifurcations have been documented to be distalized in regenerated fins (Géraudie *et al.,* 1994). In the model, this distalization is achieved without altering the mechanism for bifurcation formation between ontogeny and regeneration. Therefore, the mechanism in regeneration is identical to that in ontogeny.

The equation for joint substance production (equation 7b) in the model presented here that best recreates the trends and experimental data in ray patterning, has the same form as the equation for fin growth:

$$\tilde{A}_{r,t} = \frac{\tilde{h}_r}{(t+t_0)^e} \qquad (7b)$$

The cellular model presented by Rolland-Lagan *et al.* (2012) suggested the control of growth was dependent on the interaction of two morphogens – as outlined in Section 1.6.1. This model suggested that the control of growth and joint formation was dependent on the interaction of multiple morphogens. The growth curve, determined from experimental data, presented in this model (as described by equation 1) has a similar shape to that obtained in the cellular model. This suggests that our equation for growth could represent the result of morphogen interactions. Similarly, the equation used in our joint formation mechanism follows a similar shape, therefore, it could also be consistent with the role of morphogen interactions in the control of joint formation. Since the equation for growth (equation 1) represents the interaction of two morphogens, this equation for joint formation (equation 7b) suggests the interactions of morphogens could be involved in the formation of joints. The cellular model supports this as well, because joint formation is the result of morphogen interaction (Rolland-Lagan *et al.*, 2012).

We describe the substances for joint and bifurcation formation being produced, accumulating to a threshold, and inducing either joint or bifurcation formation. However, the specific action of the substance *in vivo* is unclear. The model presented by Rolland-Lagan *et al.* (2012) suggests that the morphogen involved in joint formation is an inhibitory substance. Within this whole fin model, we can alter the model such that the joint forming substance has an inhibitory effect. A source of joint forming substance can be present at the base of each ray, as well as at each joint along the ray. These substances could have an inhibitory effect at a high concentrations near the sources (i.e. preventing joint formation near one another), and only through diffusion or degradation of these substances below threshold, will a joint or bifurcation be able to form. This is converse to the model presented here, in which the joint forming substance induces joint formation. The reason we choose not to model an inhibitory joint forming substance is that the inductive mechanism currently in use recreates the appropriate trends in joint patterning. The purpose of this model is not to explain the cellular interactions between these patterning substances and the tissues they affect (i.e. whether they are inductive or inhibitory). Rather, the model attempts to determine the developmental rules behind joint formation to produce accurate joint and bifurcation patterns. The substances presented in this model ($B_{r,t}$ and $J_{r,t}$) reflect the potential to form a joint or bifurcation. As mentioned earlier, the equation used for the joint formation mechanism suggests the interaction of multiple morphogens in joint formation. Similarly, the equation for growth is dependent on the equation for growth (which also represents the interaction of morphogens). Therefore, these substances could represent part of the pathway responsible for joint and bifurcation formation. Further targets may have inhibitory actions similar to those presented by Rolland-Lagan *et al.* (2012).

We refrain from presenting the joint and bifurcation forming as any substances or morphogens currently known to play a role in fin patterning. This is because the substances involved in joint and bifurcation formation are not well known. Multiple genes have been linked to both processes, but it is unclear whether these genes are responsible for the formation of joints and bifurcations, or whether factors up- or down-stream of these genes

are responsible. However, we can postulate candidates for the joint and bifurcation forming substances based on the current literature.

There are two candidate substances for the joint formation substance in the model, and they are cx43 and evx1. In the current model (i.e. with the joint forming substance increasing in concentration and inducing joint formation), we postulate that the joint forming substance represents *evx1*. We do not believe it represents *cx43* because in fin mutants with altered *cx43* levels (*sof* and *alf*), not only do they exhibit altered segment length, but also altered fin length (Iovine *et al.*, 2005, Sims *et al.*, 2009). Within the model, the mechanism of joint formation does not affect growth. Therefore, if we were to alter the joint formation mechanism in the model to increase the levels of joint forming substance, segment length will be altered; however, we would not see the appropriate change in ray length.

On the other hand, *evx1* mutants, which lack evx1 function, have no joints in their rays and their fins are of normal length. In the model, if we prevent the production of joint forming substance we can achieve this phenotype. Further, *evx1* is expressed at the position of each joint in the rays (Schulte *et al.*, 2011), which could indicate that it is involved in joint formation, not necessarily in determining the position of the joint. Therefore, *evx1* is a possible candidate for the joint forming substance in the model.

Far less is known about the substances involved in bifurcation formation within the fin. *Shh*, its receptor *ptc1* and a downstream target of *shh*, *bmp2b*, have all been linked to the formation of bifurcations. However, we can hypothesize that the bifurcation forming substance in the model is *shh*. Ectopic expression of *Shh* has been shown to fuse branches of bifurcations, and the splitting of endogenous *shh* expression domains before bifurcation imply a strong link between *shh* and bifurcation induction (Laforest *et al*., 1998, Akimenko *et al.*, 2003). In the model, the splitting of the source of bifurcation forming substance results in the splitting of the bony ray. In addition, if we ectopically express *shh* in the model, we could induce bifurcation or fuse branch, since the bone points can detect multiple sources of bifurcation forming substance.

An important aspect of modelling, is learning from the models that did not give us the results expected. For the mechanism of joint and bifurcation formation, we tested the situation where they both formed at given time intervals (in the Appendix). We determined that these mechanisms are not sufficient to reproduce the fin patterns expected, so we rejected them. Although simplicity is aimed for when creating models, simple mechanism may not always be able to explain the phenomena of interest. Many different substances have been shown to interact in joint and bifurcation formation (Laforest *et al.,* 1998, Borday *et al.,* 2001, Quint *et al.,* 2002, Akimenko *et al.,* 2003, Iovine *et al.,* 2005, Sims *et al.,* 2009, Schulte *et al.,* 2011, Rolland-Lagan *et al.,* 2012); therefore, a mechanism based solely on time in unlikely. Similarly, for both the mechanisms of joint and bifurcation formation we tested situations where the rate of patterning substance production did not vary between rays. In most cases, this resulted in little variation in segment length or bifurcation location between rays, which is not what is expected. We know that growth rates vary between rays; therefore, it is likely that other substances or properties (such as segmentation and bifurcation) also vary between rays. Finally, from the bifurcation mechanism, we learned that the concentration of bifurcation forming substance needs to be reset to zero after bifurcation. Initially, we postulated the concentration of bifurcation forming substance to be split in half (with half being allocated to each source point) after bifurcation; however, this did not reproduce the correct bifurcation pattern. Rather, the substance needs to be completely depleted, and production begin anew, for proper S2 ray section lengths. This could indicate that the bifurcation forming substance is consumed in the formation of the bifurcation, Since we know that *shh* expression domains persist after bifurcation (Laforest *et al.,* 1998, Borday *et al.,* 2001, Quint *et al.,* 2002, Akimenko *et al.,* 2003), perhaps our bifurcation substance does not represent *shh* or that it is really another substance (acting downstream of *shh*) that is responsible for bifurcation.

5.2 Future Directions

5.2.1 Improvements to the Model

There is a lack of quantitative experimental data on the rates of regeneration and the length of regeneration; often the rate of regeneration is only stated as being more rapid than ontogenetic development. Regeneration is a highly variable process that depends on a variety of environmental factors. The rate of regeneration and development can vary depending on age of the fish (Nabrit 1929), ambient water temperature (Johnson and Weston 1995), and amputation level (Morgan 1902, Tassava and Goss 1966, Lee *et al.*, 2005). There is also a lack of quantitative information on the patterning of joint and bifurcations in the regenerated rays.

We use a small experimental data set on regeneration to calibrate regenerative growth in the model; however, it does not encompass the variability associated with regeneration. To this end, regeneration experiments have been conducted in the laboratory to determine the rates of regeneration at various amputation levels, the patterning of joints and bifurcations in the regenerate, and the length of time required for complete regeneration. However, the results of these experiments have not yet been processed for use in the model.

Once these data are available, we can improve fin regeneration in the model. We can incorporate various rates of regeneration, dependent on amputation level; be able to make quantitative comparisons between regenerate joint and bifurcation patterns and model regenerate patterns; and ensure regeneration occurs in an appropriate amount of time. From the comparisons between model and experimental data of joint and bifurcation patterning in the regenerate, we will be able to determine whether the mechanisms from ontogenetic development for joint and bifurcation pattern formation would be able to recreate the appropriate patterns in regeneration. If not, what alterations to the mechanisms would recreate these patterns?

5.2.2 Model Predictions

Little information is available on fin patterning in fins beyond the caudal fin. Because the caudal fin is readily accessible, it allows for easier imaging and manipulation during experimentation. However, all the fins in the fish are composed of the same exoskeletal elements (Akimenko *et al.*, 2003) and therefore it can be assumed that the processes of joint and bifurcation formation may be similar in each type of fin. A property of theoretical models is that if they are based on solid experimental data, they can have predictive power (Kholodenko *et al.,* 2005). Therefore, we can alter the model to recreate various fin types (pectoral, pelvic, anal, or dorsal) and predict the patterning of joints and bifurcations in the bony rays.

Thanks to new custom-made programs created by Rolland-Lagan *et al.* (*in prep*), we have a methodology for extracting quantitative data on fin patterns on any type or shape of fin. This methodology uses time-lapse images of the fin and digitizing programs to convert an image of the fin into a computational representation. Data analysis programs can then extract various quantitative fin pattern data. Some examples of the fin pattern variables that can be extracted include: segment numbers, segment lengths, ray section lengths (eg. S1, S2, S3), ray lengths, ray base positions, fin lengths, fin area, fin width, and the position of bifurcations.

To test whether or not the model of ray patterning has predictive power, we can alter the growth rates between rays (similar to Figure 4.15A-C) to recreate different fin shapes, such as a pectoral, pelvic, anal or dorsal fin. Then, through the collection of experimental fin pattern data using the methodology briefly described above, we can compare how well the model joint and bifurcation patterning fits with the experimental ray patterning.

Similarly, we can attempt to model the caudal fins of different fin species. For example, we can create a mono-lobe fin, similar to the killifish, and compare joint and bifurcation patterns between experimental and model data. Alternatively, we can compare the model fin mutants (Figure 4.15E and F) to the experimental fin mutants. We are able to manipulate the parameters in the model to recreate fin outputs that resemble the mutants *sof*

and *alf* already, but additionally we can attempt to recreate other fin mutants by altering other parameters within the model.

This comparison of the various model fins to experimental data can provide insight into the mechanisms responsible for joint and bifurcation patterning, in addition to illustrating how these mechanisms may differ depending on fin type, species or mutation.

5.2.3 Multi-level Modelling

To create a true model of joint and bifurcation pattern formation, we would need to incorporate the mechanisms of growth control, joint formation, and bifurcation into one single model. A single model describing the mechanisms of growth and patterning at the tissue level, including the signalling between cells, would be the closest model to biological reality. However, this would be too computationally intensive. Therefore, we need to either limit the size of the model, or limit its detail. We can either create a model that describes this cell-to-cell signalling in a limited number of cells, or restrict the level of detail (i.e. not model cell-to-cell signalling) and maintain the same scale. However, there are downfalls to either method. In the small-scale, detailed model, we cannot perform quantitative comparisons between experimental and model data. In the large-scale, general model, we can make these comparisons; however, the interactions of morphogens cannot be determined.

Therefore, to overcome the weaknesses of each model type, we can use a combination of the two models. We can use a cellular-level model to determine the mechanisms of growth and patterning, and a higher-level model, which uses fin development rules that recreate the patterns in the cellular level model, to quantitatively compare experimental and model data.

The model presented here of fin ray patterning is a high-level, whole-fin ray, particle model of ray growth, testing mechanisms of joint and bifurcation pattern formation. We make no assumptions about the mechanics of growth, nor try to identify specific cellular interactions involved in the processes of joint and bifurcation formation. Rather,

patterning rules are implemented, and quantitative data on fin ray patterns can be extracted and compared to experimental data.

In parallel to this particle model, Rolland-Lagan *et al.* (2012) created a cell-based theoretical model of growth and joint formation in the zebrafish caudal fin during ontogenetic and regenerative growth. In the model, ray growth and regeneration are controlled by the interaction of two morphogens, and joint formation is controlled by the interactions of these two morphogens in addition to a third. Qualitative results from the theoretical model on fin size, fin shape, and joint patterning provide support for the mechanisms of growth control and joint formation proposed.

For growth control and joint formation, we have models on each level, the cellular and the whole fin ray level. However, the mechanism for bifurcation formation is only tested at the whole-fin ray level. Therefore, to complete our understanding of the mechanisms involved in fin development, a cellular level model of ray bifurcation needs to be created.

From the literature, we know that *shh* and the presence of interray tissue play important roles in bifurcation, so we can begin building the model from that information. We can also examine the role of *shh* in other systems, such as trachea branching in mammalian lungs, to further identify its role in bifurcation patterning. *bmp2* has also been shown to be expressed in a coordinated fashion with *shh*, and it has been implicated in the formation of bifurcations by inducing synthesis of lepidotrichial matrix (Laforest *et al.*, 1998); therefore, it could be worthwhile to investigate other members of the Shh signalling pathway.

Chapter 6 – Conclusions

Here we present a whole-fin ray level theoretical model of fin ray joint and bifurcation pattern formation. We test multiple mechanisms of joint and bifurcation pattern formation and determine that the mechanisms that recreates experimental patterns of joint and bifurcations the best are based on the production of patterning substances to threshold. Within these mechanisms, we test various methods of substance production and conclude that when the rate of production of these substances varies in space and time, the joint and bifurcation patterns are best achieved. Finally, we optimize the parameters in the mechanisms of joint and bifurcation formation to ensure the best fit between the model and experimental data. Overall, the model ray pattern parameters fit reasonably well with the experimental ray pattern parameters, with greater than half the model data falling within the error bars associated with the experimental data.

Future work on the model would incorporate more accurate regeneration rates, taking into account the variation in regeneration rates between proximal and distal amputations as well as age variations. In addition, once quantitative experimental data on fin patterns have been collected, the regenerate joint and bifurcation patterns in the model can be compared to the experimental data to determine whether they have been accurately recreated in the model. If so, further support will be provided to the mechanisms of joint and bifurcation patterning, and the model can be used to predict the joint and bifurcation patterns in various size and shaped fins. From this, we can investigate whether the mechanisms of joint and bifurcation patterns in the zebrafish caudal fin also apply to other fin types, fish species and fish mutants.

Chapter 7 – Bibliography

Akimenko M.-A. and Ekker M. (1995). Anterior Duplication of the *Sonic hedgehog* Expression Pattern in the Pectoral Fin Buds of Zebrafish Treated with Retinoic Acid. *Developmental Biology* **170**: 243-247.

Akimenko M.-A., Marí-Beffa M., Becerra J., Géraudie J. (2003). Old Questions, New Tools, and Some Answers to the Mystery of Fin Regeneration. *Developmental Dynamics* **226**: 190-201.

Ashe G.L., and Briscoe J. (2006). The Interpretation of Morphogen Gradients. *Development* **113**: 358-394.

Bard J.B.L. (1977). A Unity Underlying the Different Zebra Striping Patterns. *Journal of Zoology, London* **183**:527-539.

Baur S.T., Mai J.J., Dymecki S.M. (2000). Combinatorial Signaling Through BMP Receptor IB and GDF5: Shaping of the Distal Mouse Limb and the Genetic of Distal Limb Diversity. *Development* **127**: 605-619.

Becerra J., Junqueira L.C.U., Bechara I.J., Montes G.S. (1996). Regeneration of Fin Rays in Teleosts : A Histochemical. Radioautographic, and Ultrastructural Study. *Archives of Histology and Cytology* **59 (1):** 15-35.

Becerra J., Montes G.S., Bexiga S.R.R., Junqueira L.C.U. (1983). Structure of the Tail Fin in Teleosts. *Cell Tissue Research* **230**: 127–137.

Borday V., Thaëron C., Avaron F., Brulfert A., Casane D., Laurenti P., Géraudie J. (2001). *evx1* Transcription in Bony Fin Rays Segment Boundaries Leads to a Reiterated Pattern During Zebrafish Fin Development and Regeneration. *Developmental Dynamics* **220**: 91-98.

Branney P.A., Faas L., Steane S.E., Pownall M.E., Isaacs H.V. (2009). Characterisation of the Fibroblast Growth Factor Dependent Transcriptome in Early Development. *PloS One* 4(3) : e4951.

Broussonet M. (1786). Observations sur la Régénération de Quelques Parties du Corps des Poissons. *Mémoires de L'Académie Royale* 684-688.

Dale K.J., Pourquié O. (2000). A Clock-Work Somite. *BioEssays* **22** :72-83.

Géraudie J., Brulfert A., Monnot M.J., Ferretti P. (1994). Teratogenic and Morphogenetic Effects of Retinoic Acid on the Regenerating Pectoral Fin in Zebrafish. *The Journal of Experimental Zoology* **269**: 12-22.

Géraudie J., Monnot M.J., Brulfert A., Ferreti P. (1995). Caudal Fin Regeneration in Wild Type and *long-fin* Mutant Zebrafish is Affected by Retinoic Acid. *International Journal of Developmental Biology* **39**: 373-381.

Goldsmith M.I., Fisher S., Waterman R., Johnson S.L. (2003). Saltatory Control of Isometric Growth in the Zebrafish Caudal Fin is Disrupted in *long fin* and *rapunzel* Mutants. *Developmental Biology* **259**: 303-317.

Goldsmith M.I., Iovine M.K., O'Reilly-Pol T., Johnson S.L. (2006). A Developmental Transition in Growth Control During Zebrafish Caudal Fin Development. *Developmental Biology* **296**: 450-457.

Goss R.J. and Stagg M.W. (1959). The Regeneration of Fins and Fin Rays in *Fundulus heteroclitus*. *Journal of Experimental Zoology* **136(3)**: 487-507.

Haas H.J. (1962). Studies on Mechanisms of Joint and Bone Formation in the Skeleton Rays of Fish Fins. *Developmental Biology* **5**: 1-34.

Haffter P., Granato M., Brand M., Mullins M.C., Hammerschmidt M., Kane D.A., Odenthal J., van Eeden F.J.M., Jiang, Y.-J., Heisenberg C.-P., Kelsh R.N., Furutani-Seiki M., Vogelsang E., Beuchle D., Schach U., Fabian C., Nüsslein-Volhard C. (1996). The Identification of Genes with Unique and Essential Functions in the Development of the Zebrafish, *Danio rerio*. *Development* **123**: 1-36.

Ingham P.W., McMahon A.P. (2001). Hedgehog Signalling in Animal Development: Paradigms and Principles. *Genes and Development* **15**: 3059-3087.

Iovine M.K. (2007). Conserved Mechanisms Regulate Outgrowth in Zebrafish Fins. *Nature Chemical Biology* **10(3)**: 613-618.

Iovine M.K., Higgins E.P., Hindes A., Coblitz B., Johnson S.L. (2005). Mutations in *connexin43* (*GJA1*) Perturb Bone Growth in Zebrafish Fins. *Developmental Biology* **278**: 208-219.

Iovine M.K., Johnson S.L. (2000). Genetic Analysis of Isometric Growth Control Mechanisms in the Zebrafish Caudal Fin. *Genetics* **155**: 1321-1329.

Jain I., Stroka C., Yan J., Huang W.-M., Iovine M.K. (2007). Bone Growth in Zebrafish Fins Occurs via Multiple Pulses of Cell Proliferation. *Developmental Dynamics* **236**: 2668-2674.

Johnson S.L. and Weston J.A. (1995). Temperature-Sensitive Mutations That Cause Stage-Specific Defects in Zebrafish Fin Regeneration. *Genetics* **141**:1583-1595.

Johnson S.L., and Bennett P. (1999). Growth Control in the Ontogenetic and Regenerating Zebrafish Fin. *Methods in Cell Biology* **59**: 301-311.

Kholodenko B. N., Bruggeman F.J., Sauro H.M. Mechanistic and Modular Approaches to Modeling and Inference of Cellular Regulatory Networks. In Alberghina, Lilia; Westerhoff, Hans V., Systems Biology: Definitions and Perspectives. *Topics in Current Genetics* **13**, Berlin: Springer-Verlag, 2005, pp. 357–451.

Kondo S., and Asai R. (1995). A Reaction-Diffusion Wave on the Skin of the Marine Angelfish *Pomacanthus*. *Nature* **376**: 765-768.

Korc M., ana Friesel R.E. (2009) The Role of Fibroblast Growth Factors in Tumor Growth. *Current Cancer Drug Targets* **9(**5): 639-651.

Laforest L., Brown C.W., Poleo G., Géraudie J., Tada M., Ekker M., Akimenko M.-A. (1998). Involvement of the *Sonic Hedgehog, patched 1* and *bmp2* Genes in Patterning of the Zebrafish Dermal Fin Rays. *Development* **125**: 4175-4184.

Lee Y., Grill S., Sanchez A., Murphy-Ryan M., Poss K.D. (2005). Fgf Signalling Instructs Position-Dependent Growth Rate During Zebrafish Fin Regeneration. *Development* **132**: 5173-5183.

Marí-Beffa M., Mateos I., Palmqvist P., Becerra J. (1996). Cell to Cell Interactions During Teleosts Fin Regeneration. *International Journal of Developmental Biology* **Suppl.1**: 179S-180S.

Marí-Beffa, M., Plamqvist P., Marín-Girón F., Montes G.S., and Becerra J. (1999). Morphometric Study of the Regeneration of Individual Rays in Teleost Tail Fins. *Journal of Anatomy* **195**: 393-405.

Macdonald P.M., Ingham P., Stuhl G. (1986). Isolation, Structure and Expression of *Even-skipped* Gene of Drosophila Containing a Homeo Box. *Cell* **47(5)**: 721-734.

Morgan T.H. (1902). Further Experiments on the Regeneration of the Tail of Fishes. *Archiv für Entwicklungsmechanik der Organismen* **14**:539–561.

Murciano C., Fernández T.D., Durán I., Maseda D., Ruiz-Sánchez J., Becerra J., Akimenko M.-A., Marí-Beffa M. (2002). Ray–Interray Interactions During Fin Regeneration of *Danio rerio. Developmental Biology* **252**, 214–224.

Nabrit S.M. (1929). The Role of the Fin Rays in the Regeneration in the Tail-Fins of Fishies (in *Fundulus* and Goldfish). *Biological Bulletin* **56(4)**: 235-266.

Nomura R., Kamei E., Hotta Y., Konishi M., Miyake A., Itoh N. (2006). Fgf16 is Essential for Pectoral Fin Bud Formation in Zebrafish. *Biochemical and Biophysical Research Communications* **347**: 340-346.

Pepicelli C.V., Lewis P.M., McMahon A.P. (1998). Sonic Hedgehog Regulates Branching Morphogenesis in the Mammalian Lung. *Current Biology* **8(19)**: 1083-1086.

Poss K.D., Keating M.T., Nechiporuk A. (2003) Tales of Regeneration in Zebrafish. *Developmental Dynamics* **226**: 202–210.

Poss K.D., Shen J., Nechiporuk A., McMahon G., Thisse B., Thisse C., Keating M.T. (2000). Roles for Fgf Signalling During Zebrafish Fin Regeneration. *Developmental Biology* **222**: 347-358.

Pourquié O. (2003). The Segmentation Clock: Converting Embryonic Time into Spatial Pattern. *Science* **301**:328-330.

Quint E., Smith A., Avaron F., Laforest L., Miles J., Gaffield W., Akimenko M.-A. (2002). Bone Patterning is Altered in the Regenerating Zebrafish Caudal Fin After Ectopic Expression of *sonic hedgehog* and *bmp2b* or Exposure to Cyclopamine. *PNAS* **99(13)**: 8713-8718.

Rafal W., Witold D. Computational Science – ICCS 2008: Particle Based Model of Tumor Progression Stimulated by the Process of Angiogenesis. Springer Berlin/Heidelberg 2008 pp. 177 – 186,

Risau W. (1997). Mechanisms of Angiogenesis. *Nature* **386**: 671-674.

Roellig D., **Morelli L.G., Ares A., Jülicher F., Oates A.C.** (2011). Enhanced SnapShot: The Segmentation Clock. *Cell* **145**(5): 800.

Rolland-Lagan A.-G., Paquette M., Tweedle V., Akimenko M.-A. (2012). Morphogen-Based Simulation Model of Ray Growth and Joint Patterning During Fin Development and Regeneration. *Development* **139**: 1188–1197.

Santamaría J.A. and Becerra J. (1991). Tail Fin Regeneration in Teleosts: Cell-Extracellular Matrix Interaction in Blastemal Differentiation. *Journal of Anatomy* **176**: 9-21.

Schebesta M., Lien C.-L., Engel F.B., Keating M.T. (2006). Transcriptional Profiling of Caudal Fin Regeneration in Zebrafish. *The Scientific World Journal* **6(S1)**: 38-54.

Schwank G., and Basler K. (2010). Regulation of Organ Growth by Morphogen Gradients. *Cold Spring Harbor Perspectives in Biology* **2(1)**: 1-16.

Scott G.G. (1907) Further Notes on the Regeneration of the Fins of *Fundulus heteroclitus*. *The Biological Bulletin* **12**: 385-400.

Schulte C.J, Allen C., England S.J., Juárez-Morales J.L., Lewis K.E. (2011). Evx1 is Required for Joint Formation in Zebrafish Fin Dermoskeleton. *Developmental Dynamics* **240**: 1240-1248.

Sims Jr. K., Eble D.M., Iovine M.K. (2009). Connexin43 Regulates Joint Location in Zebrafish Fins. *Developmental Biology* **327**: 410-418.

Storm E.E., and Kingsley D.M. (1996). Joint Patterning Defects Caused by Single and Double Mutations in Members of the Bone Morphogenetic Protein (BMP) Family. *Development* **122**: 3969-3979.

Szebenyi G., and Fallon J.F. (1999) Fibroblast Growth Factors as Multifunctional Signaling Factors. *International Review of Cytology* **185**: 45-106.

Tal T.L., Franzosa J.A., Tanjuay R.L. (2010) Molecular Signaling Netowrks That Choreograph Epimorphic Regeneration in Zebrafish – A Mini-Review. *Gerontology* **56**(2): 231-240.

Tassava R.A. and Goss R.J. (1966). Regeneration Rate and Amputation Level in Fish and Lizard Tails. *Growth* **30**: 9-12.

van Eeden F.J.M., Granato M., Schach U., Brand M., Furutani-Seiki M., Haffter P., Hammerschmidt M., Heisenberg C.-P., Jiang Y.-J., Kane D.A., Kelsh R.N., Mullins M.C., Odenthal J., Warga R.M., Nüsslein-Volhard C. (1996). Genetic Analysis of Fin Formation in the Zebrafish, *Danio rerio*. *Development* **123**: 255-262.

Willmott C.J., and Matsuura K. (2005). Advantages of the Mean Absolute Error (MAE) Over the Root Mean Square Error (RMSE) in Assessing Average Model Performance. *Climate Research* **30**: 79-82.

Wolpert L. (1969). Positional Information and the Spatial Pattern of Cellular Differentiation. *Journal of Theoretical Biology.* **25**: 1-47.

Wolpert L. Principles of Development, second edition., Oxford University Press, New York, 2002.

Xiao Y.-T., Xiang L.-X., Shao J.-Z. (2007). Bone Morphogenetic Protein. *Biochemical and Biophysical Research Communications* **326**: 550-553.

Yamaoue Y., Setiamarga D.H.E., Matsuura K. (2010). Pelvic Fins in Teleosts: Structure, Function and Evolution. *Journal of Fish Biology* **77**: 1173-1208.

Chapter 8 – Appendices

8.1 Starting Angles and Positions

To determine the angles ($\theta_{r,0}$) at which rays grow *in vivo,* we use previously collected fin data from one fish, imaged and digitized at 33 dpf (shown in Figure 8.1A). In this figure, the thick black lines represent the ray segments and the orange circles represent the joints, for 16 bony fin rays.

From the first segment in each ray, we extrapolate lines proximally (thin black lines). We do this to determine the *y*-coordinate at which the extrapolation line reaches zero on the *x*-axis (represented by the blue squares in Figure 8.1B). We take the average *y*-coordinates of these points and determine the average intersection point for all rays (red circle in Figure 8.1B). We center this average intersection point on (0, 0), which represents the origin in the polar coordinates system. Then through a Cartesian to Polar Coordinates data conversion function in MATLAB, we determine the angles of the first segment in each ray to the origin.

We also determine the *x*- and *y*-coordinates of each ray base to determine the starting positions ($\rho_{r,0}$) of each ray and use those coordinates as a guide to determine the starting positions of the model rays. Since the digitized fin only contains 16 rays, we cannot use the exact starting positions calculated, since there would be two rays missing. Therefore, we approximate starting positions that follow the same curve seen in the digitized image.

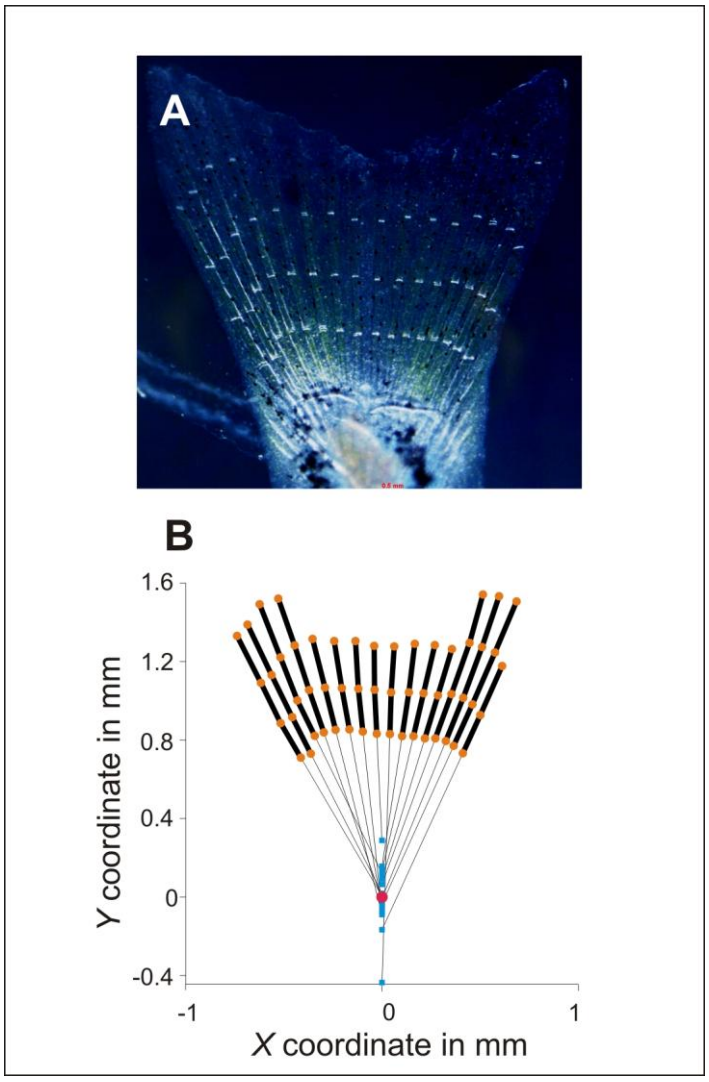

Figure 8.1. Angles and positions of the fin rays from experimental data. **A:** Image of a fin at 33 days post fertilization **B:** the digitized image of **A**, with thick black lines representing segments and orange dots representing joints. Extrapolation lines (thin black lines) extend proximally to zero on the *x*-axis. Blue dots represent where each line crosses the *x*-axis at zero, and the red dot represents the average intersection point.

8.2 Determining Growth and Regeneration

Since the model aims to recreate joint and bifurcation patterns in developing rays, we want ray growth to be identical to growth *in vivo*. Therefore, we use unpublished data on fin development and regeneration previously collected to determine realistic growth rates.

Between my undergraduate and graduate degrees, I performed a long-term experiment on fin development and regeneration. The development data set was collected on 18 fish, which were subdivided into five batches of fish. These fish were followed from 28 to 170 dpf and imaged every three days. The images were processed by another student in the Rolland-Lagan laboratory using custom-made programs for fin digitization and data analysis. The length of the fin was calculated based on the third ray from the right, since it is one of the longest fins and has been used as a measure of fin length in a previous study (Iovine and Johnson 2000). This data set contains information on various fin parameters including fin length, segment length, segment numbers, and ray section lengths. For this thesis, I utilized this data set to calculate various growth rates.

8.2.1 Development Data Set

The amount of change in fin length between days tells us the amount of growth that occurs in that period of time. Therefore, to determine a fin growth rate, we plot the fin length as a function of time (in dpf) and perform a curve fitting analysis in SPSS. We select the best model (an inverse model, of the form $y = a + \frac{b}{x}$) based on each curve's R^2 value (R^2=.864). We then determine the equation of the line (hereafter known as the fin length equation). The results of the curve fitting analysis are provided in Table 8.1 and the resulting inverse line of best fit is shown in Figure 8.2A.

To determine an equation of fin growth, we take the derivative of the fin length equation (hereafter known as the fin growth equation). We use this fin growth equation within the model to determine the amount of growth at each iteration. However, this equation represents fin growth, not individual ray growth, and thus will not create the

variations in ray growth between rays. Therefore, we adjust the fin growth equation for each ray to reflect inter-ray growth variations.

To this end, we use data collected by Rolland-Lagan *et al.* (*in prep*) on the regression of ray length as a function of fin length for 18 rays. The slope of the regression lines for each ray provides us a value that we can use to scale the fin growth rate to each individual ray. The calculation for determining individual ray growth rates is the following:

$$G_{r,t} = L_r G_{f,t} \quad (13)$$

Where $G_{r,t}$ is the growth rate for ray *r* at time t, L_r is the slope of the linear regression for ray *r,* and $G_{f,t}$ is the fin growth rate at time t. The slopes of the linear regression from Rolland-Lagan *et al.* (*in prep*) are listed in Table 8.2.

From this fin length equation, we can also determine at what point the rays should first appear. We can accomplish this by solving the fin length equation for *x* when *y*=0. If we perform this calculation, *x* = 26.12 dpf. Therefore, we can assume that ray growth starts at 26.12 dpf. This compares well to images taken of juvenile zebrafish caudal fin buds between 22 and 28 dpf where some fins have visible bony rays and segments, and some do not (unpublished data).

8.2.2 Regeneration Data Set

The regeneration data set was collected on the same fish described in the development data set experiment. Regeneration experiments were performed on the 18 fish from the development experiment; however only 12 survived past 3 dpa. Amputations were either made once first bifurcations had occurred in all rays, or once the fish reach 170 dpf. The reason we amputated at 170 dpf is that we worried if we waited more than 170 dpf that the fish would die before regeneration experiments could be performed. The amputated fins were imaged every three days and these images were digitized using custom-made programs for image analysis. Once again, the length of the fin was calculated based on the third ray from the right, since it is one of the longest rays and has been used in a previous study to measure fin length (Iovine and Johnson 2000).

We follow a similar process to the determination of ontogenetic ray growth rates for the regenerative ray growth rates. We assume since an inverse function fit ontogenetic fin length data, that it would also fit regenerative data. The resulting R^2 value for the inverse line of best fit was 0.722 and we determine the equation of the line to get a regenerate length equation (the regenerate length data and line of best fit are shown in Figure 8.2B). We take the derivative of this regenerate length equation to determine the fin regeneration equation and scale it by the regression slopes to get individual regeneration rates for each ray.

From this inverse regenerate length equation, we can also determine at what day the first regenerating ray should start growing. We can do this by solving the regenerate length equation (see Figure 8.2B) for x when y=0. If we perform this calculation, x = 2.36 dpa. Therefore, we can assume that ray outgrowth starts at 2.36 dpa. This fits with images taken of amputated zebrafish caudal fins that had reached 3 dpa (n =12, ambient water temperature 28.5ºC), where in some of the regenerating fin rays the first segments are visible (unpublished data). A study done by Becerra *et al.* (1996) on regeneration in three teleost species (false mouth-breeding cichlid fish, carp, and goldfish) showed that the first signs of ray blastema differentiation occur at 4 dpa when water temperature is between 19-21ºC. Therefore, model ray regeneration beginning at 2.36 dpa appears justified.

Table 8.1. Curve fitting results from SPSS for the experimental data on fin length**.**

	Ontogenetic Growth Model Summary				
Equation	R Square	F	df1	df2	Sig.
Linear	.670	1307.02	1	645	.000
Logarithmic	.800	2582.80	1	645	.000
Inverse	.864	4112.65	1	645	.000
Quadratic	.833	1603.78	2	644	.000
Cubic	.858	1296.14	3	643	.000
Compound	.541	759.587	1	645	.000
Power	.702	1523.88	1	645	.000
D	.832	3201.40	1	645	.000
Growth	.541	759.587	1	645	.000
Exponential	.541	759.587	1	645	.000
Logistic	.541	759.587	1	645	.000

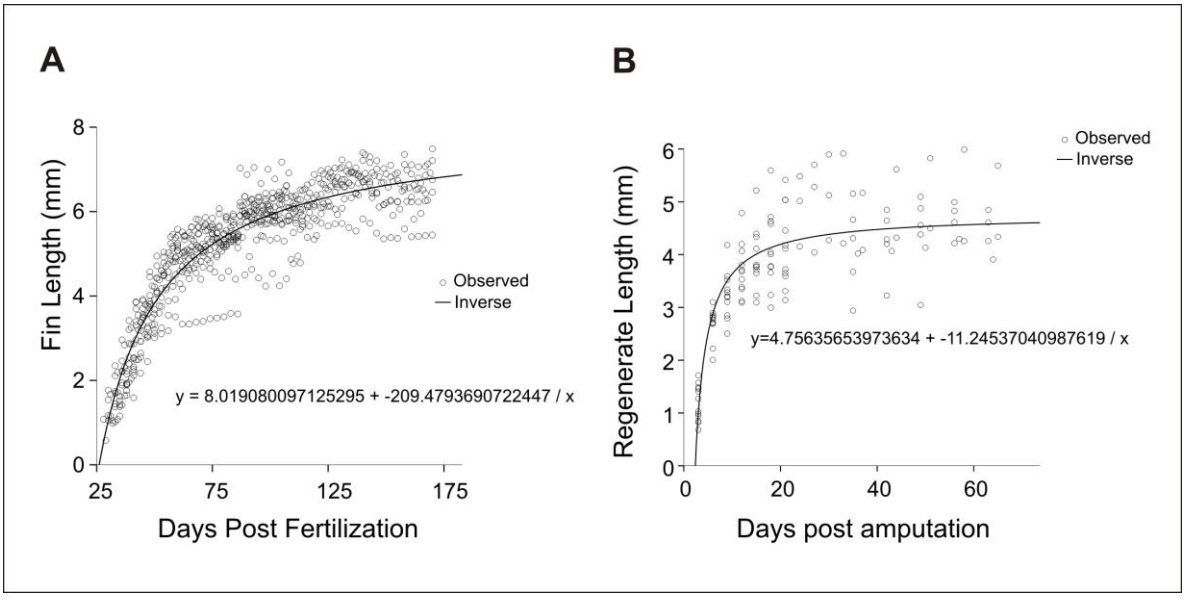

Figure 8.2. Determination of growth and regeneration equations. **A:** data on ontogenetic ray length over time (individual data points), and the inverse equation of best fit (solid line). **B:** data on regenerate length over time (individual data points), and the inverse equation of best fit (solid line).

Table 8.2. Relative ray lengths as a proportion of total fin length.

	Value Assigned																	
	Ray Number																	
Parameter*	**-9**	**-8**	**-7**	**-6**	**-5**	**-4**	**-3**	**-2**	**-1**	**1**	**2**	**3**	**4**	**5**	**6**	**7**	**8**	**9**
L_r	0.934	0.950	0.919	0.846	0.759	0.675	0.595	0.522	0.492	0.511	0.573	0.658	0.728	0.794	0.848	0.883	0.896	0.923

* Where L_r represents the slope of the linear regression of ray length as a function of fin length.

8.2.3 Optimization Data Set

To optimize the best model, we need to compare model output to experimental data on various joint and bifurcation patterns within the fin. The data set we use for this comparison is from Rolland-Lagan *et al.* (*in prep*). It was collected by a previous student in the laboratory, and we use a subset of the data to determine how well the model recreates real fin patterns.

The data was collected by following two tanks of fish (approximately 30 fish per tank, water temperature 31°C) over development and imaging 30 fish per week. The images were analyzed using custom-made programs for image analysis and data extraction. The data was organized by fin length and eight fin size classes were devised, corresponding to 1.3, 1.8, 2.2, 2.7, 3.2, 3.7, 4.1, 4.6, 5.1, and 5.5 mm (Rolland-Lagan *et al., in prep*). We only use data for fish in size class 5.1 mm since at this stage the fish is an adult and the sample size at that stage was sufficient (n=12). The sample size of the fish in the 5.5 mm fin class was too small to provide us with a sufficient data set (n=2). The parameters extracted using these programs include fin, ray, ray section and segment lengths, as well as segment numbers.

8.3 Model

8.3.1 Plotting

Model output can be visualized in three different ways, as illustrated in Figure 8.3. The first method (Figure 8.3A) highlights overall fin shape and the different ray sections (plotted in different colors). The second method (Figure 8.3B) illustrates the difference in segment numbers and segment positions within and between rays. The first five segments are plotted in different colors and those colors repeat for the remaining segments. The last method (Figure 8.3C), illustrates the variation in segment length within the fin, where a segment's color represents its length as represented in the color bar.

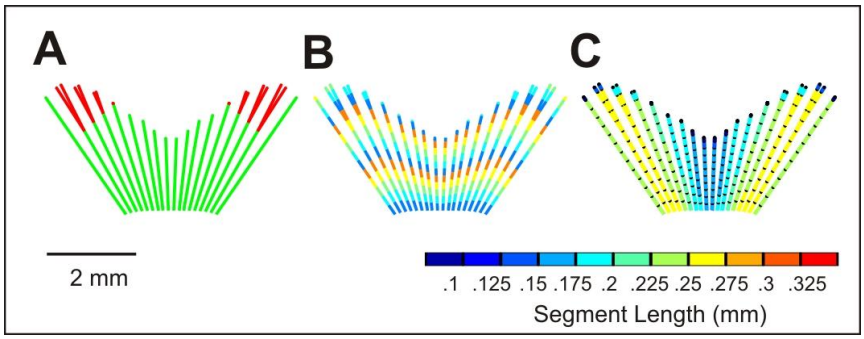

Figure 8.3. Plotting methods for the visualization of the modeled fin. **A:** fin plotted according to section length, with S1 shown in green, S2 in red, and S3 in blue (not shown). **B:** segments plotted by segment ID number for each ray; where the most proximal segments (segment ID number =1) are coloured the same, followed by the second, and so on. **C:** segments plotted by length, according to the colour bar below the fins.

8.3.2 Information Storage

For data analysis of the model, every *x* and *y* coordinate of the bone points is stored in a matrix. In addition to bone point coordinates, other relevant information is stored in the following matrix:

$$xycoord = \begin{bmatrix} x_0 & y_0 & j_0 & r_0 & S1_0 & S2_0 & S3_0 & S4_0 & t_o & M_0 \\ x_1 & y_1 & j_1 & r_1 & S1_1 & S2_1 & S3_1 & S4_1 & t_1 & M_1 \\ \dots & \dots & \dots & \dots & \dots & \dots & \dots & \dots & \dots & \dots \\ x_n & y_n & j_n & r_n & S1_n & S2_n & S3_n & S4_n & t_n & M_n \end{bmatrix}$$

Where $xycoord$ is the matrix where all the information is stored. x_0 is the bone point coordinate on the *x*-axis at $t = 0$, (x_1 at $t = 1$, x_n at $t = n$, where n is the last iteration of the simulation, for all cases). y_0 is the bone point coordinate on the *y*-axis at $t = 0$, (y_1 at $t = 1$, y_n at $t = n$). j_0 is the number of the segment to which the bone point belongs at $t = 0$ (j_1 at $t = 1$, j_n at $t = n$); r_0 is the ray number to which the bone point belongs at $t = 0$ (r_1 at $t = 1$, r_n at $t = n$). $S1_0$, $S2_0$, $S3_0$, $S4_0$ represent the ray section the point belongs to, at $t = 0$, and can either be filled with a 1 (part of that ray section) or a 0 (not part of that ray section) ($S1_1$, $S21$, $S3_1$, $S4_1$ at $t = 1$, $S1_n$, $S2_n$, $S3_n$, $S4_n$ at $t = n$). Once a 0 changes to a 1 is in one of these columns in the matrix, the 1 will always remain. This provides a method to track the ray section history of a point. t_0 is the time, in days, at $t = 0$, (t_1 at $t = 1$, t_n at $t = n$). M_0 is whether or not an amputation has occurred at $t = 0$, (M_1 at $t = 1$, M_n at $t = n$). If no amputation has occurred, this value is 0; with amputation the value becomes 1.

Tracking this information allows data analysis at the end of the simulation to determine fin parameters of interest, such as ray, section and segment length.

8.3.3 Mechanisms Tested

We tested multiple models for the formation of joint and bifurcation patterns, with the aim of reproducing trends reported in the literature. In particular, we tested models where joint formation was based on time or on substance accumulation. In parallel we also tested models where bifurcation formation was based on time, distance from the fin base, and substance accumulation. In the main thesis, we present the models of joint and bifurcation formation based on the accumulation of patterning substances. Therefore, here we will briefly explain the other mechanisms we test.

8.3.3.1 Joint Mechanism

The trends in joint patterning in the fin state that segment length decreases along the proximo-distal axis, that segment length is shorter in the medial rays than the lateral rays, and that segments are fewer in the medial rays as well (Haas 1962; Iovine and Johnson 2000, Goldsmith *et al.,* 2006, Rolland-Lagan *et al.*, 2012). The length of a segment depends on the amount of bone deposition that occurs between joint formation events. Since we know there is variation in the growth rates between rays during juvenile development (Goldsmith *et al.,* 2006), we supposed that these differences in growth rate could be sufficient to explain the trends in joint patterning. Therefore, we created a model in which joints formed at a given time interval in the model. Figure 8.4A shows the model fin visualization when joint formation is based on this mechanism.

The second mechanism we tested was joint formation based on the accumulation of a patterning substance to threshold. We found with this mechanism, we could still test the hypothesis that joints formed at specific time intervals if we kept the rate of accumulation constant over time. Therefore, the time-based model of joint formation was just a particular case of the substance accumulation model. In addition, we could alter the rate of accumulation over time in a variety of ways to create various joint patterns within the fin.

8.3.3.2 Bifurcation Mechanism

Since we were testing joint formation based on time, we decided to test bifurcation formation based on time as well. In some instances of bifurcation (i.e. in the medial

bifurcating rays), it appeared that the S2 ray section was shorter than the S1 ray section before it. If bifurcation formation was based on time, the decrease in ray growth later in life could recreate this shorter S2 ray section length.

Another hypothesized mechanism of bifurcation that we tested was based on distance from the base of the fin. We observed a slight bi-modal distribution to the ray bases in the earliest stages of development (Rolland-Lagan et al., *in prep*) that could potentially account for the bi-modal distribution of the bifurcations. Therefore, we investigated bifurcations occurring based on distance. A ray length was chosen as the bifurcating length, and the model tracked ray length. When a ray equalled or exceeded the bifurcation length, a bifurcation occurred. For second and third bifurcations, separate bifurcation lengths were assigned to the model. Problems arose with this model in determining the bifurcation lengths. Lengths were just arbitrarily chosen to recreate the trends in bifurcation patterning, but we could not identify any underlying mechanism that could explain the choice of these bifurcations lengths. In addition, there was no evidence in the literature that indicated once a ray reached a certain length it bifurcated therefore we rejected this mechanism.

The final mechanism of bifurcation formation was based on substance accumulation. Similar to joint formation, we found we could easily manipulate this mechanism to recreate bifurcations based on time (by keeping the rate of accumulation constant over time). Therefore, we could get rid of the time-based mechanism as a particular case of the substance accumulation model. We could also manipulate the rate of accumulation over time in many ways that resulted in appropriate bifurcation patterns, so we chose to proceed with this bifurcation mechanism.

8.3.4 Fin development Program

```
function findevelopment_final(r,steps,dt)
% Model of bony ray growth and patterning in teleosts, calibrated with
% experimental growth rates and optimized to recreate experimental data.
% INPUTS
%   The model requires 3 user inputs:
%     r = the number of rays to be studied in the simluation (model is set up to use 18)
%           if fewer is desired the matrices will be to be changed)
%     steps = the number of iterations the model should be run for
%     dt = the time interval that passes with each iteration (unit is days)
%
%     If steps=4400 (optimized simulation length) and dt=0.01 the length of the similation represents 44
days

% Global parameters, for use in other programs related to the ray growth program (eg. plotting program,
regeneration)
global xycoord xycoord_reg r r1 ray0 hJ_orig pB_orig TB TJ J rays B steps regen scale dt bone_theta_orig
plotting1

%Setting up the base positions of the rays - based on experimental data
x=[-0.2525 -0.2222 -0.1919 -0.1616 -0.1313 -0.1010 -0.0707 -0.0454 -0.0152 0.0152 0.0454 0.0707 0.1010
0.1313 0.1616 0.1919 0.2222 0.2525];
y=[0.3666 0.3855 0.3977 0.4043 0.4075 0.4085 0.4090 0.4093 0.4093 0.4093 0.4093 0.4090 0.4085 0.4075 0.4043
0.3977 0.3855 0.3666];
%Determining the positions in the polar coordinates system
[bone_theta,bone_rho]=cart2pol(x,y);

%The bone_theta, bone_rho, source_theta and source_rho matrices store the current position of the respective
%points row 1) and the previous position of the points (row 2)
bone_theta=[bone_theta; bone_theta]; bone_rho=[bone_rho; bone_rho];
source_rho=bone_rho*1.01; source_theta=bone_theta;
bone_theta_orig=bone_theta;

%Creating matrices to be used in the model
seg=[1:r]; seg=[seg; seg]; %Matrix of segment numbers (each column represents a ray)
```

```
s1=ones(1,r); %Tracking s1 ray section for each ray (1 - it has a parent ray)
s2=zeros(1,r); %Tracking s2 ray sections for each ray (1 - left branch of a bifurcation, 2 - right)
s3=zeros(1,r); %Tracking s3 ray sections for each ray (1 - left branch of a bifurcation, 2 - right)
s4=zeros(1,r);  %Tracking s4 ray sections for each ray (1 - left branch of a bifurcation, 2 - right)

%|These matrices  will contain the last and second to last theta and rho values for the s1, s2, s3 or s4 ray
%sections for source and bone points. Once a ray section has progressed from it's current type to the next
%(eg. s1 to s2), the old matrix (s1) is no longer updated.
source_rho_s1=zeros(2,r);source_rho_s2=zeros(2,r);source_rho_s3=zeros(2,r);source_rho_s4=zeros(2,r);
source_theta_s1=source_theta;source_theta_s2=zeros(2,r);source_theta_s3=zeros(2,r);source_theta_s4=zeros(2,r
);
bone_rho_s1=source_rho_s1;bone_rho_s2=source_rho_s2;bone_rho_s3=source_rho_s3;bone_rho_s4=source_rho_s4;
bone_theta_s1=source_theta_s1;bone_theta_s2=source_theta_s2;bone_theta_s3=source_theta_s3;bone_theta_s4=sour
ce_theta_s4;

step=zeros(1,r); %Matrix to store the current step (in days) of the model
reg=zeros(1,r); %Matrix to store whether or not the current bone point belongs to ray that has been
regenerated (0-nonamputated, 1-amputated)
ray0=[-r/2:-1,1:r/2]; %Creating the matrix to store the ray numbers (-9 to 9, excluding 0)

% Joint Formation Mechanism
TJ=0.012; %Threshold for joint formation
J=zeros(1,r);%Matrix to store the concentration of joint forming substance (J) for all rays
hJ=5.4.*[1 1 1 .93 0.85 0.84 0.8 0.73 0.68 0.68 0.73 0.8 0.84 0.85 .93 1 1 1]; %Joint substance production
equation.
%The constant in the joint substance production equation to make the rate of production vary between rays,
we multipled it by varying proportions
e=1.86;

%Bifurcation Formation Mechanism
TB=1.05; %Threshold for bifurcation formation
B=zeros(1,r);%Matrix to store the concentration of bifurcation forming substance (B) for all rays
pB=0.95.*([0.53 0.5 0.44 0.42 0.43 0.46 0.48 0.5 0.51 0.51 0.5 0.48 0.46 0.43 0.42 0.44 0.5 0.53]);
%The constant in the bifurcation substance production equation - to make the rate of production vary between
rays,
%we multipled it by varying proportions

deg=0.001; %The decay constant for both the joint and the bifurcation forming substances
```

```
hJ_orig=hJ; r1=r; r2=r; co=zeros(1,r);

%The values used to scale the fin growth rate to each ray, these represent the slope of
%the linear regression of ray length as a function of fin length
scale=([0.934 0.950 0.919 0.846 0.759 0.675 0.595 0.522 0.492 0.511 0.573 0.658 0.728 0.794 0.848 0.883
0.896 0.923]);

%Determining the x and y coordinates of the starting
[x,y]=pol2cart(bone_theta(1,:),bone_rho(1,:));
xycoord=cat(1,xycoord,[x' y' seg(1,:)' ray0(1,:)' s1(1,:)' s2(1,:)' s3(1,:)' s4(1,:)' step(1,:)'
reg(1,:)']);


for int=1:steps,
    %Step 1- determining the change in ray length for this iteration of the model
    %(the equation was derived from experimental data on fin length over time)
    growth=(209.4793690722447/(int*dt+26.12)^2);
    growth=growth.*scale; %Scaling the fin growth value to each of the rays

    %Step 2 - Bifurcation substance accumulates, based on the rate of
    %production
    B=B+(growth.*pB-deg*B)*dt;

    %Step 3 - Determining if any rays reached the threshold for bifurcation
    bifur=find(B>=TB);
    bifur=fliplr(bifur);%Inversing the matrix - this allowed an easier method of enlarging the matrices
                        %without having to change indices

    %If a ray has been triggered to bifurcation, the following occurs:
    %Step 3.1 - The bifurcation of the source points and updating all relevant matrices
    if ~isempty(bifur)
        for p=1:length(bifur), %The process of bifurcations is done ray by ray

            %Determining if the ray bifurcating is either the most dosral or ventral ray
            temp=find(bifur(p)==1);
            len=length(source_rho);
            temp1=find(bifur(p)==len);
```

```
            if isempty(temp) && isempty(temp1), %If the ray bifurcating is the most dorsal or ventral ray
                %Then it skips the bifurcation process

                %Increasing the size of the matrices used in the model
                source_rho=[source_rho(:,1:bifur(p)) source_rho(:,bifur(p):end)];
                source_rho_s1=[source_rho_s1(:,1:bifur(p)) source_rho_s1(:,bifur(p):end)];
                source_rho_s2=[source_rho_s2(:,1:bifur(p)) source_rho_s2(:,bifur(p):end)];
                source_rho_s3=[source_rho_s3(:,1:bifur(p)) source_rho_s3(:,bifur(p):end)];
                source_rho_s4=[source_rho_s4(:,1:bifur(p)) source_rho_s4(:,bifur(p):end)];

                source_theta=[source_theta(:,1:bifur(p)) source_theta(:,bifur(p):end)];
                source_theta_s1=[source_theta_s1(:,1:bifur(p)) source_theta_s1(:,bifur(p):end)];
                source_theta_s2=[source_theta_s2(:,1:bifur(p)) source_theta_s2(:,bifur(p):end)];
                source_theta_s3=[source_theta_s3(:,1:bifur(p)) source_theta_s3(:,bifur(p):end)];
                source_theta_s4=[source_theta_s4(:,1:bifur(p)) source_theta_s4(:,bifur(p):end)];

                ray0=[ray0(:,1:bifur(p)) ray0(:,bifur(p):end)];
                reg=[reg(:,1:bifur(p)) reg(:,bifur(p):end)];
                co=[co(:,1:bifur(p)) co(:,bifur(p):end)];
                pB=[pB(:,1:bifur(p)) pB(:,bifur(p):end)];
                hJ=[hJ(:,1:bifur(p)) hJ(:,bifur(p):end)];
                B=[B(:,1:bifur(p)) B(:,bifur(p):end)];
                J=[J(:,1:bifur(p)) J(:,bifur(p):end)];
                growth=[growth(:,1:bifur(p)) growth(:,bifur(p):end)];

                %Assigning new theta angles to the bifurcated ray
                source_theta(2,bifur(p))=93*pi/180;
                source_theta(2,bifur(p)+1)=87*pi/180;

                if s4(1,bifur(p))==1 || s4(1,bifur(p))==2,%If the source point bifurcating belongs to S4 ray
                %section
                    %Determining the length of the S4 section length (rho)
                    %- which is the current rho value, minus the length of
                    %all other sections
                    source_rho_s4(2,bifur(p))=source_rho(1,bifur(p))-
(source_rho_s1(1,bifur(p))+source_rho_s2(1,bifur(p))+source_rho_s3(1,bifur(p)));
```

```
                    source_rho_s4(2,bifur(p)+1)=source_rho(1,bifur(p))-
(source_rho_s1(1,bifur(p))+source_rho_s2(1,bifur(p))+source_rho_s3(1,bifur(p)));

                    %The starting theta angle for the next ray section is stored
                    source_theta_s5(:,bifur(p))=source_theta1(2,bifur(p));
                    source_theta_s5(:,bifur(p)+1)=source_theta1(2,bifur(p)+1);

                elseif s3(1,bifur(p))==1 || s3(1,bifur(p))==2,%If the source point bifurcating belongs to S3
                %ray section
                    %Determining the length of the S3 section length (rho)
                    %- which is the current rho value, minus the length of
                    %all other sections
                    source_rho_s3(2,bifur(p))=source_rho(1,bifur(p))-
(source_rho_s1(1,bifur(p))+source_rho_s2(1,bifur(p)));
                    source_rho_s3(2,bifur(p)+1)=source_rho(1,bifur(p))-
(source_rho_s1(1,bifur(p))+source_rho_s2(1,bifur(p)));

                    %The starting theta angle for the next ray section is stored
                    source_theta_s4(:,bifur(p))=source_theta(2,bifur(p));
                    source_theta_s4(:,bifur(p)+1)=source_theta(2,bifur(p)+1);

                elseif s2(1,bifur(p))==1 || s2(1,bifur(p))==2,%If the source point bifurcating belongs to
                %S2 ray section
                    %Determining the length of the S2 section length (rho)
                    %- which is the current rho value, minus the length of
                    %all other sections
                    source_rho_s2(2,bifur(p))=source_rho(1,bifur(p))-source_rho_s1(1,bifur(p));
                    source_rho_s2(2,bifur(p)+1)=source_rho(1,bifur(p))-source_rho_s1(1,bifur(p));

                    %The starting theta angle for the next ray section is stored
                    source_theta_s3(:,bifur(p))=source_theta(2,bifur(p));
                    source_theta_s3(:,bifur(p)+1)=source_theta(2,bifur(p)+1);

                else %If the source point bifurcating belongs to S1 ray section
                    %Determining the length of the S4 section length (rho)
                    %- which is the current rho value
                    source_rho_s1(1,bifur(p))=source_rho(1,bifur(p));
```

```
                source_rho_s1(1,bifur(p)+1)=source_rho(1,bifur(p));

                %The starting theta angle for the next ray section is stored
                source_theta_s2(:,bifur(p))=source_theta(2,bifur(p));
                source_theta_s2(:,bifur(p)+1)=source_theta(2,bifur(p)+1);
            end;

            %Resetting the amount of bifurcation forming substance to 0
            B(1,bifur(p))=0;
            B(1,bifur(p)+1)=0;

            %Assigning the growth rates to the bifurcated points
            growth(1,bifur(p))=growth(1,bifur(p));
            growth(1,bifur(p)+1)=growth(1,bifur(p));

            r2=r2+1; %Updating the number of source points in the model
        end;
    end;
end;

%Step 3.2 - The bifurcation of the source points and updating all relevant matrices
%Bifurcation of bone points
if ~isempty(bifur)
    %Determining the x and y coordinates of the points where they are
    %currently - these values are used only if the bone points are S1
    [sourcex,sourcey]=pol2cart(source_theta(1,:),source_rho(1,:));
    [bonex,boney]=pol2cart(bone_theta(1,:),bone_rho(1,:));

    %Otherwise, if the bone points are S2, S3, or S4 ray sections, we
    %need to take into account the previous ray sections position in
    %the current position of the bone point
    if sum(source_theta_s2(2,:))==0,%If the bone point is in ray section S2
    else,
        %Determining the last x and y coordinates of the S1 ray section
        [xray1, yray1]=pol2cart(source_theta_s1(2,:),source_rho_s1(2,:));

        %We consider the base of any ray section (S1, S2, S3, S4) as
```

```
    %the origin of a new polar coordinates system. To have growth
    %occuring properly, we need to account for the rotation between
    %polar coordinates systems.
    thetarot=source_theta_s1(2,:)-(pi/2);%Determining the rotation of the points between S1 and S2
    theta2_glob=source_theta_s2(2,:)+thetarot;%Adding the rotation to the angle of the S2 ray
    %section
    [xray2_loc, yray2_loc]=pol2cart(theta2_glob(1,:),source_rho_s2(2,:));%Determining the S2 source
    %point positions

    sourcex=xray2_loc+xray1;%Adding the S1 and S2 source point positions together to get %the total
    position of the source point
    sourcey=yray2_loc+yray1;

    %Doing the same for the bone points
    [xray1b, yray1b]=pol2cart(bone_theta_s1(2,:),bone_rho_s1(2,:));
    thetarotb=bone_theta_s1(2,:)-(pi/2);
    theta2_globb=bone_theta_s2(2,:)+thetarotb;
    [xray2_locb, yray2_locb]=pol2cart(theta2_globb(1,:),bone_rho_s2(2,:));

    bonex=xray2_locb+xray1b;
    boney=yray2_locb+yray1b;
end;
if sum(source_theta_s3(2,:))==0 %If the bone point is in ray section S3
else,
    %If the point belongs to S3, it will go through the if
    %statement above and then will also go through this section -
    %adding the length of the S3 ray section.
    thetarot2=source_theta_s2(2,:)-(pi/2);
    theta3_glob=source_theta_s3(2,:)+thetarot2+thetarot;
    [xray3_loc, yray3_loc]=pol2cart(theta3_glob(1,:),source_rho_s3(2,:));

    sourcex=xray3_loc+sourcex;
    sourcey=yray3_loc+sourcey;

    %Doing the same for the bone points
    thetarot2b=bone_theta_s2(2,:)-(pi/2);
    theta3_globb=bone_theta_s3(2,:)+thetarot2b+thetarotb;
    [xray3_locb, yray3_locb]=pol2cart(theta3_globb(1,:),bone_rho_s3(2,:));
```

```
    bonex=xray3_locb+bonex;
    boney=yray3_locb+boney;
  end;

if sum(source_theta_s4(2,:))==0 %If the bone point is in ray section S4
else,
    %If the point belongs to S4, it will go through the if
    %statements above and then will also go through this section -
    %adding the length of the S4 ray section.
    thetarot3=source_theta_s3(2,:)-(pi/2);
    theta4_glob=source_theta_s4(2,:)+thetarot3+thetarot2+thetarot;
    [xray4_loc, yray4_loc]=pol2cart(theta4_glob(1,:),source_rho_s4(2,:));

    sourcex=xray4_loc+sourcex;
    sourcey=yray4_loc+sourcey;

    %Doing the same for the bone points
    thetarot3b=bone_theta_s3(2,:)-(pi/2);
    theta4_globb=bone_theta_s2(2,:)+thetarot3b+thetarot2b+thetarotb;
    [xray4_locb, yray4_locb]=pol2cart(theta4_globb(1,:),bone_rho_s4(2,:));

    bonex=xray4_locb+bonex;
    boney=yray4_locb+boney;
end;

for i=r:-1:1, %Going through each bone point individually
    %Determining the distance of the current bone point to all
    %source points in the model
    datab=[bonex(1,:)' boney(1,:)'];
    datas=[sourcex(1,:)' sourcey(1,:)'];

    d=distance(datas,datab(i,:));
    [v,c]=min(d);
    d=sortrows(d);

    if d(2)-d(1)==0, % If there are two equidistant source points, the bone point will bifurcate
```

```
 %Increasing the size of the matrices used in the model
s1=[s1(:,1:i) s1(:,i:end)];
s2=[s2(:,1:i) s2(:,i:end)];
s3=[s3(:,1:i) s3(:,i:end)];
s4=[s4(:,1:i) s4(:,i:end)];
seg=[seg(:,1:i) seg(:,i:end)];
scale=[scale(:,1:i) scale(:,i:end)];

bone_theta=[bone_theta(:,1:i) bone_theta(:,i:end)];
bone_theta_s1=[bone_theta_s1(:,1:i) bone_theta_s1(:,i:end)];
bone_theta_s2=[bone_theta_s2(:,1:i) bone_theta_s2(:,i:end)];
bone_theta_s3=[bone_theta_s3(:,1:i) bone_theta_s3(:,i:end)];
bone_theta_s4=[bone_theta_s4(:,1:i) bone_theta_s4(:,i:end)];

bone_rho=[bone_rho(:,1:i) bone_rho(:,i:end)];
bone_rho_s1=[bone_rho_s1(:,1:i) bone_rho_s1(:,i:end)];
bone_rho_s2=[bone_rho_s2(:,1:i) bone_rho_s2(:,i:end)];
bone_rho_s3=[bone_rho_s3(:,1:i) bone_rho_s3(:,i:end)];
bone_rho_s4=[bone_rho_s4(:,1:i) bone_rho_s4(:,i:end)];

%Assigning new theta angles to the bifurcated ray
bone_theta(2,i)=93*pi/180;
bone_theta(2,i+1)=87*pi/180;

if s4(1,i)==1 || s4(1,i)==2 %If the bone point belongs to S4
    %Determining the length of the S4 section length (rho)
    %- which is the current rho value, minus the length of
    %all other sections
    bone_rho_s4(2,i)=bone_rho(1,i)-(bone_rho_s1(1,i)+bone_rho_s2(1,i)+bone_rho_s3(1,i));
    bone_rho_s4(2,i+1)=bone_rho(1,i)-(bone_rho_s1(1,i)+bone_rho_s2(1,i)+bone_rho_s3(1,i));

    %The starting theta angle for the next ray section is stored
    bone_theta_s5(:,i)=bone_theta(2,i);
    bone_theta_s5(:,i+1)=bone_theta(2,i+1);

elseif s3(1,i)==1 || s3(1,i)==2 %If the bone point belongs to S3
```

```
    %Changing the value in the S4 matrix so that the matrix
    %now recognizes the S3 sections as having bifurcation
    s4(1,i)=1;
    s4(1,i+1)=2;
    %Determining the length of the S3 section length (rho)
    %- which is the current rho value, minus the length of
    %all other sections
    bone_rho_s3(2,i)=bone_rho(1,i)-(bone_rho_s1(1,i)+bone_rho_s2(1,i));
    bone_rho_s3(2,i+1)=bone_rho(1,i)-(bone_rho_s1(1,i)+bone_rho_s2(1,i));

    %The starting theta angle for the next ray section is stored
    bone_theta_s4(:,i)=bone_theta(2,i);
    bone_theta_s4(:,i+1)=bone_theta(2,i+1);

elseif s2(1,i)==1 || s2(1,i)==2 %If the bone point belongs to S4
    %Changing the value in the S4 matrix so that the matrix
    %now recognizes the S2 sections as having bifurcation
    s3(1,i)=1;
    s3(1,i+1)=2;
    %Determining the length of the S2 section length (rho)
    %- which is the current rho value, minus the length of
    %all other sections
    bone_rho_s2(2,i)=bone_rho(1,i)-bone_rho_s1(1,i);
    bone_rho_s2(2,i+1)=bone_rho(1,i)-bone_rho_s1(1,i);

    %The starting theta angle for the next ray section is stored
    bone_theta_s3(:,i)=bone_theta(2,i);
    bone_theta_s3(:,i+1)=bone_theta(2,i+1);

elseif s1(1,i)==1 %If the bone point belongs to S1
    %Changing the value in the S4 matrix so that the matrix
    %now recognizes the S1 sections as having bifurcation
    s2(1,i)=1;
    s2(1,i+1)=2;
    %Determining the length of the S1 section length (rho)
    %- which is the current rho value
    bone_rho_s1(1,i)=bone_rho(1,i);
    bone_rho_s1(1,i+1)=bone_rho(1,i);
```

```
                %The starting theta angle for the next ray section is stored
                bone_theta_s2(:,i)=bone_theta(2,i);
                bone_theta_s2(:,i+1)=bone_theta(2,i+1);
            end;
        end;
    end;
    r=r2; %Updating the number of rays to be used in the model
end;

%Step 4 - changing the source point positions to represent fin growth
%Growth of the source points
for i=1:r, %Going through each source point individually
    if s4(1,i)==1 || s4(1,i)==2, %If the source point belongs to the S4 ray section
        source_rho(2,i)=source_rho(1,i)+(growth(1,i)*dt);%Moving the source point by the %amount of
        growth
        source_rho_s4(:,i)=source_rho(2,i)-(source_rho_s1(2,i)+source_rho_s2(2,i)+source_rho_s3(2,i));
        %The new position of the source point is stored, taking into account the length of the S1 & S2
        %ray sections

    elseif s3(1,i)==1 || s3(1,i)==2,%If the source point belongs to the S3 ray section
        source_rho(2,i)=source_rho(1,i)+(growth(1,i)*dt);%Moving the source point out by the amount of
        %growth
        source_rho_s3(:,i)=source_rho(2,i)-(source_rho_s1(2,i)+source_rho_s2(2,i));
        %The new position of the source point is stored, taking into account the length of %the S1 & S2
        ray sections

    elseif s2(1,i)==1 || s2(1,i)==2 %If the source point belongs to the S2 ray section
        source_rho(2,i)=source_rho(1,i)+(growth(1,i)*dt);%Moving the source point by the amount of %
        %growth
        source_rho_s2(:,i)= source_rho(2,i)-source_rho_s1(1,i); The new position of the source point is
        %stored, taking into account the length of the S1 ray section

    elseif s1(1,i)==1, %If the source point belongs to the S1 ray section
        source_rho(2,i)=source_rho(1,i)+(growth(1,i)*dt);%Moving the source point by the %amount of
        growth
```

```
        source_rho_s1(:,i)=source_rho(2,i); %The new  position of the source point is stored (Once a
        %point changes from one ray section to another (i.e S1 to S2). This matrix is no longer updated
        %and it will store the last rho value of the S1 ray section
    end;
end;

%Step 5 - changing the bone point positions to represent ray growth
%Growth of the bone points
for i=1:r,%Going through each bone point individually
    if s4(1,i)==1 || s4(1,i)==2, %If the bone point belongs to the S4 ray section
        %Determining the amount of movement between the current and
        %previous positions of the source points
        move=source_rho(2,i)-source_rho(1,i);
        bone_rho(2,i)=bone_rho(1,i)+move; %Moving the bone point by the same amount

        bone_rho_s4(:,i)=bone_rho(2,i)-(bone_rho_s1(2,i)+bone_rho_s2(2,i)+bone_rho_s3(2,i));
        %Updating the rho matrix

    elseif s3(1,i)==1 || s3(1,i)==2,    %If the bone point belongs to the S3 ray section
        %Determining the amount of movement between the current and
        %previous positions of the source points
        move=source_rho(2,i)-source_rho(1,i);
        bone_rho(2,i)=bone_rho(1,i)+move; %Moving the bone point by the same amount

        bone_rho_s3(:,i)=bone_rho(2,i)-(bone_rho_s1(2,i)+bone_rho_s2(2,i));%Updating the rho matrix

    elseif s2(1,i)==1 || s2(1,i)==2, %If the bone point belongs to the S2 ray section
        %Determining the amount of movement between the current and
        %previous positions of the source points
        move=source_rho(2,i)-source_rho(1,i);
        bone_rho(2,i)=bone_rho(1,i)+move; %Moving the bone point by the same amount

        bone_rho_s2(:,i)=bone_rho(2,i)-bone_rho_s1(2,i);%Updating the rho matrix

    elseif s1(1,i)==1, %If the bone point belongs to the S1 ray section
        %The bone points grow towards the closes source point -
        %therefore we determine which source point is the closest to
```

```
        %the bone point
        [sourcex,sourcey]=pol2cart(source_theta(1,:),source_rho_s1(1,:));
        [bonex,boney]=pol2cart(bone_theta(1,:),bone_rho(1,:));

        datab=[bonex(1,:)' boney(1,:)'];
        datas=[sourcex(1,:)' sourcey(1,:)'];

        d=distance(datas,datab(i,:));%Determining the distance between the current bone point and
                                     %every source point
        [v,c]=min(d); %c is the index for the closest source point
        d=sortrows(d);

        move=source_rho(2,c)-source_rho(1,c);%Determining the movement in the closest source point
        bone_rho(2,c)=bone_rho(1,c)+move; %Moving the current bone point by the amount of movement

        bone_rho_s1(:,i)=bone_rho(:,i);%Updating the rho matrix
    end;
end;

%Updating the matrix containing the current time (in days) - will be saved in the xycoord matrix
step=(ones(1,r)*int)*dt;

%Step 7 - Finding the current x and y coordinates of the bone points
%This step starts by identifying the last point in the s1 matrix. This will give us x and y coordinates
%We can work from. If the point is in S1, this will correspond to it's current location. If it isn't,
%this poisition will be used to then determine the rotation of the S2 or S3 sections
%This also ensures that each iteration the x and y matrices are remade and
%there is no previous information from other iterations
[x,y]=pol2cart(bone_theta_s1(2,:),bone_rho_s1(2,:));
x=[x; x];   y=[y; y];

for i=1:r,%Going through each ray individually
    %If a bifurcation has occured, for plotting purposes, we need to
    %store the previous position of the bifurcated points in the
    %xycoord matrix so the lines join up between previous and current
    %ray section types
     if s4(1,i)==1 || s4(1,i)==2, %If the bone point is S4
```

```
            %Finding the current position of the bone point - need to
            %determine the angles of rotation and lengths of each section
           thetarot=bone_theta_s1(1,i)-(pi/2);
           theta2_glob=bone_theta_s2(1,i)+thetarot;
           [x2,y2]=pol2cart(theta2_glob,bone_rho_s2(2,i));

           thetarot2=bone_theta_s2(1,i)-(pi/2);
           theta3_glob=bone_theta_s3(1,i)+thetarot+thetarot2;
           [x3,y3]=pol2cart(theta3_glob,bone_rho_s3(2,i));

           thetarot3=bone_theta_s3(1,i)-(pi/2);
           theta4_glob=bone_theta_s4(1,i)+thetarot+thetarot2+thetarot3;
           [x4,y4]=pol2cart(theta4_glob,bone_rho_s4(2,i));

           x4=x(1,i)+x2+x3+x4;
           y4=y(1,i)+y2+y3+y4;
           x(1,i)=x4;
           y(1,i)=y4;

           if co(i)==2,
               thetarot=bone_theta_s1(1,i)-(pi/2);
               theta2_glob=bone_theta_s2(1,i)+thetarot;
               [x4,y4]=pol2cart(theta2_glob,bone_rho_s2(2,i));

               thetarot2=bone_theta_s2(1,i)-(pi/2);
               theta2_glob=bone_theta_s3(1,i)+thetarot+thetarot2;
               [x5,y5]=pol2cart(theta2_glob,bone_rho_s3(2,i));
               x5=x(2,i)+x4+x5;
               y5=y(2,i)+y4+y5;

               x(2,i)=x5;
               y(2,i)=y5;
               xycoord=cat(1,xycoord,[x(2,i)' y(2,i)' seg(1,i)' ray0(1,i)' s1(1,i)' s2(1,i)' s3(1,i)'
s4(1,i)' step(1,i)' reg(1,i)']);
           end;

           co(i)=3;
```

```
        elseif s3(1,i)==1 || s3(1,i)==2,%If the bone point is S3
            %Finding the current position of the bone point - need to
            %determine the angles of rotation and lengths of each section
           thetarot=bone_theta_s1(1,i)-(pi/2);
           theta2_glob=bone_theta_s2(1,i)+thetarot;
           [x2,y2]=pol2cart(theta2_glob,bone_rho_s2(2,i));

           thetarot2=bone_theta_s2(1,i)-(pi/2);
           theta3_glob=bone_theta_s3(1,i)+thetarot+thetarot2;
           [x3,y3]=pol2cart(theta3_glob,bone_rho_s3(2,i));

           x3=x(1,i)+x2+x3;
           y3=y(1,i)+y2+y3;
           x(1,i)=x3;
           y(1,i)=y3;

           if co(i)==1,
               thetarot=bone_theta_s1(1,i)-(pi/2);
               theta2_glob=bone_theta_s2(1,i)+thetarot;
               [x4,y4]=pol2cart(theta2_glob,bone_rho_s2(2,i));
               x4=x(2,i)+x4;
               y4=y(2,i)+y4;

               x(2,i)=x4;
               y(2,i)=y4;
               xycoord=cat(1,xycoord,[x(2,i)' y(2,i)' seg(1,i)' ray0(1,i)' s1(1,i)' s2(1,i)' s3(1,i)'
s4(1,i)' step(1,i)' reg(1,i)']);
           end;

           co(i)=2;
       elseif s2(1,i)==1 || s2(1,i)==2 %If the bone point is S2
               %Finding the current position of the bone point - need to
            %determine the angles of rotation and lengths of each section
            thetarot=bone_theta_s1(1,i)-(pi/2);
           theta2_glob=bone_theta_s2(1,i)+thetarot;
           [x2,y2]=pol2cart(theta2_glob,bone_rho_s2(2,i));
           x2=x(1,i)+x2;
           y2=y(1,i)+y2;
```

```
            x(1,i)=x2;
            y(1,i)=y2;
            if co(i)==0,
                %the old position of the point - adding it to the matrix
                [x3,y3]=pol2cart(bone_theta(1,i),bone_rho(1,i));
                x(2,i)=x3;
                y(2,i)=y3;
                xycoord=cat(1,xycoord,[x(2,i)' y(2,i)' seg(1,i)' ray0(1,i)' s1(1,i)' s2(1,i)' s3(1,i)'
s4(1,i)' step(1,i)' reg(1,i)']);
            end;
            co(i)=1;
        elseif s1(1,i)==1, %If the bone point is S1 the point calculated above is the current position
        end;
    end;

    %Step 8 - storing information about the bone points for data analysis
    %Storing the x and y coordinates in the matrix with
    xycoord=cat(1,xycoord,[x(1,:)' y(1,:)' seg(1,:)' ray0(1,:)' s1(1,:)' s2(1,:)' s3(1,:)' s4(1,:)'
step(1,:)' reg(1,:)']);

    %Step 9 - Segment forming substance
    %Determining the rate of production (ROA) for this day in the model(int*dt).
    %hJ is different for each ray
    ROA=(hJ)/((int*dt+26.12)^e);
    if ROA<0 %If the rate of production is negative, it is automatically set to 0
        ROA=0;
    end;
    J=J+(ROA-deg*J)*dt; %The concentration of segment substance increases boned on the rate of
                        %production (ROA) and the amount of decay happening in a single time step

    %Step 9 - determining if any joints are formed
    for i=1:r, %Going through each ray individually
        if J(i)>=TJ, %If the segment substance is greater than the threshold for joint formation, a joint
forms
            maxi=max(seg(2,:)); %The model determines the highest segment number currently used
            seg(2,i)=maxi+1; %and the new segment that is formed is assigned the following number
            J(1,i)=0; %the concentration of the segment substance is then returned to 0
```

```
        end;
    end;

    %Updating the matrices. The "Current values" Now become the "Previous step" values (will go in row 1)
    %so the 2nd row can be updated with new positions next iteration
    bone_rho(1,:)=bone_rho(2,:); bone_rho_s1(1,:)=bone_rho_s1(2,:); bone_rho_s2(1,:)=bone_rho_s2(2,:);
bone_rho_s3(1,:)=bone_rho_s3(2,:);bone_rho_s4(1,:)=bone_rho_s4(2,:);
    source_rho(1,:)=source_rho(2,:); source_rho_s1(1,:)=source_rho_s1(2,:);
source_rho_s2(1,:)=source_rho_s2(2,:);
source_rho_s3(1,:)=source_rho_s3(2,:);source_rho_s4(1,:)=source_rho_s4(2,:);
    source_theta(1,:)=source_theta(2,:); source_theta_s1(1,:)=source_theta_s1(2,:);
source_theta_s2(1,:)=source_theta_s2(2,:);
source_theta_s3(1,:)=source_theta_s3(2,:);source_theta_s4(1,:)=source_theta_s4(2,:);
    bone_theta(1,:)=bone_theta(2,:); bone_theta_s1(1,:)=bone_theta_s1(2,:);
bone_theta_s2(1,:)=bone_theta_s2(2,:);
bone_theta_s3(1,:)=bone_theta_s3(2,:);bone_theta_s4(1,:)=bone_theta_s4(2,:);
    seg(1,:)=seg(2,:);
end;

%Saving the xycoord matrix for use in other programs - without scaling
save('xycoord - final','xycoord');

xycoord_reg=xycoord; %Saving the xycoord for use in regeneration

%Scaling the fin out along the x axis to reproduce a visually similar fin
%The scaling value was determine by looking at the change in x coordinate
%position of ray bones over development
scale=4;
starting=find(xycoord(:,9)==0); %Finding starting positions
starting1=xycoord(starting,1);

starting2=starting1*scale; %Moving the starting positions of the ray out by the scaling value
movement=starting2-xycoord(starting,1);
random=[-9:-1, 1:9];%Matrix of ray numbers

%Scaling out the remaining points of the ray by the change in ray base
%position
```

```
for i=1:18,
    raypoints=find(xycoord(:,4)==random(i));
    xycoord(raypoints,1)=xycoord(raypoints,1)+movement(i);
end;

%Plotting program - User is asked how to plot the model fin
plotting1=input('How would you like to display the fin? plot by rays (ray), plot by segment number(num) or
plot by segment length (len)','s');
plotting;

%Asks the user if they would like to run the regeneration program
regen=input('Do you want to amputate the fin? (y/n)', 's');
if regen=='y',
    regeneration_final;
end;
```

8.3.5 Regeneration Program

```
% Model of bony ray regeneration and patterning in teleosts, calibrated with
% experimental regenerative growth rates.
% INPUTS
%   The model requires 1 user input:
%       steps2=4000; which represents a fin regenerating for 40 days

%The parameter values for the number of rays (r) and the time step (dt) are
%maintained from the ontogenetic ray growth and patterning program
%(findevelopment_final(r,steps,dt)

% Global parameters, for use in other programs related to the ray regeneration
% program (eg. plotting program, regeneration)
global xycoord xycoord_reg plotting1 r r1 ray0 alpha_orig pB_orig TB TJ J B p e dt bone_theta_orig
bone_rho_orig xycoord1 scale steps dt
%Calling the xycoord matrix we saved at the end of the findevelopment
%program for use in the regeneration program. This matrix represents all
%the points in the ontogenetic fin
xycoord_orig=xycoord_reg;

%Recalling the number of rays from the findevelopment program
r=r1;
%Creating a matrix of the ray numbers for the original number of rays at
%the beginning of the findevelopment simulation
ray0=[-r/2:-1,1:r/2];

%Setting up the length at which the amputation will be performed on the fin.
regen_len=2; %Note, this parameter can be changed to represent any length along the fin

%Determining the bone points that are located along the amputation
%plane, and finding all the bone points that are located proximal to the
%amputation plane
interpol=[];    %Matrix that will be used to determine the interpolation between two points
                %if the amputation plane does not fall directly on a point
xycoord=[];     %New xycoord matrix we are creating that will contain all the bone points
                %located proximal to the amputation plane
```

```
amputation=[];  %Matrix to contain the bone points of the amputation points

for i=1:r,  %Finding the point of amputation for each ray individually

    indx=find(xycoord_orig(:,4)==ray0(i)); %Finding all the bone points associated with the ray
    indx2=min(find(xycoord_orig(indx,2)>=regen_len));   %Determining the first bone point distal
                                                        %to the amputation plane
    interpol=cat(1,xycoord_orig(indx(indx2-1:indx2),:),interpol); %Storing the values of the
                                %bone point just distal and just proximal to the amputation plane

    % Interpolating the x coordinate of the bone point at the amputation length (y=2)
    x=interpol(:,1);
    y=interpol(:,2);
    xi=interp1(y,x,regen_len);

    %Storing the values of the bone points along the amputation plane for that ray
    amputation=cat(1,[xi,regen_len,interpol(2,3:10)],amputation);
    interpol=[]; %Clearing the matrix for the next ray
    xycoord1=cat(1,xycoord_orig(indx(1:indx2-1),:),amputation(1,:)); %Storing the xycoord matrix
                                    %up to the amputation plane and then storing the amputation point as well
    xycoord=cat(1,xycoord1,xycoord); %Building the xycoord matrix to include each ray
end;
%Simply flipping the amputation matrix, since the matrices are presented
%from ray -9 to ray 9
amputation=flipud(amputation);

%Sorting the matrix containing the bone points proximal to the amputation
%so that the data is stored by time (not ray number)
xycoord=sortrows(xycoord,[9 4]);
xycoord_preamp=xycoord; %Storing the matrix for later use

%Plotting the ray stumps that remain after amputation
%Scaling the fin out the amputated fin along the x axis to reproduce a visually similar fin
%The scaling value was determine by looking at the change in x coordinate
%position of ray bones over development
scale=4;
starting=find(xycoord(:,9)==0); %Finding starting positions
```

```
starting1=xycoord(starting,1);

starting2=starting1*scale; %Moving the starting positions of the ray out by the scaling value
movement=starting2-xycoord(starting,1);
random=[-9:-1, 1:9];%Matrix of ray numbers

%Scaling out the remaining points of the ray by the change in ray base
%position
for i=1:18,
    raypoints=find(xycoord(:,4)==random(i));
    xycoord(raypoints,1)=xycoord(raypoints,1)+movement(i);
end;

save('xycoord - 2 mm amputation','xycoord'); %Saving the xycoord amputated matrix for use in data analysis

%Plotting the fin using the plotting program created within the laboratory
plotting; %The method of plotting (ray, len, num) is maintained from the findevelopment program

%Making xycoord empty so that xycoord matrix during regeneration is only the new
%fin section - at the end of the simulation we will add the amputation
%matrix to this matrix
xycoord=[];
x=[];
y=[];

%Determining the total length of ontogenetic development and regeneration
stepstot=steps+steps2;

%SETTING UP THE MODEL FOR THE REGENERATIVE OUTGROWTH PHASE OF REGENERATION
%Determining the starting positions for the regenerating ray - determined
%from the ray stumps at the amputation plane
bonex=fliplr(amputation(:,1)');
boney=fliplr(amputation(:,2)');
%Determining the theta and rho values in the polar coordinates system for
%the bone points
[bone_theta_test,bone_rho]=cart2pol(bonex,boney);
bone_theta=bone_theta_orig;
```

```
%The bone_theta, bone_rho, source_theta and source_rho matrices will store the current position of the
source and bone points (row 1) and the
%previous position of the source and bone points (row 2)
bone_rho=[bone_rho; bone_rho]; %bone_theta=[bone_theta; bone_theta];
source_rho=bone_rho*1.01; source_theta=bone_theta;

%Creating matrices to be used in the model
seg=amputation(:,3)';    %Segment numbers for segments - the segments that were amputated are continued in
the regenerate
seg=[seg; seg]; %Doubling the matrix of segment numbers (each column represents a ray)
s1=ones(1,r); %Tracking s1 ray section for each ray (1 - it has a parent ray)
s2=zeros(1,r); %Tracking s2 ray sections for each ray (1 - it's the lefthand branch of a bifurcation, 2 -
it's the righthand)
s3=zeros(1,r); %Tracking s3 ray sections for each ray (1 - it's the lefthand branch of a bifurcation, 2 -
it's the righthand)
s4=zeros(1,r);  %Tracking s4 ray sections for each ray (1 - it's the lefthand branch of a bifurcation, 2 -
it's the righthand)

%|These matrices  will contain the last and second to last theta and rho values for the s1, s2, s3 or s4 ray
sections
%for source and bone points. Once a ray section has progressed from it's current type to the next (eg. s1 to
s2),
%the old matrix (s1) is no longer updated.
source_rho_s1=zeros(2,r); source_rho_s2=zeros(2,r); source_rho_s3=zeros(2,r); source_rho_s4=zeros(2,r);
source_theta_s1=source_theta; source_theta_s2=zeros(2,r); source_theta_s3=zeros(2,r);
source_theta_s4=zeros(2,r);
bone_rho_s1=source_rho_s1; bone_rho_s2=source_rho_s2; bone_rho_s3=source_rho_s3; bone_rho_s4=source_rho_s4;
bone_theta_s1=source_theta_s1; bone_theta_s2=source_theta_s2; bone_theta_s3=source_theta_s3;
bone_theta_s4=source_theta_s4;

step=zeros(1,r)+steps*dt; %Matrix to store the current step (in days) of the model
reg=zeros(1,r); %Matrix to store whether or not the current bone point belongs to ray that has been
regeneration
                %(0-nonamputated, 1-amputated)

%Creating the ray number matrix from the amputation data - in case the
%amputation was made distal to a bifurcation
```

```
ray0=amputation(:,4)';

%Joint formation mechanism
J=zeros(1,r);
%The parameters associated with the joint and bifurcation forming
%mechanisms are almost entirely conserved for the regenerative portion of
%the model. The only parameter that changes in the constant in the joint
%formation mechanism
h=0.4;
hJ=h.*([1 1 1 .93 0.85 0.84 0.8 0.73 0.68 0.68 0.73 0.8 0.84 0.85 .93 1 1 1]);

%Bifurcation forming mechanism
B=zeros(1,r);
pB=0.95.*[0.53 0.5 0.44 0.42 0.43 0.46 0.48 0.5 0.51 0.51 0.5 0.48 0.46 0.43 0.42 0.44 0.5 0.53]; %Softening
pB values
deg=0.001;
r1=r; r2=r; co=zeros(1,r);

%The values used to scale the fin growth rate to each ray, these represent the slope of
%the linear regression of ray length as a function of fin length
scale=([0.934 0.950 0.919 0.846 0.759 0.675 0.595 0.522 0.492 0.511 0.573 0.658 0.728 0.794 0.848 0.883
0.896 0.923]);

%Determining the x and y coordinates of the starting bone points
[x,y]=pol2cart(bone_theta(1,:),bone_rho(1,:));
xycoord=cat(1,xycoord,[x' y' seg(1,:)' ray0(1,:)' s1(1,:)' s2(1,:)' s3(1,:)' s4(1,:)' step(1,:)'
reg(1,:)']);




%NOTE: the next section of the model is identical to the "int" loop in the
%findevelopment program (Steps 1 - 9). The only differences are the rate of regeneration
%is a regenerative growth rate, which is as follow:

%    growth=(11.24537040987619/(int*dt+2.36)^2); %Regenerate regeneration
```

```
%And the equation for the joint formation mechanism is as follows:

%    ROA=(hJ)/((int*dt+2.36)^e);

%This is because instead of the ontogenetic growth rate, and the starting
%date of ontogenetic growth (which was 26.12 days), this regeneration
%growth rate is different and has a new starting date (2.36)




%Updating the xycoord matrix so that it is known that these bone points
%belong to the regenerate
xycoord(:,10)=1;
xycoord=[xycoord_preamp; xycoord]; %Combining the preamputation xycoord matrix with the regenerate matrix

%Scaling the fin out along the x axis to reproduce a visually similar fin
%The scaling value was determine by looking at the change in x coordinate
%position of ray bones over development
scale=4;
starting=find(xycoord(:,9)==0); %Finding starting positions
starting1=xycoord(starting,1);

starting2=starting1*scale; %Moving the starting positions of the ray out by the scaling value
movement=starting2-xycoord(starting,1);
random=[-9:-1, 1:9];%Matrix of ray numbers

%Scaling out the remaining points of the ray by the change in ray base
%position
for i=1:18,
    raypoints=find(xycoord(:,4)==random(i));
    xycoord(raypoints,1)=xycoord(raypoints,1)+movement(i);
end;

%Plotting program - the method of plotting is the same as ontogenetic plotting
```

```
plotting;

%Saving the complete regenerated fin for use in data analysis

save('xycoord - regeneration','xycoord');
```

8.3.6 Plotting Programs

```
function plotting_final(plotting1)
% Model to plot the bony rays created in the findevelopment and
% regeneration programs
% Note: this plotting program plots the final fin at once, it does not plot
% iteration by iteration
%
% INPUTS
%   The model requires 1 user inputs:
%       plotting1 = the method of plotting desired. Options are "ray",
%       "len", and "num".
%           ray = plotting by ray section type (S1 = green, S2 = red, S3 =
%           blue)
%           len = plotting segments and joints, with coloration dependent
%           on colour length
%           num = plotting segments by their segment ID number along the
%           proximo-distal axis (1st segments in the rays are plotted one
%           colour, 2nd segments the next colour, 3rd segments the next,
%           etc. After 5 segments, the colours are restarted).

% Global parameters, for use in other programs related to the ray growth
% program (eg. plotting program, regeneration)
global xycoord r r1 rays
%Everytime the plotting program is used, a new figure is created
figure;

%Determining the number of rays in the model
r=r1; %Recalling the number of rays stored in the findevelopment model
rays=[-r/2:-1,1:r/2]; %Creating a matrix storing the ray numbers

%Depending on the option selected for plotting, different scripts are used
if plotting1=='len', %If plotting by segment length is chosen
  %Determining the ray numbers in the model data
  temp=unique(xycoord(:,4));
  %Setting up the colour matrix for plotting
  col=jet(11);
```

```
    for k=1:size(temp),%Finding the data points for each ray individually
        raypoints=find(xycoord(:,4)==temp(k));%Finding the points associated with each ray
        raypoints=xycoord(raypoints,:);%Storing all the information associated with those points
        segments=unique(raypoints(:,3));%determining the number of segments in the ray

        for i=1:size(segments,1),%Finding the data points for each segment individually
            segray=find(raypoints(:,3)==segments(i));%Finding the data points associated with that segment
            segray=raypoints(segray,:);%Storing all the information associated with that segment

            %Determining if the segments are part of the S2 ray section (rayseg) or
            %S3 ray section (Rayseg2)
            rayseg=unique(segray(:,6)==1);
            rayseg2=unique(segray(:,7)==1);
            if size(rayseg,1)==1 && size(rayseg2,1)==1 %If the segment is in the S1 ray section
                h=line(segray(1:end,1),segray(1:end,2));  %Plotting the data for each segment
                set(h,'LineWidth',4);
                hold on
            elseif size(rayseg2,1)==1 %If the segment is in the S2 ray section
                segray1=segray;%Creating a temporary matrix so the original segment data isn't changed
                s2ray=find(segray1(:,6)==1); %Finding the points associated with the left S2 ray section
                s2ray_1=segray1(s2ray,:);%Storing the data associated with those points for plotting
                segray1(s2ray,:)=[];%Removing those points from the matrix of segment data

                s22ray=find(segray1(:,6)==2);%Finding the points associated with the right S2 ray section
                s22ray_1=segray1(s22ray,:);%Storing the data associated with those points for plotting
                segray1(s22ray,:)=[];%Removing those points from the matrix of segment data

                h=line(segray1(1:end,1),segray1(1:end,2));%Plotting the data for the segments that don't
belong to S2
                set(h,'LineWidth',4);
                h2=line(s2ray_1(1:end,1),s2ray_1(1:end,2));%Plotting the data for the left S2 segments
                set(h2,'LineWidth',4);
                h3=line(s22ray_1(1:end,1),s22ray_1(1:end,2));%Plotting the data for the right S2 segments
                set(h3,'LineWidth',4);

            else, %If the segment belongs to the S3 ray section
                segray1=segray; %Creating a temporary matrix to store the data - so the original data isn't
affected
```

```
            s2ray=find(segray1(:,7)==1);%Finding the segment points associated with the left S3 ray
section
            s2ray_1=segray1(s2ray,:);%Storing the segment data for plotting purposes
            segray1(s2ray,:)=[];%Removing that data from the temporary matrix
            s22ray=find(segray1(:,7)==2);%Finding the segment points associated with the right S3 ray
sections
            s22ray_1=segray1(s22ray,:);%Storing the segment data for plotting purposes
            segray1(s22ray,:)=[];%Removing the data from the temporary matrix

            h=line(segray1(1:end,1),segray1(1:end,2));  %Plotting the data for the segments not in S3
            set(h,'LineWidth',4);
            h2=line(s2ray_1(1:end,1),s2ray_1(1:end,2));%Plotting the data for the left S3 segments
            set(h2,'LineWidth',4);
            h3=line(s22ray_1(1:end,1),s22ray_1(1:end,2));%Plotting the data for the right S3 segments
            set(h3,'LineWidth',4);
        end;

        %Determining the segment's length
        seg_len=distance(segray(1,1:2),segray(end,1:2));

        %Plotting the joint between segments
        if size(rayseg,1)==1 && size(rayseg2,1)==1%If the segment is part of the S1 ray section
            joint=plot(segray(end,1),segray(end,2),'.');%Plotting the joint
            set(joint,'Color','k','markersize',12);
        elseif  size(rayseg2,1)==1 %If the segment is part of the S2 ray section - need to plot 2 joints
            %(1 for each S2 branch)
            joint=plot(s2ray_1(end,1),s2ray_1(end,2),'.');%Plotting the left S2 joint
            set(joint,'Color','k','markersize',12);
            joint=plot(s22ray_1(end,1),s22ray_1(end,2),'.');%Plotting the right S2 joint
            set(joint,'Color','k','markersize',12);
        else %If the segment is part of the S3 ray section - need to plot 2 joints (1 for each S3
branch)
            joint=plot(s2ray_1(end,1),s2ray_1(end,2),'.');%Plotting the left S3 joint
            set(joint,'Color','k','markersize',12);
            joint=plot(s22ray_1(end,1),s22ray_1(end,2),'.');%Plotting the right S3 joint
            set(joint,'Color','k','markersize',12);
        end;
```

```
            %Determining the coloration of the segment depending on the
            %segment's length
            if seg_len(1)<=.1,
                ct=1;
            elseif seg_len(1)<=.125 && seg_len(1)>.1,
                ct=2;
            elseif seg_len(1)<=.15 && seg_len(1)>.125,
                ct=3;
            elseif seg_len(1)<=.175 && seg_len(1)>.15,
                ct=4;
            elseif seg_len(1)<=.2 && seg_len(1)>.175,
                ct=5;
            elseif seg_len(1)<=.225 && seg_len(1)>.2,
                ct=6;
            elseif seg_len(1)<=.25 && seg_len(1)>.225,
                ct=7;
            elseif seg_len(1)<=.275 && seg_len(1)>.25,
                ct=8;
            elseif seg_len(1)<=.3 && seg_len(1)>.275,
                ct=9;
            elseif seg_len(1)<=.325 && seg_len(1)>.3,
                ct=10;
            elseif seg_len(1)>.325
                ct=11;
            end;
            %Setting the segment color
            set(h,'Color',col(ct,:));
            if size(rayseg,1)>1 || size(rayseg2,1)>1;
                set(h2,'Color',col(ct,:));
                set(h3,'Color',col(ct,:));
            end
        end;
    end;

elseif plotting1=='ray'%If plotting by ray section type is chosen
      %Determining the ray numbers in the model data
      temp=unique(xycoord(:,4));
```

```
for i=1:r, %Finding all data associated with each ray individually
    raypoints=find(xycoord(:,4)==temp(i));%Finding the points associated for this ray
    raypoints=xycoord(raypoints,:);%Storing all the information associated with that ray

    %Because there are many different ray sections which must be
    %plotted, the points associated with each ray section are
    %determined and plotted individually

    %Finding the points in the left S4 ray sections
    ray4=find(raypoints(:,8)==1);
    ray4_1=raypoints(ray4,:); %Storing the information associated with the left S4 ray section
    raypoints(ray4,:)=[];%Removing the information associated with this section from the main matrix

    %Finding the points in the right S4 ray sections
    ray42=find(raypoints(:,8)==2);
    ray4_2=raypoints(ray42,:);%Storing the information associated with the right S4 ray section
    raypoints(ray42,:)=[];%Removing the information associated with this section from the main matrix

    %Finding the points in the left S3 ray sections
    ray3=find(raypoints(:,7)==1);
    ray3_1=raypoints(ray3,:);%Storing the information associated with the left S3 ray section
    raypoints(ray3,:)=[];%Removing the information associated with this section from the main matrix

    %Finding the points in the right S3 ray sections
    ray32=find(raypoints(:,7)==2);
    ray3_2=raypoints(ray32,:);%Storing the information associated with the right S3 ray section
    raypoints(ray32,:)=[];%Removing the information associated with this section from the main matrix

    %finding the points in the left S2 ray sections
    ray2=find(raypoints(:,6)==1);
    ray2_1=raypoints(ray2,:);%Storing the information associated with the left S2 ray section
    raypoints(ray2,:)=[];%Removing the information associated with this section from the main matrix

    %finding the points in the right S2 ray sections
    ray22=find(raypoints(:,6)==2);
    ray2_2=raypoints(ray22,:);%Storing the information associated with the right S2 ray section
```

```
    raypoints(ray22,:)=[];

    %Plotting the S1 ray sections first
    h=line(raypoints(:,1),raypoints(:,2));
    hold on;
    set(h,'Color',[0 1 0],'LineWidth',3);

    %To plot the right and left S2 ray sections
    if ~isempty(ray2_1),
        k=line(ray2_1(:,1),ray2_1(:,2));
        k2=line(ray2_2(:,1),ray2_2(:,2));

        set(k,'Color',[1 0 0],'LineWidth',3);
        set(k2,'Color',[1 0 0],'LineWidth',3);
    end;

    %To plot s3_1 and s3_2 ray sections
    if ~isempty(ray3_1)
        %Plotting the left S3 ray section for both S2 ray sections
        ray_s3s2=find(ray3_1(:,6)==1);
        ray_s3s22=find(ray3_1(:,6)==2);
        l=line(ray3_1(ray_s3s2,1),ray3_1(ray_s3s2,2));
        l2=line(ray3_1(ray_s3s22,1),ray3_1(ray_s3s22,2));

        %Plotting the right  S3 ray section for both S2 ray sections
        ray_s32s2=find(ray3_2(:,6)==1);
        ray_s32s22=find(ray3_2(:,6)==2);
        l3=line(ray3_2(ray_s32s2,1),ray3_2(ray_s32s2,2));
        l4=line(ray3_2(ray_s32s22,1),ray3_2(ray_s32s22,2));

        set(l,'Color',[0 0 1],'LineWidth',3);
        set(l2,'Color',[0 0 1],'LineWidth',3);
        set(l3,'Color',[0 0 1],'LineWidth',3);
        set(l4,'Color',[0 0 1],'LineWidth',3);
    end;
end;
```

```
elseif plotting1=='num' %If plotting by ray number is desired
    colsize=5;%Determining the number of colours to use in the "num" method of plotting
    col=jet(colsize);%Creating the colour matrix
    colct=0;%Setting up a colour counter to cycle through the colour matrixcount1=0;

    cnt=0;

    %Determining the ray numbers in the model data
    temp=unique(xycoord(:,4));
    for k=1:size(temp), %Going through each ray individually
        count=1; %Setting up the count matrix, which is used to determine the segment colouration

        raypoints=find(xycoord(:,4)==temp(k));%Finding all data associated with each ray individually
        raypoints=xycoord(raypoints,:);%Storing all the data associated with this point
        segments=unique(raypoints(:,3));%Finding the unique segments in the ray

        for i=1:size(segments,1),%Going through each segment within the ray individually
            segray=find(raypoints(:,3)==segments(i));%Finding all the points associated with that segments
            segray=raypoints(segray,:);%storing the data associated with that segment

            ray_s3=find(segray(:,7)==1);%Finding the segments which are part of the left S3 ray section
            ray_s3_1=segray(ray_s3,:);%Storing the data associated with those segment points
            segray(ray_s3,:)=[];%Removing that data from the main matrix
            ray_s32=find(segray(:,7)==2);%Finding the segments which are part of the right S3 ray section
            ray_s32_1=segray(ray_s32,:);%Storing the data associated with those segment points
            segray(ray_s32,:)=[];%Removing that data from the main matrix

            ray_s2=find(segray(:,6)==1);%Finding the segments which are part of the left S2 ray section
            ray_s2_1=segray(ray_s2,:);%Storing the data associated with those segment points
            segray(ray_s2,:)=[];%Removing that data from the main matrix
            ray_s22=find(segray(:,6)==2);%Finding the segments which are part of the right S2 ray section
            ray_s22_1=segray(ray_s22,:);%Storing the data associated with those segment points
            segray(ray_s22,:)=[];%Removing that data from the main matrix


            if count>5,%If the counter exceeds the number of colours we are using
                count=1;%The counter resets to 1, and colouration begins anew
```

```
            end;

            %Plotting the segments which are in the S1 ray section
            if ~isempty(segray)
                h=line(segray(:,1),segray(:,2));
                set(h,'Color',col(count,:),'Linewidth',3);
            end;

            hold on;
            axis equal;

            %Plotting the segments which are in the left S2 ray section
            if ~isempty(ray_s2_1)
                h2=line(ray_s2_1(:,1),ray_s2_1(:,2));
                set(h2,'Color',col(count,:),'Linewidth',3);
                if isempty(ray_s3_1) && isempty(segray), %If the segment occurs in a bifurcation, the
segment
                                            %colouration needs to continue into the next ray section
                                            %by subtracting 1 from the
                                            %colour counter this ensure
                                            %colouration is the same
                    count=count-1;
                end;
            end;
            %Plotting the segments which are in the right S2 ray section
            if ~isempty(ray_s22_1)
                h3=line(ray_s22_1(:,1),ray_s22_1(:,2));
                set(h3,'Color',col(count,:),'Linewidth',3);
            end;
            %Plotting the segments which are in the left S3 ray section
            if ~isempty(ray_s3_1)
                h4=line(ray_s3_1(:,1),ray_s3_1(:,2));
                set(h4,'Color',col(count,:),'Linewidth',3);

                if isempty(ray_s2_1)&& isempty(ray_s22_1)%If the segment occurs in a bifurcation, the
segment
                                            %colouration needs to continue into the next ray section
                                            %by subtracting 1 from the
```

```
                                        %colour counter this ensure
                                        %colouration is the same
                    count=count-1;
                end;
            end;
            %Plotting the segments which are in the right S3 ray section
            if ~isempty(ray_s32_1)
                h5=line(ray_s32_1(:,1),ray_s32_1(:,2));
                set(h5,'Color',col(count,:),'Linewidth',3);

                if ray_s32_1(1,6)==1,
                    count=count-1;
                end;

            end;
            count=count+1; %After the plotting of this segment, the colour counter is increased
                           %so that the next segment is the following
                           %colour in the pattern
        end;
    end;
end;
%Ensuring the axes are equal in the figure
axis equal;
```